UNIVERSITY OF OKLAHOMA

GRADUATE COLLEGE

OBSERVATION OF MARS ANALOGOUS BASALT IN NEAR SATURATED BRINES

A THESIS

SUBMITTED TO THE GRADUATE FACULTY

In partial fulfillment of the requirements for the

Degree of

MASTER OF SCIENCE

By

ANDREW RODRIGUEZ

Norman, Oklahoma

2020

OBSERVATION OF MARS ANALOGOUS BASALT IN NEAR SATURATED BRINES

A THESIS APPROVED FOR THE

SCHOOL OF GEOSCIENCES

BY THE COMMITTTEE CONSISTING OF

Dr. Megan Elwood Madden, Chair

Dr. Andrew Elwood Madden

Dr. Lindsay Hunt

Table of Contents

I sincerely wish to thank my advisor, Dr. Megan Elwood Madden, for her flexibility during the ups and downs of my study, and my committee for their openness for positive criticism and outspoken optimism for this project. I am grateful for my funding institutions NASA and the OU College of Geosciences. I wish to thank Daniel Mason, Cansu Demirel Floyd, Emily Simpson, Katie Welch, and Katy Garrett for being great coworkers who have been available to give feedback on many situations and research strategies. I wish to thank my wife, Anna Rodriguez. If not for her support and daily encouragement, I would not have felt accomplished from the start nor have made it this far. And I wish to thank my children, Luke, Joseph, Evelyn, and Samuel. Each of you remind me in your own special way the awesomeness of being a dad and how special the ordinary things in life really are. Each of you have helped create, mold, and refine the person that I have been and am. With each day you morph and guide the acts, decisions, words, and thoughts that when taken together make my life, mine.

Thank you

"The future is in the hands of those who explore and from all the beauty they discover while crossing perpetually receding frontiers, they develop for nature and for humankind an infinite love."

Jacques Yves Cousteau

Abstract

The Mars 2020 rover and the ExoMars rover will include a Raman spectrometer as part of the suite of instruments onboard the rovers and will be the first times a Raman spectrometer will take direct measurements on the surface of Mars. This experiment looked to bridge the understanding of basalt dissolution in near saturated brines, Raman spectroscopy, and brine chemistry. This experiment used basalt chips from the Craters of the Moon National Monument as an analogous basalt and left them to react in solutions of ultra-pure water, NaCl, Na_2SO_4, $NaClO_4$, $MgCl_2$, $MgSO_4$, $CaCl_2$, and two mixed brines of $NaClO_4$+Na_2SO_4 and $MgSO_4$+$MgCl_2$. After 365 days of reacting in the solutions, the basalt chips show iron oxide, sulfate, and carbonate secondary mineral precipitation that is identifiable by Raman spectroscopy. The formation of carbonate secondary minerals in solutions absent of carbon suggest CO_2 from the experiment atmosphere dissolved into solution then salted out of solution. The implication of carbonates forming in this experiment combined with observation of carbonates on Mars could suggest a past environment near neutral or slightly acidic in pH.

Introduction

Recent and early Mars probe studies have shown mafic minerals are plentiful on the Martian surface. As early as the Viking I lander, we had evidence that mafic minerals such as pyroxene and olivine are important components of the surface dust and rock (Clark, 1978). A study from the more recent Mars Express Orbiter (Bibring et al., 2006) shows that mafic and ultramafic rocks are very common in the southern hemisphere of Mars and can also be found across the planet in fine-grained sand..

Gooding et al. (1978) made the argument that gaseous H_2O, as well as gaseous O_2 and CO_2, should be included in the thermodynamic and kinetic models of Mars geochemistry after the Viking I and II landers provided early evidence of hydrated minerals on the surface near the polar regions of Mars (Carr, 1979). Gooding's argument assumed that there was no evidence of liquid water was on the surface, and therefore liquid-solid interactions are nonexistent. However, multiple indirect observations, such as the possible briny droplet growth on a Phoenix landing strut (Rennó et al., 2009) and the formation of recurring slope lineae allude to liquid water on the surface of current day Mars (Berger et al., 2009; Fairén et al., 2009; Martínez and Renno, 2013; Ojha et al., 2015).

As we continue to send rovers, landers, and orbiters to Mars our understanding of the past geologic landscape has broadened to include liquid water interactions as well as other aqueous phenomena associated with a working hydrologic cycle. New evidence, including the possible aqueous transport of sulfates and the size and shape of apparent deltas seen from suggests hydrologic activity extends later in the history of Mars (Bhattacharya et al., 2005; Ojha et al., 2015; Rennó et al., 2009; Schon et al., 2012).

Studies of Mars' past hydrologic cycle gained importance after the Viking I and II orbiters returned images suggesting liquid flow on the Martian surface (Cutts et al., 1976) and the Mariner 9 lander returned images of drainage patterns suggesting aqueous activity occurred on Mars in the past. (Martínez and Renno, 2013). Recurring slope lineae observed in orbital images may also form due to deliquescence of water vapor (McEwen et al., 2014) or possibly an upwelling of groundwater (Abotalib and Heggy, 2019). Martinez et. al. (2013) discussed the possibility of liquid water at or near the surface of current day Mars, as evidenced by droplet looking growths on the Phoenix lander struts, images of possible liquid induced recurring slope lineae at Richardson Crater, and dark discoloration from CO_2 off-gassing in the Richardson Crater as it causes possible liquid brines to form rings in the crater (Kieffer, 2007; Martínez et al., 2012). This work by Martinez et al. demonstrates that pure liquid water is not thermodynamically stable under Mars surface conditions and will evaporate rapidly. However, Martinez and others make the argument that certain minerals and salts observed by the Curiosity rover could either maintain water in a briny state or incorporate water as a hydrated mineral. While we continue to investigate ways liquid water could possibly exist on Mars, no instrument currently operated on Mars has directly detected liquid water (Ojha et al., 2015). Past studies suggest that Mars still has an active hydrologic cycle on the surface, albeit diminished in the amount of water (Hecht et al., 2009; Kounaves et al., 2010; McEwen et al., 2014; Ojha et al., 2015). Studies also suggest liquid water is vital to the understanding of how Mars was shaped to its current state and how Mars continues to change to this day. Renno et al. (2009) discuss the conditions necessities for brine to exist on Mars and their models support evidence of such brines based on images from the Phoenix Lander struts and trench

Recent orbiter images also suggest evidence for liquid water could possibly persist on the surface of Mars as recurring slope lineae (Ojha et al., 2015). The appearance of these lineae may form via salts found on the Martian surface and their ability to deliquesce liquid from the meager amount of water vapor in the Martian atmosphere (Nikolakakos and Whiteway, 2018). Salts can lower the freezing point of water to within the range of temperate and pressure conditions found at Gale Crater, Gusev Crater, and Meridiani Planum (Cull et al., 2010; Rennó et al., 2009). These theories of past, and possibly current, aqueous processes on Mars could be key to determining not only the past geological history of Mars, but also its past habitability (Baker et al., 1991; Bish et al., 2003; Carter et al., 2013; Clifford and Parker, 2001; Goudge et al., 2016; Haskin et al., 2005; Kite, 2019; Solomon et al., 2005). These hypotheses underscore the importance of understanding how aqueous geochemical processes could operate at the locations chosen for our rovers, as well as regional areas of interest investigated by orbiters, so we can better understand aqueous systems throughout Mars' history (Greenwood and Blake, 2006; Grotzinger et al., 2015, 2005; Massé et al., 2014; Milliken et al., 2010; Ming et al., 2006; Peslier et al., 2019; Rampe et al., 2017; Rapin et al., 2018).

Since basalt, salts, and water are likely to co-exist on the surface of Mars event today, one area of particular interest is understanding of how basaltic minerals may be chemically altered in brines. This area of research is important and of interest because, as far we know, life on Earth began in wet, salty conditions, likely in the presence of early mafic crust (Dodd et al., 2017; Hazen, 2012; Marshall et al., 2010; Westall, 2005). Evidence of salts on Mars was first predicted by the Viking landers, but the Phoenix Lander, using the wet chemistry lab, was the first mission to directly observe evidence of salts (Hecht et. al., 2009a). The Mars exploration rovers also found volatile enrichments indicative of salts (Cull et al., 2010; Möhlmann and

Thomsen, 2011; Wray et al., 2010), and the Mars reconnaissance orbiter observed planet wide evidence of salts (Beck et al., 2020; Ehlmann and Edwards, 2014; Feldman et al., 2004; Marshall et al., 2010; Ojha et al., 2015; Solomon et al., 2005; Vaniman et al., 2004). Since then, several studies have focused on weathering in acidic, cold, salty, or radiated conditions that we expect to see on Martian surfaces (Boynton et al., 2007; Chemtob et al., 2017; Hausrath and Brantley, 2010; Schröder et al., 2004). These studies, however, looked at these interactions with relatively dilute concentrations of salts. Given the abundance of salts and the low temperature and pressure conditions, any liquid water present at the surface today will likely be a nearly-saturated brine (Carr, 1979; Chevrier and Rivera-Valentin, 2012; Martínez and Renno, 2013; Primm et al., 2017; Tosca and McLennan, 2009).

Orbiter data also suggests that the surface of Mars is plentiful in basalt (Edwards et al., 2008), so a focused understanding of how brines react with basalt is crucial to understanding key assumptions that we must make in order interpret information we attain from our orbiters, landers, and rovers. Past experiments have focused on dissolution of basalts with a mixture of cold or acidic conditions that replicate conditions on Mars (Jones et al., 2012; Peretyazhko et al., 2018; Schröder et al., 2004; Smith et al., 2017) or analogous to the salty conditions of Earth's current oceans (Hausrath and Brantley, 2010). Salts are of particular interest due to the ability of certain salts to lower the eutectic point of liquid water to within the mean surface conditions recorded on Mars (Marion et. al. 2010; Gough et. al. 2011; Toner et. al. 2014). Previous studies produced salts in Mars-like conditions either by the ionization of chlorine to produce perchlorates (Schuttlefield et al., 2011) or with the introduction of halite to a soil of similar bulk chemistry to Mars soils (Carrier and Kounaves, 2015). Other experiments have taken in depth approaches to the geochemistry of acidic-sulfate rich solutions and their interaction with Mars

analogous mafic rock samples (Banin et al., 1997; Hurowitz et al., 2010; Tosca and McLennan, 2009; Yant et al., 2016). These experiments suggest that soils on Mars are possibly acidic, rich in salts, and water-limited in its aqueous interactions.

Other experiments suggest that the clays observed on the surface of Mars were possibly from alteration of basalt (Berger et al., 2014). These prior experiments suggest that basalt weathering in near saturated brines could produce Ca-rich alterations that are detectable with instruments either in orbit or on the surface. These characteristics of the altered basalt can also be used to make geochemical hypotheses about the characteristics of Martian soils. Additional studies tried to replicate and explain how certain brines can dissolve mafic rocks and precipitate minerals that have been observed on Mars (Berger et al., 2014; Golden et al., 2005; Peretyazhko et al., 2018; Phillips-Lander et al., 2019, 2017). Under acidic and water-limiting conditions pyroxene observed on the surface can react with brines predicted to be on the Martian surface and create characteristic textures (Phillips-Lander et al., 2019). These textures, indicative of basalt dissolution and subsequent secondary mineral and clay formation, give evidence for either sporadic, limiting water-rock interactions or a low water activity environment. Unique secondary minerals such as akageneite ($(Fe^{3+},Ni^{2+})_8(OH,O)_{16}Cl_{1.25} \cdot nH_2O$) can also form in chloride-rich solutions over a wide range of pH condittions (Peretyazhko et al., 2018). Experiments in assessing acidic alteration of low-to-high glass silica show correlations to the data collected from Pathfinder rock and Irvine which alludes to the conditions that best support silicate dissolution observed on Mars despite little global evidence of alterations (Yant et al., 2016). These conclusions form Yant, Phillips-Lander, Peretyazhko, and others suggest either localized low pH or a global moderately low pH, which has the potential to drive future missions to locations on the Martian surface. These experiments are important as rovers, landers, and orbiters can only

give us so much information and the complexity of the Martian past requires us to test theories with new tools to better understand the geology of Mars than instruments that could be a decade old depending on when final assembly occurred and if the mission is lasting longer than designed, such as the Mars Exploration Rovers. Being able to test theories on Earth with new techniques or ideas allows us to expand our understanding of the Martian history without demanding time and data from instruments that may not be able to accomplish the goal due to engineering constraints or deteriorating conditions as well as help define future missions to Mars.

These studies are important to understand the limits of the environment of past Mars as well as attempt to piece together the necessary factors in how certain brines can exist in liquid form by lowering the freezing point of water to within Martian high temperatures (Brass, 1980; Primm et al., 2017; Toner et al., 2014). Other experiments focus on the environmental conditions necessary for these brines to remain liquid (Dickinson and Rosen, 2003; Primm et al., 2017; Robertson and Bish, 2011; Smith et al., 2014) such as the effect of relative humidity on the water activity of a brine, or the effects on melting and eutectic temperatures. What hasn't been found in my literature research is how a Mars analog basalt will react in a near-saturated liquid brine and how this alteration can be characterized with a Raman spectroscopy. The literature discusses the conditions on Mars or the utility of a Raman spectrometer with salts at less than saturated condition, but what is missing is how a Raman spectrometer will detect the products of basalt reacting with brines of salts we have confidence are present on Mars.

Key knowledge gaps

Previous experiments found that iron-rich olivine will dissolve before magnesium rich olivine in acidic conditions observed on Mars (Hausrath and Brantley, 2010) and that diurnal cycling combined with a fine salt layer can affect rock weathering due to thermal fracturing (Viles et al., 2010). Studies have shown how the high salinity NaCl and Na_2SO_4 brines have a significant effect on the dissolution of diopside despite low water activity (Phillips-Lander et al., 2019). These dissolution experiments show how Ca-, Mg-, and Fe- cations are able to dissolve out of the primary minerals and potentially produce secondary sulfate minerals similar to what was found in drill samples in Yellowknife Bay in Gale Crater (Vaniman et al., 2014). It is unclear, however, if such alterations will be observable with the Raman spectrometer.

Horgan et. al. (2017) demonstrate that low pH solutions aid in weathering and alteration of basalt. However, this study also highlights the limitations of the tools by suggesting that if a basalt or silica glass is altered in a moderately acidic condition (~pH 3) the near infrared signature is minimal and due to superficial depolymerization of the silicates. This illustrates how instruments currently on Mars may not readily detect alteration phases or they require preparation of sample materials. Horgan et al. (2017) does, however, allude to the idea that weathering events could be interpreted by spectral signatures in the surface features of the host rock. Others have shown evidence of Horgan's idea, specifically the shift in near infrared spectrum of glass in highly acidic environments (Chou and Wang, 2017). The limitations of FTIR spectroscopy may be overcome by employing in situ Raman spectroscopy. With Raman spectrometers set to arrive on Mars with the next two rover missions, the value of understanding how weathered material will appear as opposed to its unaltered parent material using Raman spectroscopy will allow geochemists to further decipher the Martian past.

Raman spectroscopy has the ability to quantitatively measure covalently bonded materials without the need to prepare or disturb the sample. In addition, Raman spectroscopy does not require the instrument to interact with the specimen nor requires any preparation of the specimen. The instrument is based on the principle of inelastic scattering of light through a medium first demonstrated theoretically by Sir Chandrashekhara Venkata Raman (Raman and Krishnan, 1928) and later made a usable tool once laser technology in the 1960's increased the irradiance of the light source, improving the Raman signal. Studies show that Raman spectroscopy is able to detect sulfate minerals with differing hydration states (Chou and Wang, 2017) as well as inferring the presence of organic hydrocarbons (Marshall et al., 2010; Marshall and Marshall, 2014). Additional studies have also looked at sediment samples from Permian lakes in North America and report how the Raman spectra of fluid inclusions in these sediments give evidence of acidic conditions in the lakes during the Permian period, even after eons of deposition and alteration (Benison et al., 1998). The ability of the Raman spectroscopy to determine percent abundance of minerals and discern between the hydration states of the same minerals even after millennia makes it a valuable tool for future Mars explorations.

The European Space Agency will soon send their second rover to Mars as part of the *ExoMars* Mission (Rull et al., 2017). Recently christened the Rosalind Franklin, this rover will include a Raman spectrometer as part of the suite of instruments in the analytical chamber. Vago et. al. (2017) discuss the importance of the Raman as part of the Rosalind Franklin's scientific mission as it is capable of taking measurements of a sample without needing preparation, and can be capable of deciphering any liquid water interactions. The spectrometer will also be able to discern mineral phase changes due to aqueous chemistry as different minerals will produce a different Raman spectra due to the unique intramolecular forces between each covalently bonded

element (Chou and Wang, 2017; Nikolakakos and Whiteway, 2018). The National Aeronautics and Space Administration (NASA) will also utilize the Raman spectrometer as part of the suite of instruments on their Mars 2020 rover. A Raman spectrometer does not rely on a radioactive source for subatomic particles such as the alpha particle x-ray spectrometer (APXS), nor does this instrument require a large amount of energy to power the laser necessary to take measurements. Perseverance will utilize two Raman spectrometers on its mission; a 532nm green laser on the SuperCam which will be used to study mineralogy of the Martian surface, and a 548.6 green laser on SHEROCK which will focus more on organic molecules. With these instruments, we can make interpretations about past and current liquid chemistry on Mars as well as take measurements on a score of organic functional groups if they exist on Mars. Therefore, this study provides important ground truthing that is needed to see how our current understandings of mineral dissolution, precipitation, and weathering events can be observed with a Raman spectrometer.

Few studies have used Raman as a tool to look for evidence of aqueous weathering on igneous rocks. While Smith et al. (2017) demonstrated that it is difficult to interpret weathering patterns with near infrared spectroscopy and Philips-Lander et. al. (2017) show difficulties in interpreting the dissolution of pyroxene based on texture patterns based on denticle length, Raman is a promising analytical tool for observing weathering products *in situ* on Mars. In this study we will test the utility of Raman spectroscopy for discerning weathering products by reacting Mars-analog basalt with near-saturated brines for up to a year. These moderate-term experiments allow the brines to dissolve the basalt and precipitate secondary minerals at a scale which can be discerned with the Raman spectrometer. We will also characterize the weathering products and reaction fronts with scanning electron microscopy (SEM), wavelength dispersive

spectroscopy (WDS), and backscatter scanning electron (BSE) imaging. Through these experiments and analyses we aim to demonstrate how Raman spectroscopy can be used in future efforts to characterize aqueous processes on Mars and other planetary bodies and to learn about the effects of brine chemistry on basalt dissolution and secondary minerals formed.

The next rovers sent to Mars will each include Raman spectrometers as part of the suite of instruments. These will be the first Raman spectrometers on Mars. The Raman spectrometer is useful in identifying minerals based on the inelastic scattering of energy from phonons within a target, and is able to distinguish minerals that are similar in chemical composition (Das and Hendry, 2011). This study investigates how different near-saturated brines react with a Mars analogous basalt to observe the impact of these brines on the rocks over time and determine how we can observe these changes using a Raman spectrometer. We use a 532 nm laser similar to that used by the Scanning Habitable Environments with Raman & Luminescence for Organics & Chemicals (SHERLOC) and SuperCam Raman/LIBS system on NASA's Mars 2020 rover, and the RLS Raman Spectrometer on the European Space Agency's ExoMars 2020 rover.

Methodology

A hand sample of the basalt from the Craters of the Moon National Monument was broken into pieces 0.75 mm to 2 mm in diameter. These pieces were sonicated to remove fine dust and microscopic grains, then placed on a clean cloth to dry. Fourteen of the larger samples were taken to the microprobe lab where I cut the samples and ground a single planar surface into each chip. These pieces were initially polished by hand with an abrasive lapping film pad equivalent to a 220-grit sandpaper and water to roughly grind a side into each chip. This process

was repeated to the now flattened side with lapping film pads equivalent to 400, 1000, 1800, and 8000 grit sandpaper. Further polishing on the chips were attained with felt pads lubricated with Al_2O_3 powder with 0.3 µm and 0.05 µm Al_2O_3 powder. The result for each polished chip is a single flat surface with as little topography as possible with respect to the newly created plain of reference on each chip.

These ground and polished samples are referred to as "polished" in this thesis to distinguish them from the rough, unpolished samples. Nine of the polished chips that appeared to have the best polished surface were chosen for the brine experiments and two were selected as control samples. One polished chip and 11 rough chips of roughly equal size and gross mass were grouped together to be reacted with brine in each experiment.

Before the chips were placed in their respective solutions, 100 mL of saturated brines NaCl, Na_2SO_4, $NaClO_4$, $MgSO_4$, $MgCl_2$, $CaCl_2$ or 100 mL of ultra-pure water was placed in separate Nalgene bottle reactors. The brines were produced by adding laboratory grade salts to ultra-pure water in non-reactive plastic containers and constantly agitating the reactors until no further salts dissolved. Two additional reactors contained mixed brines. The first contained a mixture of 50mL of the $NaClO_4$ brine and 50 mL of Na_2SO_4 brine and the second mixed brine reactor contained 50 mL of $MgSO_4$ brine and 50 mL of $MgCl_2$ brine.

Five mL of each solution were extracted before the experiment started as a control. The pH was measured using an Orion 3 star pH benchtop probe. Three mL of each solution was extracted into a clean centrifuge tube for measurement so as to not contaminate the whole batch with any ions released from the probe. An additional four mL of each brine was extracted and stored in new 10 mL centrifuge tubes for Raman spectroscopy.

Raman spectra were collected for each brine by extracting 0.3 mL into a well on a porcelain painter's dish. This dish gives low background signatures and produces no observable artifacts in the spectra of a sample (McGraw et al., 2018). These brine samples were placed in a Renishaw InVia Raman Spectrometer and measured with a 532nm green laser using streamline laser settings, centered at 1500 wavenumbers with a 1200 lines/cm grating. This provides a wide enough range to include peaks from the polyatomic ions in the brine, the water peak at 1640 wavenumbers, possible secondary minerals in suspension, new polyatomic ions from chemical reactions, and any unforeseen peaks that may arise. This change in the spectra over time and from any secondary minerals observed will be the results of this experiment and what will be discussed in detail.

Once we collected the brine samples, the basalt chips were added to each of the nine containers. Within one hour, the pH of each container was measured again by extracting three mL of each solution, and the nine bottles, each containing brine and 12 chips were then placed on a shaker table set for a moderate speed to agitate the solutions for the duration of this experiment.

After one month of reaction, three rough basalt chips of different sizes were removed from each reactor and rinsed three times with ultrapure water to remove any salt crystal buildup or fine dust. Each rock chip was weighed and placed in a sealed plastic bag with a dry paper towel for storage. Seven mL of each brine solution was extracted for further testing. Three mL was used for pH measurements and 0.4 mL of the extraction was used for Raman spectroscopy using the same settings for solution measurements from the control solutions. The bottles were then resealed and returned to the shaker table to continue agitation.

Within 24 hours of sampling, Raman spectra from the reacted rock samples was collected. I used the 2400 grating with the 532 nm laser and conducted spot analyses using the edge laser focusing mechanism at 10% of the full laser power. The edge setting focuses the laser at a point rather than a line to more precisely measure a single point on the surface rather than an elliptical area. The spectrometer was centered at 1500 cm^{-1}. Spectra was collected for 240 seconds at each spot on the surface. Raman spectra were collected at different locations on the sample until at least three separate spectra were collected that were indicative of each of the primary minerals: plagioclase (with two primary peaks near 483 and 508 wavenumbers and secondary peaks near 151, 196, 278, 407, 562, and 562); olivine (double peak near 819 and 850 wavenumbers); and pyroxene (a wide peak near 687 wavenumbers with a range from 577 to 748 wavenumbers and secondary peaks near 162, 329, and 493). In instances where the CCD detector was oversaturated with signal from the returned light, the collection was aborted then repeated with a reduction in laser power down to 5% power.

Locations were chosen based on surface morphology, as well as color, fracture pattern, or opacity. Locations that were visually glassy or translucent to milky in color were also chosen for spectroscopy. Previous studies note that this rock contains some glass (Adcock et al., 2018); however, these locations produce Raman spectra that contain mostly background noise. As such, while glass is part of the chemical makeup of our samples and may provide elements for reactions, this thesis will not include Raman analyses of the glass, since no discernable peaks appeared in this experiment, making it difficult to consistently analyze.

We used Renishaw's WiRE 4.2 software to subtract the background noise and normalize the spectra. I then analyzed each spectra further using *CrystalSleuth*, a free search engine software created by the RRUFF™ Project (Lafuente et al., 2015) that compares each spectrum to

the library of Raman spectra in the RRUFF™ database. RRUFF™ files were compared to each spectrum and matches were based on the calculated similarity between spectra, regardless of the color laser used. This has the downside of suggesting minerals that have different spectra between different color lasers. Another downside to the program that requires attention is that some minerals in the database give sporadic signatures or fluoresced during collection. This will appear as a false match due to the limitations of the program code, and any noise from the spectra being compared to the database adds to the likelihood of a false match. These limitations can be overcome and still allow the software to be a valuable tool to this thesis with a more controlled collection to reduce the noise of the spectra collected, or by material understanding of what can or cannot be observed with Raman spectroscopy due to fluorescence. The database will also be improved with higher quality grade spectra as more scientists work on the project and contribute to its use.

After the Raman spectra were collected, a single chip from each brine experiment was prepared for scanning electron microscopy (SEM) by sputter coating with Au-Pd. The sputter coater was set for automatic pulsations to create a fine grain coating so to provide better resolution at the expense of possible charging and shadowing effects. Images were collected at 100x, 500x, 5,000x, and 10,000x using the Zeiss Neon SEM located at the University of Oklahoma's Samuel Roberts Noble Microscopy Laboratory. Images were taken at 5 KV accelerating voltage with a 30 mm aperture. Multiple locations on each rock sample were examined for changes to surface characteristics. On each chip we analyzed at least one location where a fracture or a vesicular opening exposed a portion of the interior of the rock chip, one location with a mostly smooth surface where chemical weathering may be restricted due to a lower surface area, and one location with a rough texture where chemical weathering may be

increased due to a higher surface area. After imaging, the accelerating voltage was increased to 20 kV for EDS analysis. The proprietary software *Aztec* was used to calculate the elements of best fit for the samples. Data from the EDS analysis was then processed with the proprietary statistics software SPSS from IBM. This software was then able to show us the distribution of the elements C, O, Na, Mg, Al, Si, P, K, Ca, Ti, Mn, and Fe. The data was able to be grouped by mineral, allowing for a comparison of means of independent groups. The software is also able to say which elements were most significant to say statistically the elemental difference between the three most prominent minerals, pyroxene, plagioclase, and olivine.

This process of extraction, pH measurement, rinsing and drying, Raman analysis of the brine and rocks, and finally SEM imaging was repeated for the 3-month, 6-month, and 12-month observations. The timing of extractions provides an evaluation of chemical weathering and analysis over a longer period of time. We ended the experiment after one year to provide moderate-term reaction data within the timeframe of a master's thesis.

The 6-month extractions included two rough chips and one polished sample from each solution. The polished chip was prepared similar to the other chips with the exception that during Raman spectroscopy the samples were measured on both the rough and polished surfaces. The polished sample was then sent to the electron microprobe lab for carbon coating for SEM. The choice to carbon coat rather than sputter coating in AuPl is to reduce the number of elements coating the sample that could add error for the final electron microprobe analysis. SEM imaging was performed with the Jeol 840-A located at the Samuel Roberts Noble Microscopy Lab and achieved modestly similar imaging to the Zeiss Neon SEM used for the previous sample collections and for the 12-month imaging. The spectrometer was set for 20 KV with a 4 mm aperture.

Results

Brine analyses

A sample of the brine liquid was extracted from the reactors to look for any changes to the solute spectra and determine if any secondary minerals could be observed in suspension**.** Within each solution, the peak position for the polyatomic ion of the brine did not change, nor did the ratio of the ion peak area relative to the water peak change as time progressed. The spectra of each brine also did not show any indication of new peaks to suggest any secondary minerals in suspension. As no discernable difference could be seen in the spectra of the solutions, this thesis will not include further discussion of the brine Raman analyses.

Unreacted Samples

A polished control sample was analyzed using the electron microprobe for wavelength dispersive spectroscopy. Along with this data, backscatter imaging was taken at the same time to show crystal structure (fig.1) and for easier identification of targets for WDS analysis.

Raman Spectroscopy

Raman spectroscopy of a control sample shows three main minerals in the Craters of the Moon (COTM) Grassy Cone sample; pyroxene, plagioclase, and olivine. Olivine has a pair of intense peaks 819 and 850 wavenumbers (fig. 2). Plagioclase has a primary peak at 508 wavenumbers and a secondary peak at 483 (fig. 2). The unreacted sample from Craters of the Moon shares a minor peak with a plagioclase from the RRUFF™ database at 407 wavenumbers, but lacks the sharp, minor peaks in the range <400 wavenumbers. The Raman spectra of pyroxene from the unreacted sample has a primary peak between 680 and 679 wavenumbers (fig.

2). The spectra from the RRUFF™ database shows a narrower peak in this spectral range of 678 to 680, while the COTM sample exhibits a broader curve. Vandenabeele (2013) asserts the broadness in the spectra is due to natural impurities in the sample. SEM imaging of the control polished sample supports this claim as the pyroxene matrix shows exsolution throughout the sample (fig. 1) which would also influence the peak broadening observed in the pyroxene is likely due to variations in the chemistry.

Minor minerals in the basalt include ilmenite. Ilmenite is identified by XRD analysis, but no Raman spectra indicative of ilmenite were collected from the control samples; XRD analysis suggests that this mineral accounts for about 3.0% of the basalt by weight. Therefore, it is within reason that any ilmenite in the control samples are either too small to be resolved or no sample of ilmenite exists on the surface of the sample for Raman analysis.

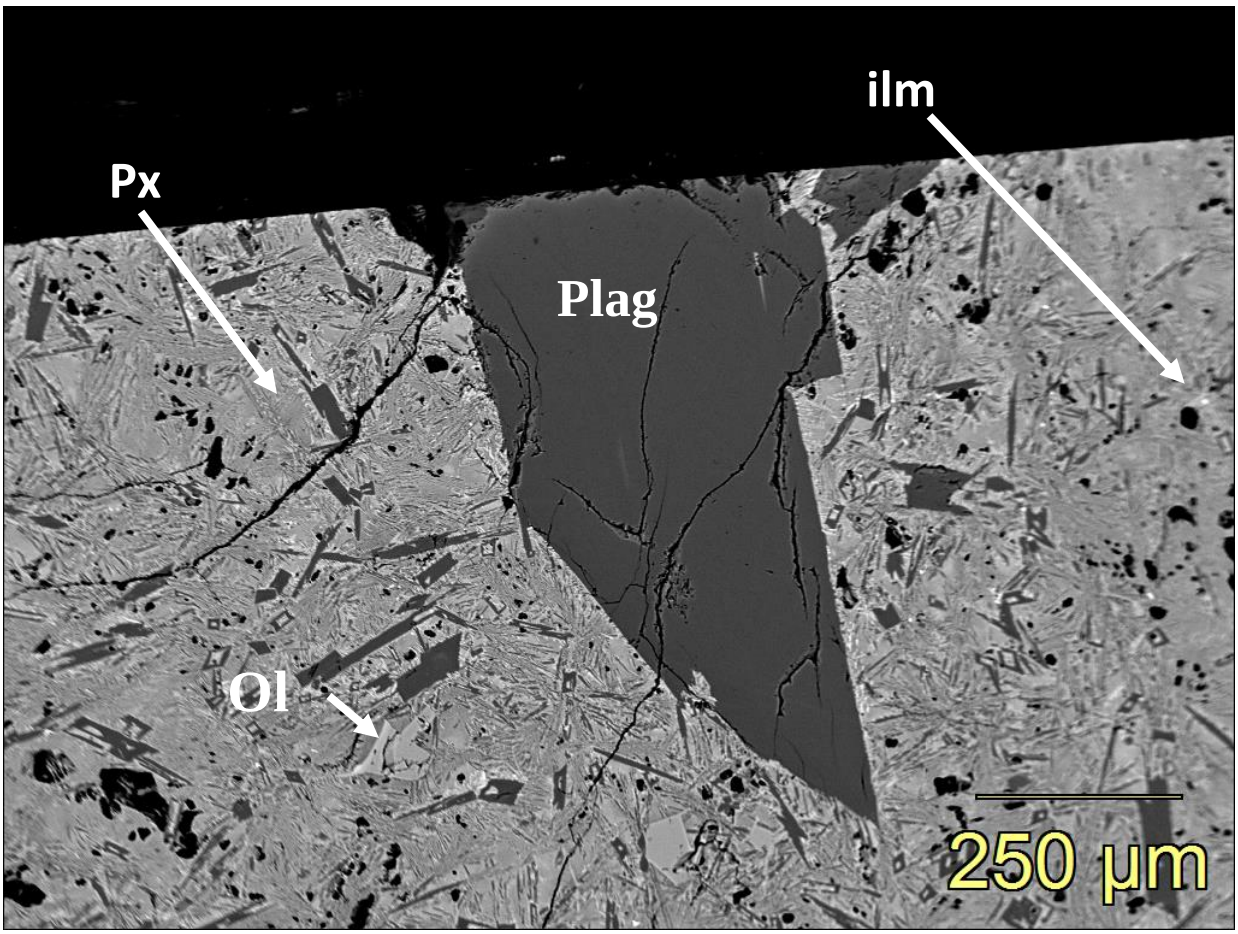

Figure 1. BSE image of a control sample of the Craters of the Moon basalt. A large plagioclase (Plag) crystal is center with many smaller plagioclase crystals throughout the basalt. Small olivine (Ol) crystals are of a light gray color and pyroxene (Px) makeup the rest of the matrix of the basalt. Tiny bright spots on the right side of the large plagioclase crystal is ilmenite (ilm). The pyroxene shows exsolution throughout the matrix and is particularly prevalent near the plagioclase crystals.

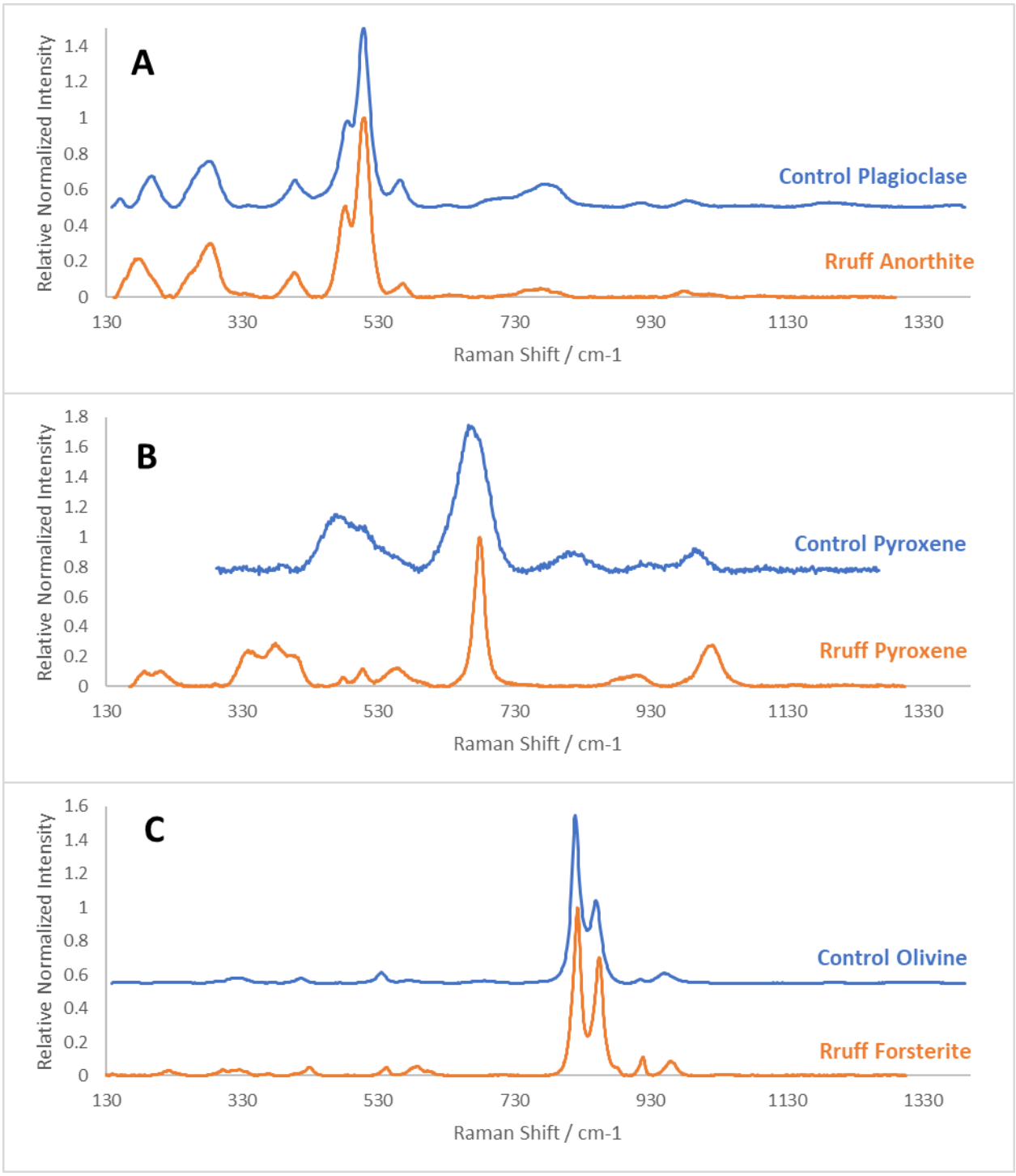

Figure 2. Raman spectra of plagioclase (A), pyroxene (B), and olivine (C) from a control sample of the Craters of the Moon Grassy Cone basalt as compared to spectra of anorthite, pyroxene, and forsterite from the online database www.rruff.info.

Table 1. Raman peak positions of the major and minor minerals in the Craters of the Moon sample. Values are in the units wavenumber (cm^{-1}) and are based on spectra produced by a 532nm green laser. Bold values denote a primary peak.

Mineral	Raman excitation position of primary and secondary peaks (λ/cm-1)						
Pyroxene				466	**679**		
Olivine				534		**819**	**850**
Plagioclas	196	278	407	**483**	**509**	562	
Ilmenite	240	325	445			**680**	
Augite	324	390			**665**		1008

We also employed WDS and EDS and to understand the bulk chemistry of our samples and as a comparison to previous bulk chemistry analyses (Adcock et al., 2018). For EDS analysis, a control sample that was polished but not used in the experiments was sputter coated with AuPd for SEM and analyzed using the Zeiss Neon SEM with the EDS detector to determine the bulk chemistry of the sample (Table 2).

Table 2. Statistical information of the control sample of the Craters of the Moon: Grassy Cone lava flow from EDS analysis. No Cl or S is shown as these elements are below the detection limit. Values are in weight %.

Mineral		O	Na	Mg	Al	Si	P	K	Ca	Ti	Mn	Fe
Forsterite	Mean	44.6025	0	20.7842	0	16.1825	0	0	0.0383	0	0.2517	18.2342
	Minimum	40.70	0	19.39	0	14.66	0	0	0	0	0.11	16.06
	Maximum	48.86	0	22.10	0	17.70	0	0	0.24	0	0.40	19.90
	Median	45.7600	0	20.1550	0	15.7250	0	0	0	0	0.2350	18.1800
	Variance	10.173	0	1.274	0	1.331	0	0	0.008	0	0.006	1.274
	Std. Deviation	3.18950	0	1.12886	0	1.15356	0	0	0.08963	0	0.07481	1.12859
	n	12	12	12	12	12	12	12	12	12	12	12
Mineral		O	Na	Mg	Al	Si	P	K	Ca	Ti	Mn	Fe
Labradorite	Mean	54.0258	2.5217	0.0092	14.3617	20.7200	0	0	7.9808	0	0	0.3817
	Minimum	51.48	0	0	13.42	18.79	0	0	7.34	0	0	0.26
	Maximum	57.49	3.20	0.11	15.00	21.82	0	0	8.32	0	0	0.48
	Median	53.7600	2.6900	0	14.4250	20.7000	0	0	8.0300	0	0	0.3750
	Variance	2.441	0.668	0.001	0.161	0.580	0	0	0.078	0	0	0.004
	Std. Deviation	1.56244	0.81704	0.03175	0.40154	0.76190	0	0	0.27891	0	0	0.06013
	n	12	12	12	12	12	12	12	12	12	12	12
Mineral		O	Na	Mg	Al	Si	P	K	Ca	Ti	Mn	Fe
Pyroxene	Mean	55.4325	0.7125	1.4667	3.2433	17.9592	0.0492	1.0617	8.4208	2.0192	0.0250	9.6067
	Minimum	53.82	0	0.94	2.76	16.96	0	0.74	5.95	1.50	0.00	8.33
	Maximum	57.55	1.04	1.86	4.00	18.94	0.30	1.41	9.75	3.42	0.30	12.35
	Median	55.3400	0.7700	1.5250	3.1350	17.8750	0	1.1150	8.8000	1.9100	0	9.3450
	Variance	1.360	0.077	0.106	0.151	0.402	0.013	0.056	1.234	0.319	0.008	1.055
	Std. Deviation	1.16640	0.27838	0.32575	0.38904	0.63404	0.11485	0.23648	1.11101	0.56518	0.08660	1.02700
	n	12	12	12	12	12	12	12	12	12	12	12

Mineral		O	Na	Mg	Al	Si	P	K	Ca	Ti	Mn	Fe
Total	Mean	51.3536	1.0781	7.4200	5.8683	18.2872	0.0164	0.3539	5.4800	0.6731	0.0922	9.4075
	Minimum	40.70	0	0	0	14.66	0	0	0	0	0	0.26
	Maximum	57.55	3.20	22.10	15.00	21.82	0.30	1.41	9.75	3.42	0.40	19.90
	Median	53.7450	0.7500	1.5250	3.1350	17.8750	0	0	7.8250	0	0	9.3450
	Variance	28.171	1.393	92.650	39.000	4.312	0.005	0.275	15.677	1.032	0.017	55.390
	Std. Deviation	5.30765	1.18024	9.62550	6.24503	2.07651	0.06854	0.52460	3.95942	1.01601	0.13152	7.44242
	n	36	36	36	36	36	36	36	36	36	36	36

XRD Analysis

XRD analysis (fig. 3) of a micronized sample of our Craters of the Moon sample suggests the rock is composited of mostly a plagioclase that closely fits with labradorite (54.3 wt. %), followed by forsterite (27.5%) as the second most common mineral. An iron bearing pyroxene similar to hendengbergite-ferroan makes up 13.4% of the sample. All three of these minerals were also observed in the Raman spectra collected from each sample. While ilmenite (3.0%) and quartz (1.3%) were also indicated in the XRD analysis, they were not consistently observed in the Raman analyses. Of the two minor minerals, ilmenite has the potential to be most impactful as it is the only other source of titanium whereas silicon and oxygen are prevalent in all three of the main minerals.

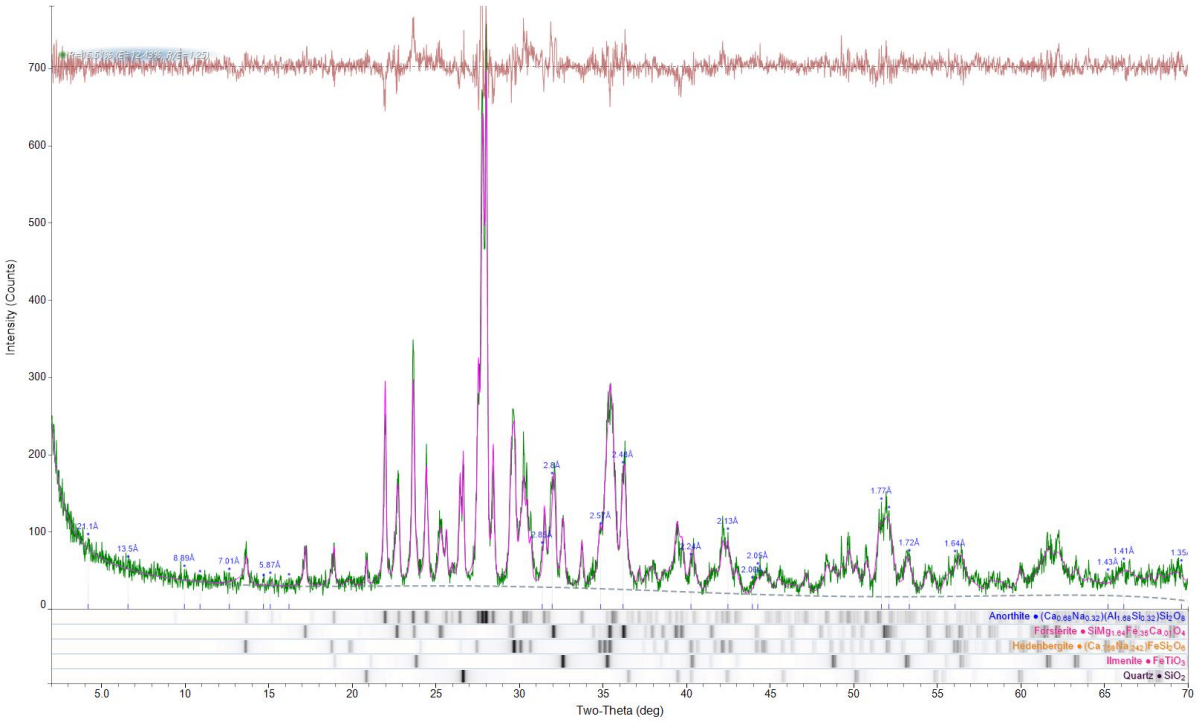

Figure 3. Whole-pattern XRD fitting of a sample from the Craters of the Moon Grassy Cone lava event. Analysis shows this basalt is a majority plagioclase with olivine and a pyroxene making up the bulk of the remainder. Less than 5% of the basalt is quartz and ilmenite. ICDD PDF 4+, Jade Pro software.

Table 3. XRD analysis of a sample from the Craters of the Moon Grassy Cone lava flow showing the primary minerals, the best fit chemical formula of the mineral and their respective PDF file number. Weight percent is given with the estimated percent error.

Phase ID	Chemical Formula	PDF-#	Wt%(esd)
Anorthite (PO)	$(Ca_{0.68}Na_{0.32})(Al_{1.68}Si_{0.32})Si_2O_8$	01-089-1469	55.9(1.1)
Forsterite (PO)	$SiMg_{1.64}Fe_{0.35}Ca_{0.01}O_4$	98-000-1373	26.3(0.8)
Hedenbergite (PO)	$(Ca_{0.758}Na_{0.242})FeSi_2O_6$	98-000-5223	12.6(0.5)
Ilmenite	$FeTiO_3$	98-000-0255	3.2(0.3)
Quartz	SiO_2	98-000-0369	1.9(0.2)

Month 1

After one month of reaction, no evidence was found to suggest any change in the Raman spectra observed from the primary minerals. The peak position and shape of the spectra of the five primary minerals- pyroxene, olivine, ilmenite, quartz, and plagioclase- did not appear to shift or alter from the control samples. The most notable difference in the spectra collected was the inclusion of secondary iron oxide minerals within the spectra collected from the primary minerals and the identification of a sulfate mineral and a carbonate mineral in $NaClO_4$ and $NaClO_4$+Na_2SO_4 brines.

Of the spectra that showed the highest degree of alteration, pyroxene had the most noise in the spectra as well as additional peaks consistent with iron oxides. Hematite was identified within one spectra of pyroxene in the ultra-pure water reactor, but the other spectra indicative of hematite and magnetite observed in $MgSO_4$ and the Na_2SO_4 brines did not contain peaks associated with the primary minerals. Lepidocrocite, or another iron oxide with a hydrogen bond, appeared alongside pyroxene in the $MgCl_2$+$MgSO_4$ solution (Fig. 4). Spectra consistent with hematite and magnetite were observed in association with quartz in the ultra-pure water experiment (Fig. 5). This spectra also includes a broad peak at 1310. A study by Bridges et al. (2010) suggests that this peak is likely associated with hematite and magnetite. J. Dunnwald et al. (1989) also report a hematite band at ~1320, but the hematite spectra from the RRUFF™ Project do not extend past 1301 wavenumbers.

Spectra consistent with macfallite ($Ca_2Mn^{3+}{}_3(SiO_4)(Si_2O_7)(OH)_3$) were observed in the $MgCl_2$+$MgSO_4$ experiment (Fig. 6). The mixed Na_2SO_4 and $NaClO_4$ experiment also produced a

spectrum consistent with thenardite (Na_2SO_4) (fig. 7). One chip in from the $NaClO_4$ brine experiment produced a spectrum with a sharp peak at 1084, alluding to the formation of calcite.

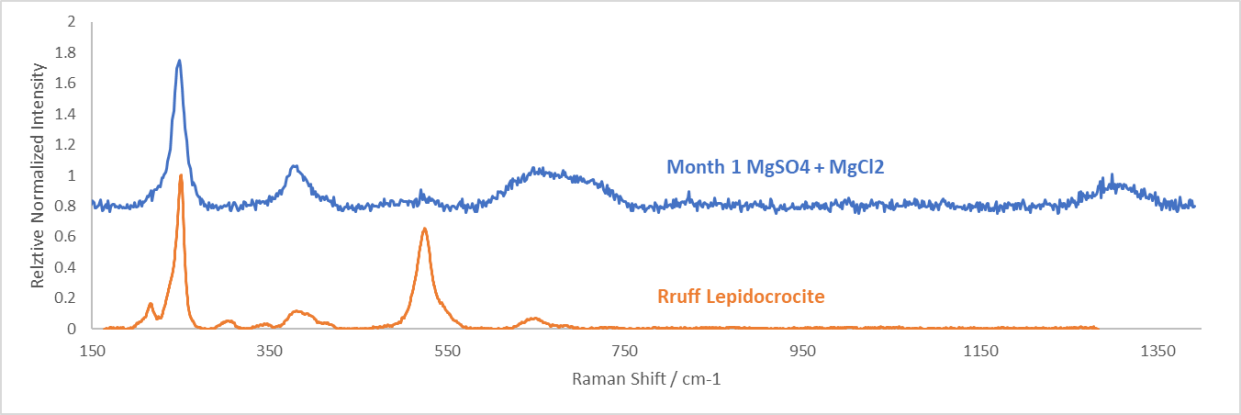

Figure 4. A spectra from a Craters of the Moon sample that reacted in a mixed brine of $MgSO_4$ and $MgCl_2$ as compared to a spectra of lepidocrocite from the online database www.rruff.info. The peak near 200 from the reacted sample is a good fit for lepidocrocite but the secondary peak near 500 is a good fit by position but not in intensity.

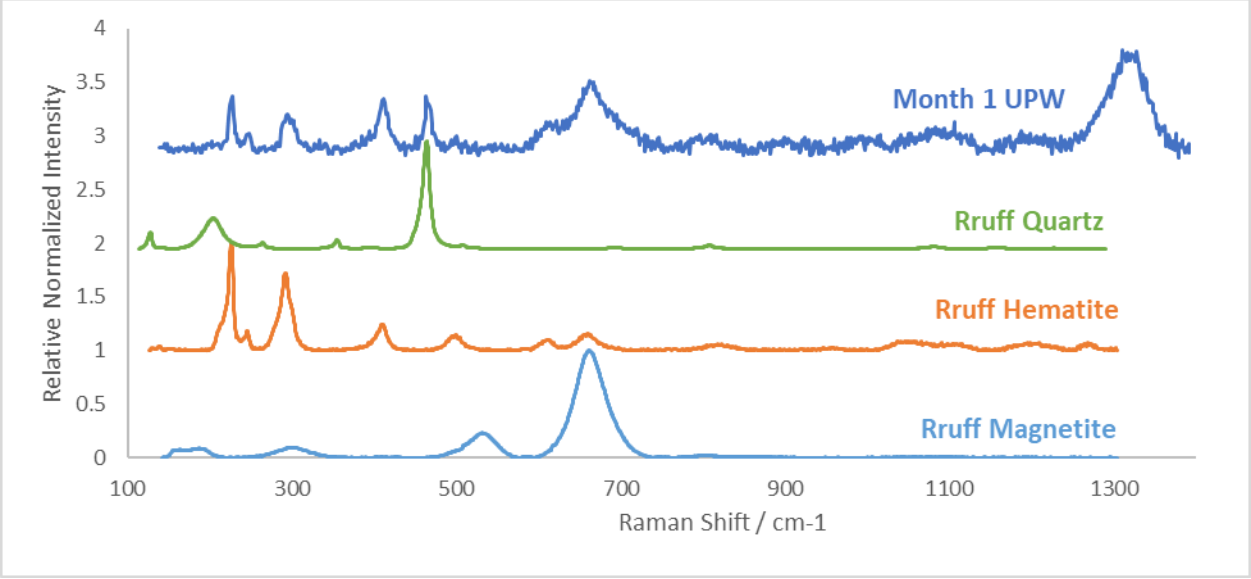

Figure 5. Spectra of a Craters of the Moon Basalt after reacting with Ultra-Pure water as compared to Quartz, Hematite, and Magnetite from www.Rruff.info database.

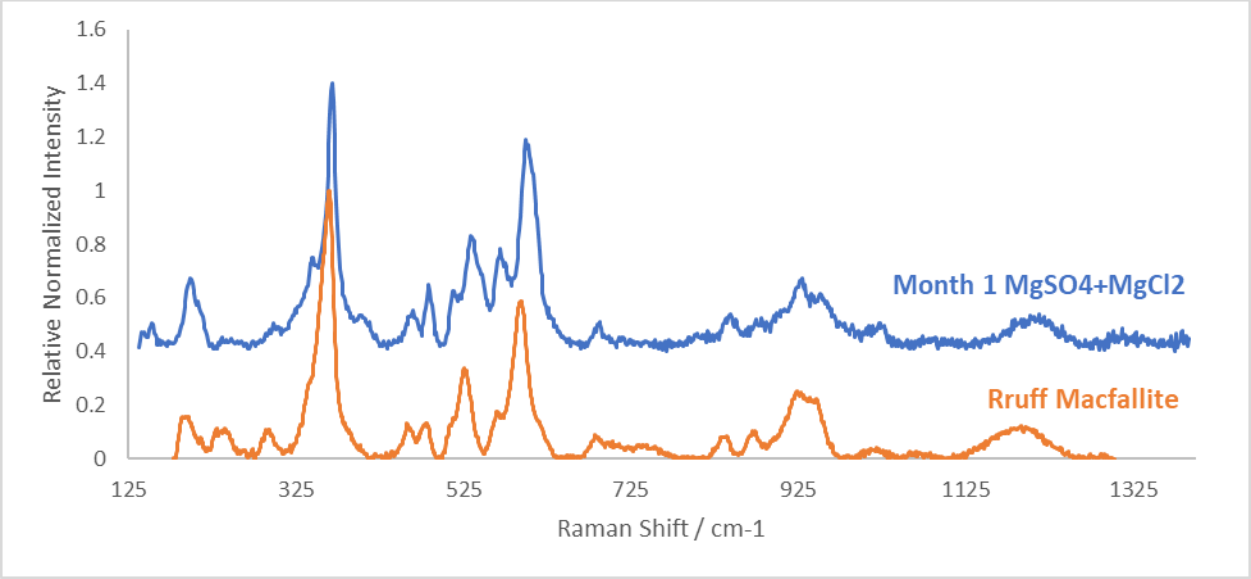

Figure 6. Raman Spectra of a Craters of the Moon Basalt Chip after reacting with $MgCl_2$ and $MgSO_4$ for 30 days (top) compared to a spectrum of Macfallite from www.Rruff.info database.

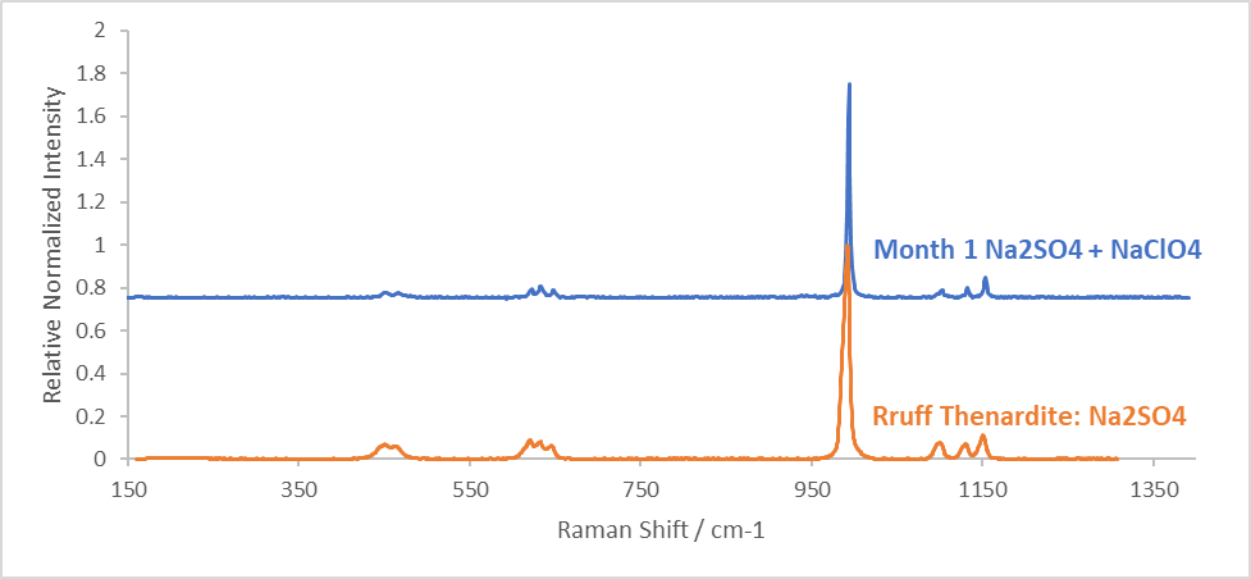

Figure 7. Raman spectra of a Craters of the Moon basalt after reacting in Na_2SO_4 and $NaClO_4$ for 30 days as compared to spectra from www.Rruff.info database of Thenardite ($Na_2(SO_4)$) (bottom).

Month 3

Observations of spectra indicative of iron oxides increased in this group of samples compared to the one month experiments. Five of the solutions ($NaClO_4$, $NaClO_4$+Na_2SO_4, $MgCl_2$, $MgSO_{4+,}$ and $MgSO_4$+$MgCl_2$) produced spectra consistent with hematite on the surface of the basalt chips. More carbonates and sulfates also appeared in these samples compared to the month one analyses.

The basalt chips reacted in $NaClO_4$ produced spectra consistent with lepidocrocite and goethite (fig. 8). An iron oxide spectrum was also observed on a basalt chip after reacting in the mixed $MgCl_2$ and $MgSO_4$ brine. This spectrum is unique in that it contains the peak positions of both hematite and quartz, suggesting the deposition of the hematite onto the quartz crystal original to the basalt (Fig. 9). Spectra consistent with hematite were observed on the basalt chips reacted in the $NaClO_4$ + Na_2SO_4 mixed brine. Chips reacted with $NaClO_4$ brine also produced spectra consistent with hematite, with an additional peak associated with hydroxylapatite (fig. 10).

Two spectra consistent with thenardite were observed in association plagioclase after reaction with Na_2SO_4 brine (Fig. 11). Spectra consistent with epsomite, or another hydrated

sulfate mineral, were observed from chips that reacted in $MgSO_4$ (fig. 12). Spectra consistent with gypsum were observed on the basalt chips reacted with $CaCl_2$ brine (Fig. 13).

Spectra indicative of calcite, aragonite, or rhodochrosite were observed in the samples that reacted with NaCl brine (Fig. 14). Basalt reacting in $MgSO_4$ and $MgCl_2$ solutions produced spectra that also fit with a carbonate phase (fig. 15).

Finally, the Raman spectra collected from the basalt chips reacted with ultra-pure water show no change in peak position or width of the peaks associated with the three main primary minerals compared to the control samples. However, an additional band at 1002 wavenumbers is consistent with amorphous silica (fig. 16). The best spectra that fits the peak is opal.

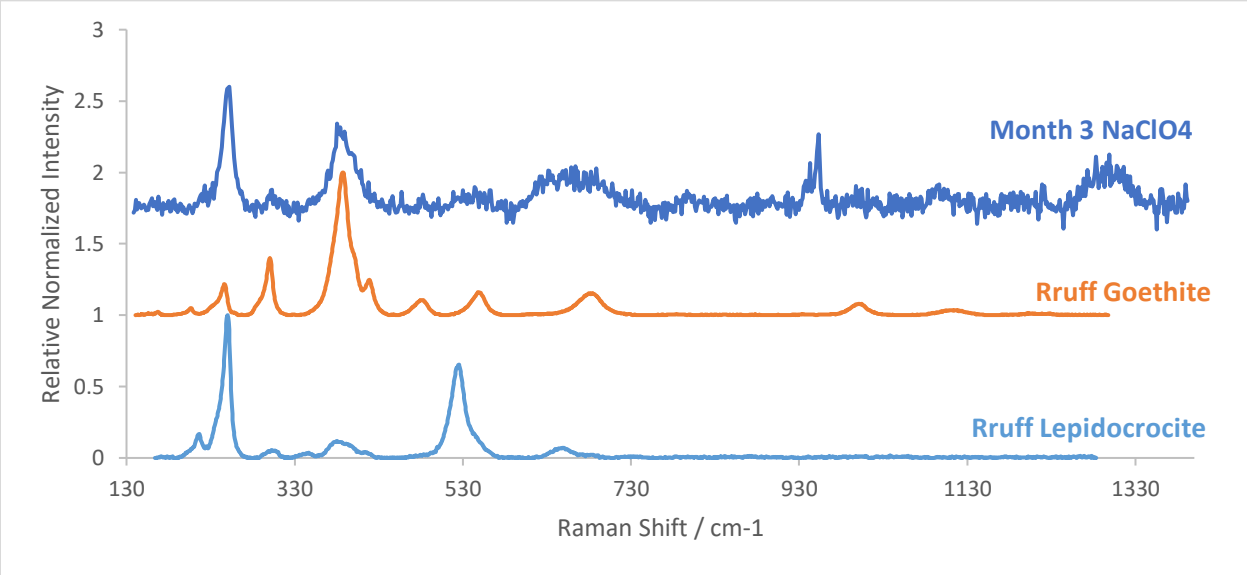

Figure 8. Raman spectra of a Craters of the Moon chip after reacting in $NaClO_4$ after 90 days (Top) as compared to www.rruff.info database spectra of goethite (middle) and lepidocrocite (bottom).

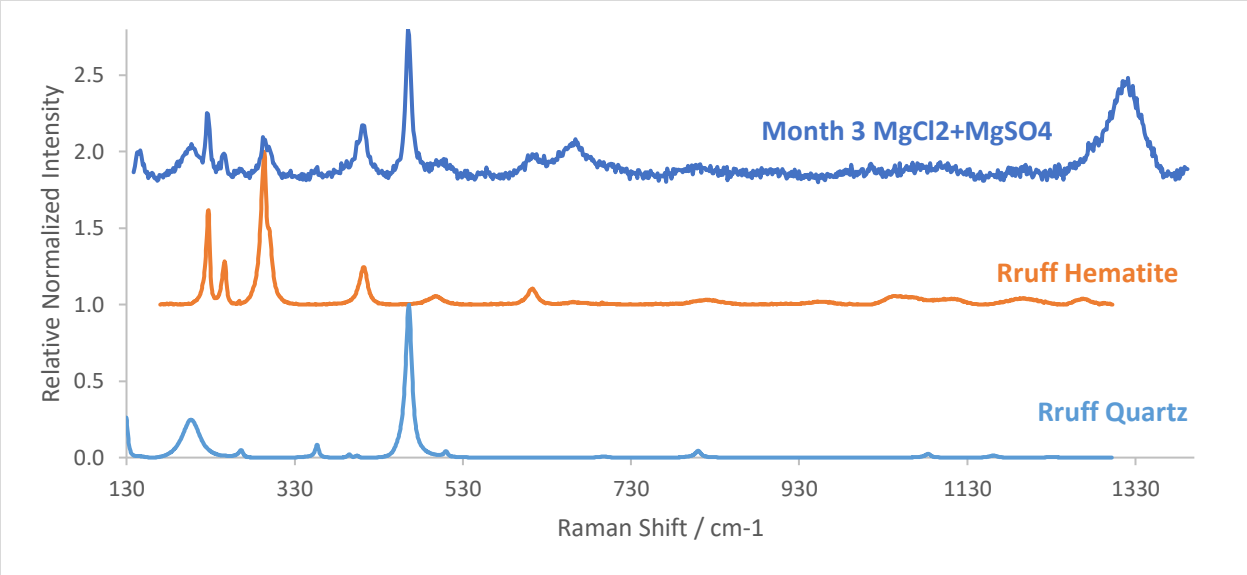

Figure 9. Raman spectra of a Craters of the Moon chip after reacting in $MgCl_2$ and $MgSO_4$ for 90 days as compared to the spectra of Hematite and Quartz from the online database at www.rruff.info.

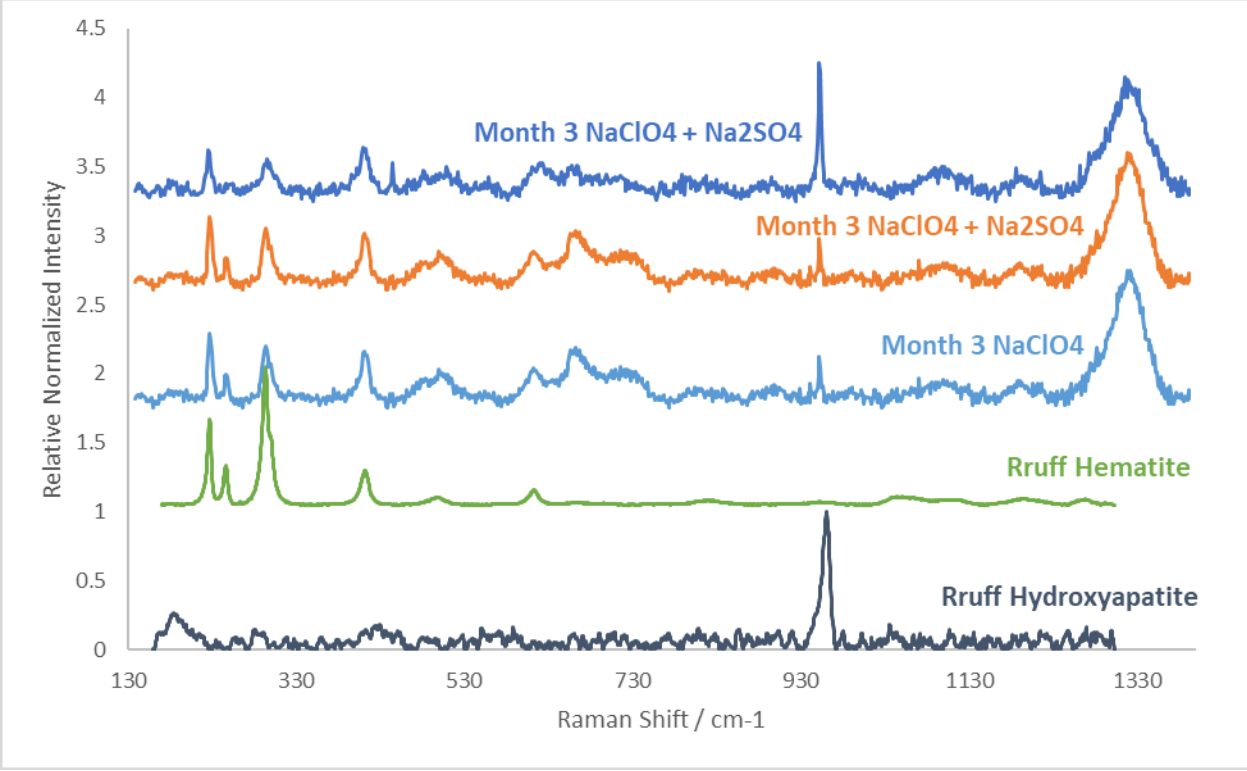

Figure 10. Raman Spectra of Crater of the Moon samples after 90 days reacting in a mixed brine of $NaClO_4$ and Na_2SO_4 and a brine of $NaClO_4$, as compared to the www.rruff.info database of Hematite and Hydroxylapatite. The broad peak near 1330 is a peak for hematite and magnetite supported by work from the study by Das et al. (2011).

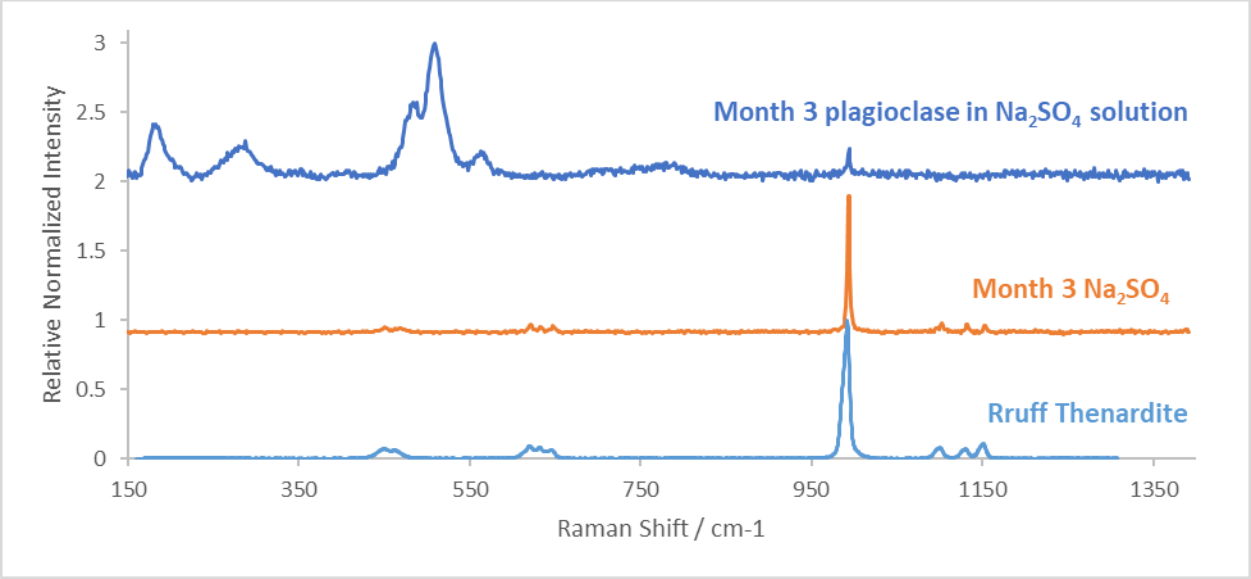

Figure 11. Raman spectra of plagioclase from a Craters of the Moon sample reacting in Na_2SO_4 for 90 days including a thenardite peak at 984, spectra from a Craters of the Moon sample that reacted with Na_2SO_4 for 90 days, and a spectra of thenardite from www.rruff.info database.

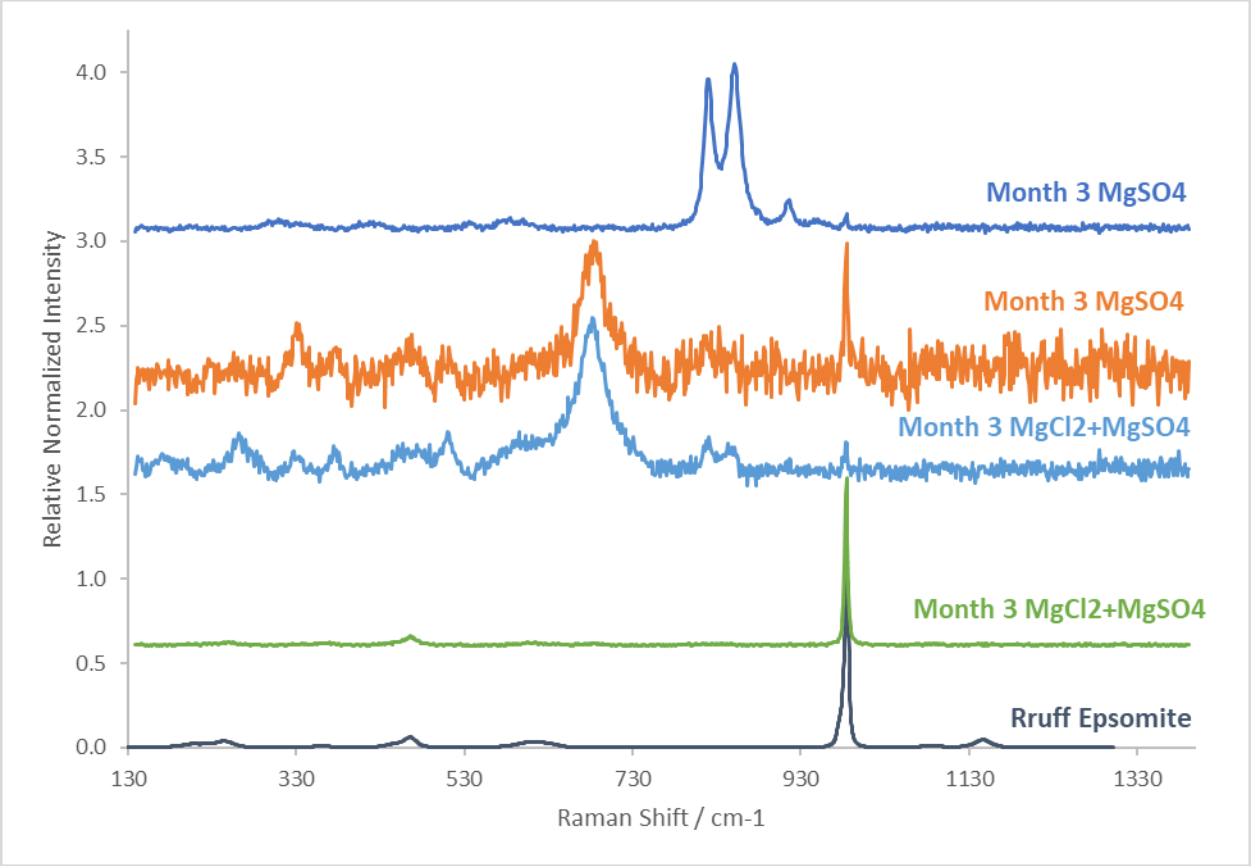

Figure 12. Spectra of COTM ships reacting in Mg cation solutions for 3 months as compared to epsomite (MgSO4·7H2O) from the online database www.rruff.info.

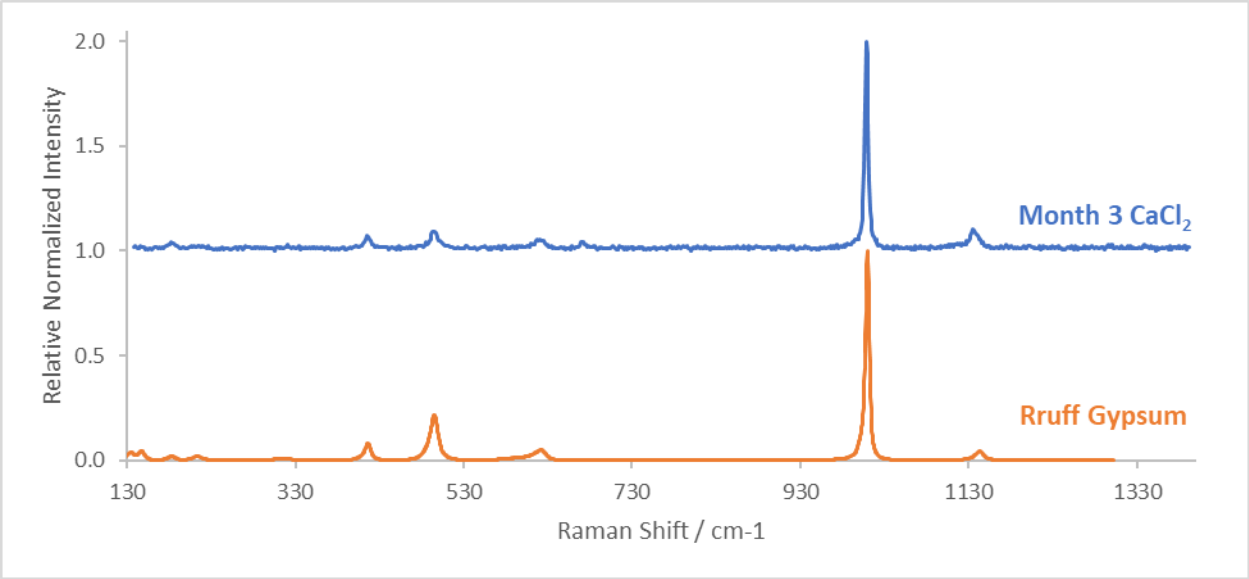

Figure 13. Raman spectra of a Craters of the Moon chip after reacting in $CaCl_2$ for 90 days as compared to a spectra of Gypsum from the online database www.rruff.info.

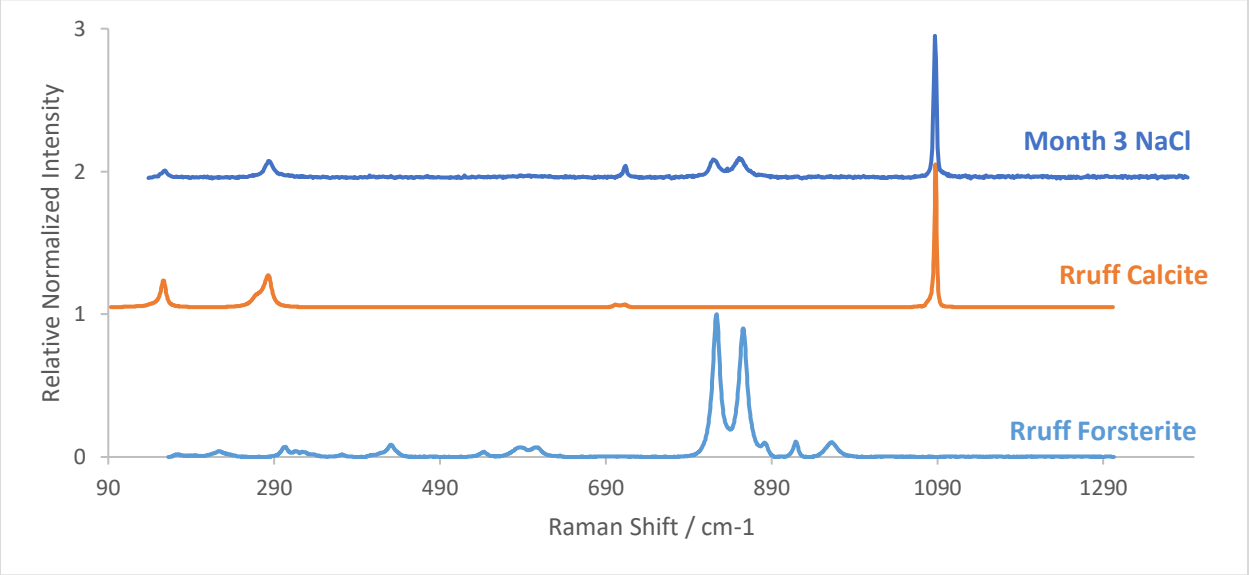

Figure 14. Raman spectra of a Craters of the Moon chip after reacting in NaCl for 90 days (A) as compared to calcite (B) and forsterite (C) from the online database www.rruff.info.

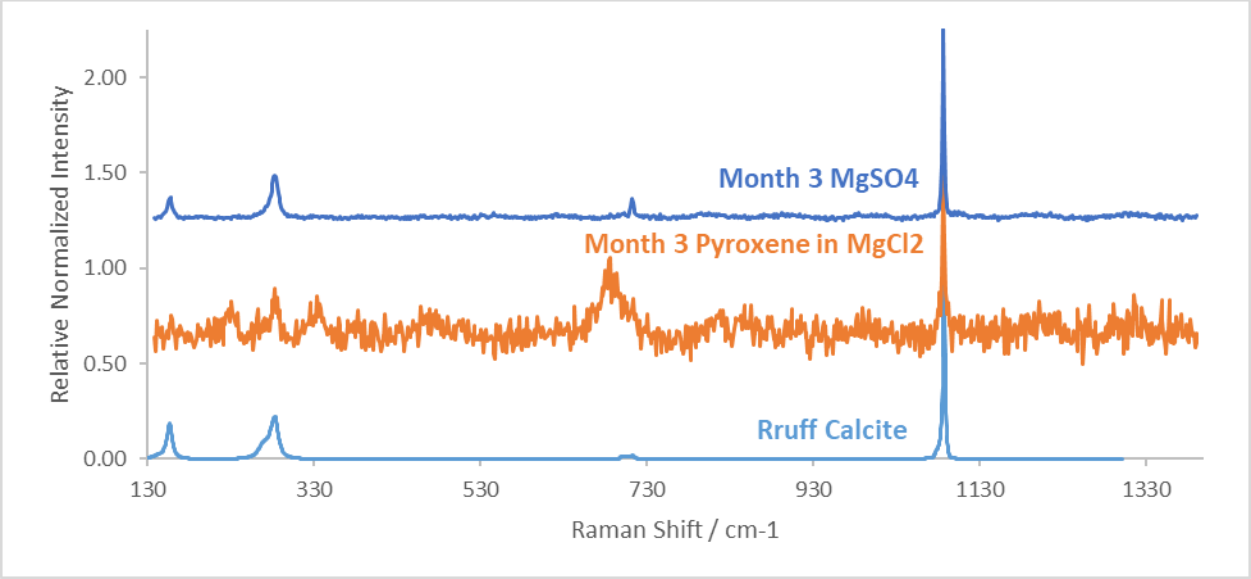

Figure 15. Raman spectra of a Craters of the Moon sample after reacting in $MgSO_4$ (A) and $MgCl_2$ (B) for 90 days as compared to calcite (C) from www.rruff.info database.

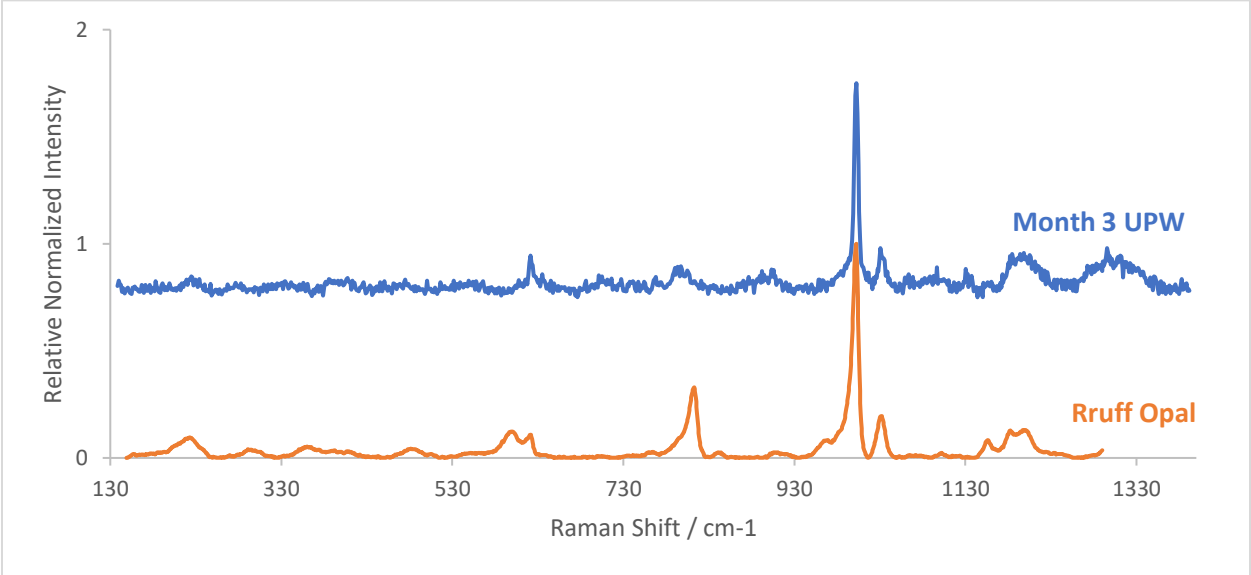

Figure 16. Raman spectra of a Craters of the Moon chip after reacting in ultra-pure water after 90 days (A) as compared to the spectra of opal (B) from the online database www.rruff.info.

Month 6

The spectra of the primary minerals continue to remain unchanged in the peak position for pyroxene, olivine, plagioclase, and ilmenite. No quartz was observed on these basalt chips. Iron oxides, sulfates, and carbonates were the secondary minerals observed in these samples. Overall, identifying specific minerals from the spectra became more difficult after 6 months of reaction, as the spectra include more hydrated states, hydroxyl groups, and wider peaks.

Samples that reacted with $NaClO_4$ show a trend of expanding the width of the peak often observed near 680 (Fig. 18), which could fit multiple hydrated iron oxide samples but could be a best fit for trevorite ($Ni^{2+}Fe^{3+}{}_2O_4$) (fig. 19). This trend of a wide peak near 700 wavenumbers is also common among minerals with three oxygens bonding to a single metallic element such as the examples in figure 17. Samples reacting in ultra-pure water continue to show formation of secondary iron oxides (fig. 19&20)

The chips reacting with Na_2SO_4 also show a widening of the peak at 700, but also exhibit spectra that suggest more diversification in the secondary minerals created. Among the secondary minerals present are hematite, epsomite hexahydrate, and possibly a hydrated iron oxide. However, positive identification is difficult as many minerals have a peak near 675 to 710 which could be due to a wide range of secondary minerals and hydrated states. One spectra is consistent with magnetite, however additional peaks in the spectra are not easily identifiable as the program *CrystalSleuth* encounters problems in finding a mineral file to match the peaks near

813, 918, and 1003 (fig. 21). Kidwellite ($NaFe^{3+}_{9+x}(PO_4)_6(OH)_{11} \cdot 3H_2O$, x = 0.33) is a close match to the peak near 1003 but produced no other matches to the smaller secondary peaks.

Basalt chips reacted in brines for 6 months produced spectra indicative of a wide range of hydrated sulfate minerals. Basalt chips reacted with magnesium-bearing brines produced peaks similar in characteristics with sodium-bearing brines. However, *Crystalsleuth* shows a higher match percentage with pentahydrite ($Mg(SO_4)\cdot 5H_2O$) in magnesium sulfate and magnesium chloride brines (fig. 22), whereas the program shows a higher percent match with hexahydrite ($Mg(SO_4)\cdot 6H_2O$) in sodium perchlorate and sodium sulfate experiments. The difference of these two hydrated forms of $MgSO_4$ is 13 wavenumbers, 984 for hexahydrite and 997 for pentahydrite. Pentahydrite was also produced in a large enough area to be observed without any primary minerals in the spectrum, providing enough clarity to clearly identify the peak position (Fig. 23). Similar to the other secondary minerals, the pentahydrite peak often appears in spectra that also contain peaks for plagioclase and olivine.

Samples reacted in NaCl brine also produced spectra that are less clear than previous samples. Of the spectra collected, one sample that showed a clear deviation from the primary minerals and is consistent with trona (Fig. 24), a hydrated sodium carbonate.

The samples reacted in $CaCl_2$ brine produce spectra are less clear than the other samples, yet there are some peaks within the 1000 wavenumber range that might allude to a hydrated mineral. While *Crystalsleuth* suggests a better fit for kidwellite ($NaFe^{3+}_{9+x}(PO_4)_6(OH)_{11}\cdot 3H_2O$, x = 0.33) due to the width of the peak, however, the mineral starkeyite ($Mg(SO_4)\cdot 4H_2O$) is an 85% match to the spectra taken with the peak position in the same location (Fig. 21).

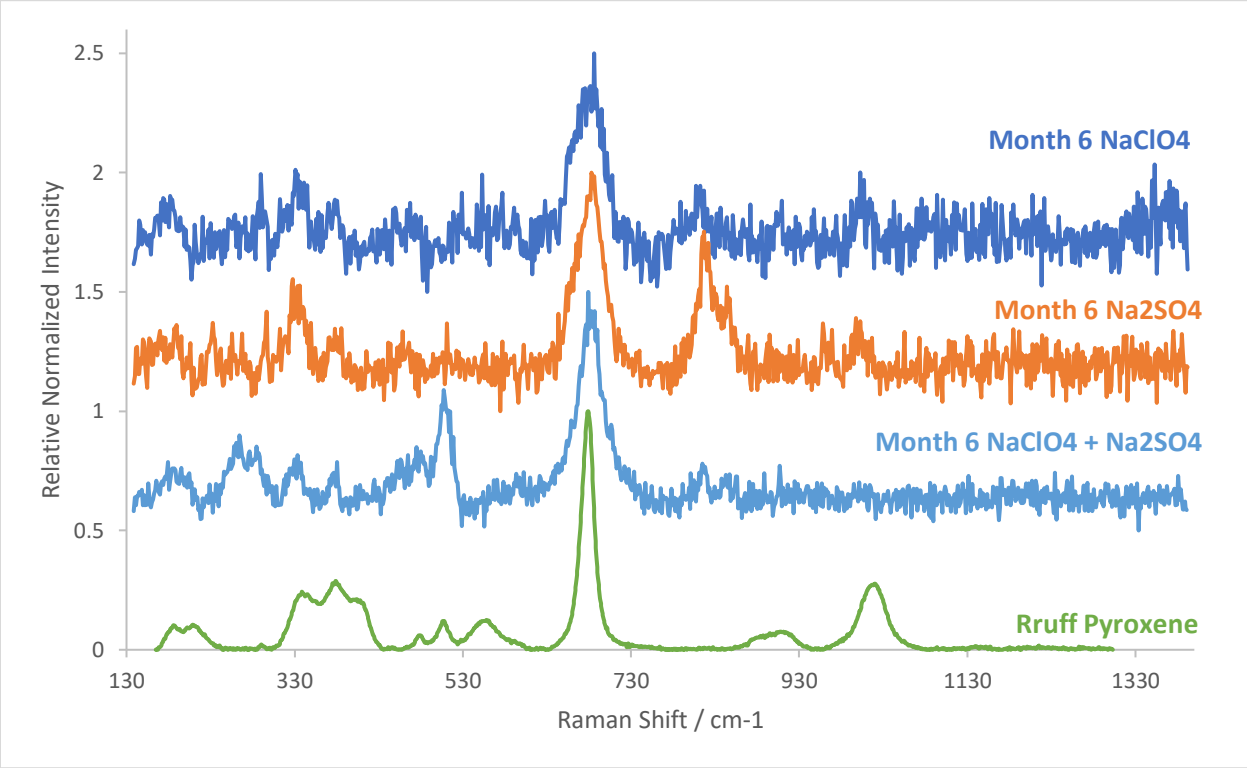

Figure 17. Raman spectra of Craters of the Moon chips after reacting for 6 months in $NaClO_4$ (A), Na_2SO_4 (B), and a mixed solution of $NaClO_4$ and Na_2SO_4 (C) as compared to pyroxene from the database www.rruff.info. Each spectra shows widening of the 680 peak.

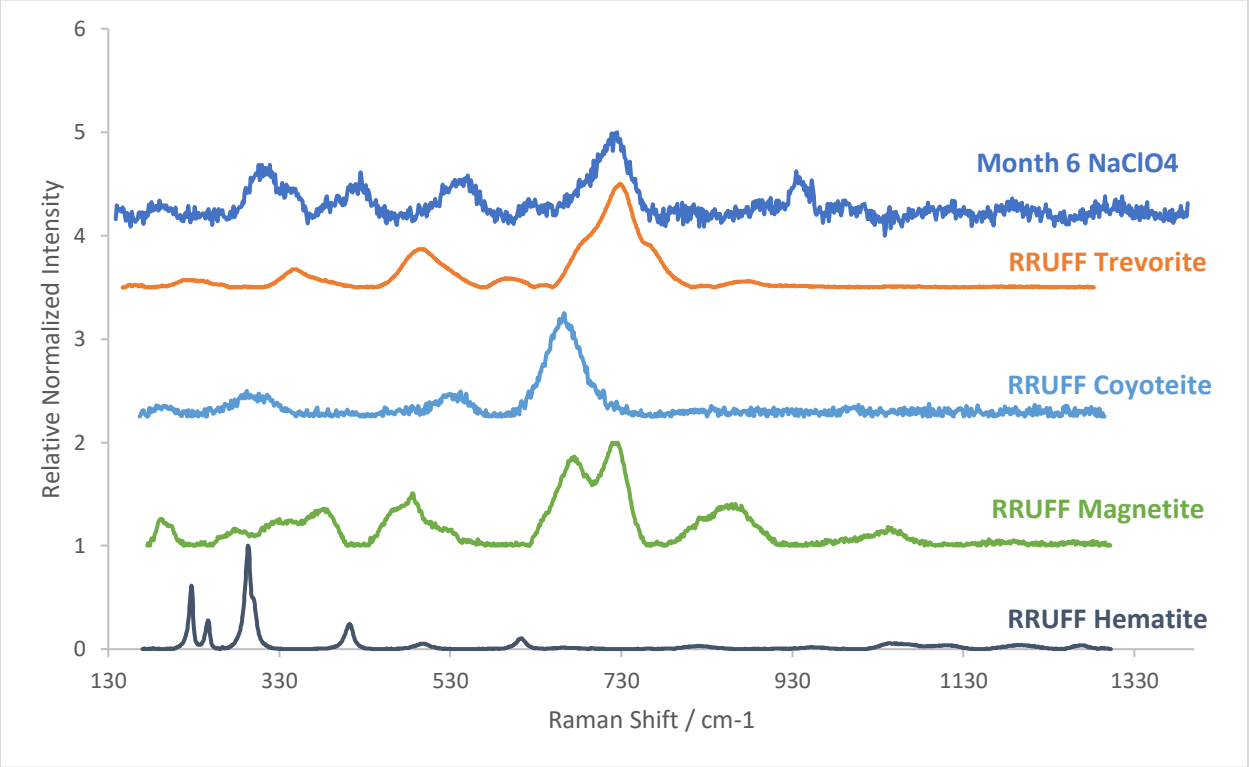

Figure 18*. Raman spectra of a Craters of the Moon sample after reacting in $NaClO_4$ for 6 months as compared to trevorite and other iron oxides from the online database www.rruff.info. The primary peak position and shape fail to fit any iron oxide with a high degree of confidence, but the iron oxide trevorite ($Ni_2Fe_2O_3$) fit best although no nickel was confirmed to exist in the basalt. Magnetite is another candidate.*

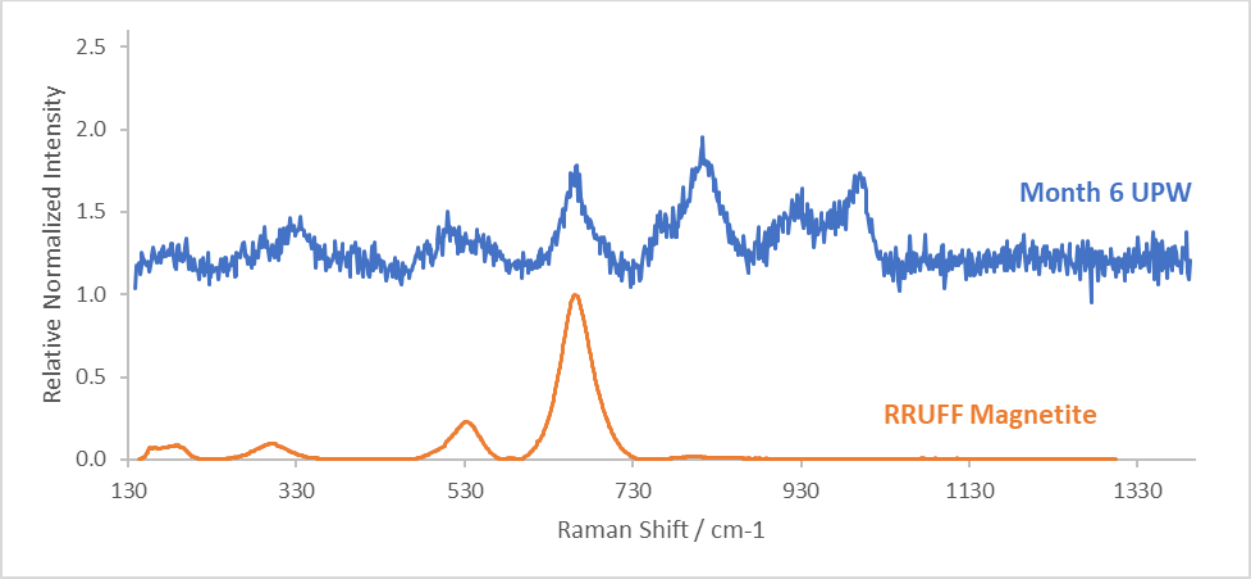

Figure 19. Raman spectra of a sample of the Craters of the Moon basalt after reacting in ultra-pure water for 6 months compared to a spectra of magnetite from the online database www.rruff.info. The peaks at 918 and 1003 are unidentified.

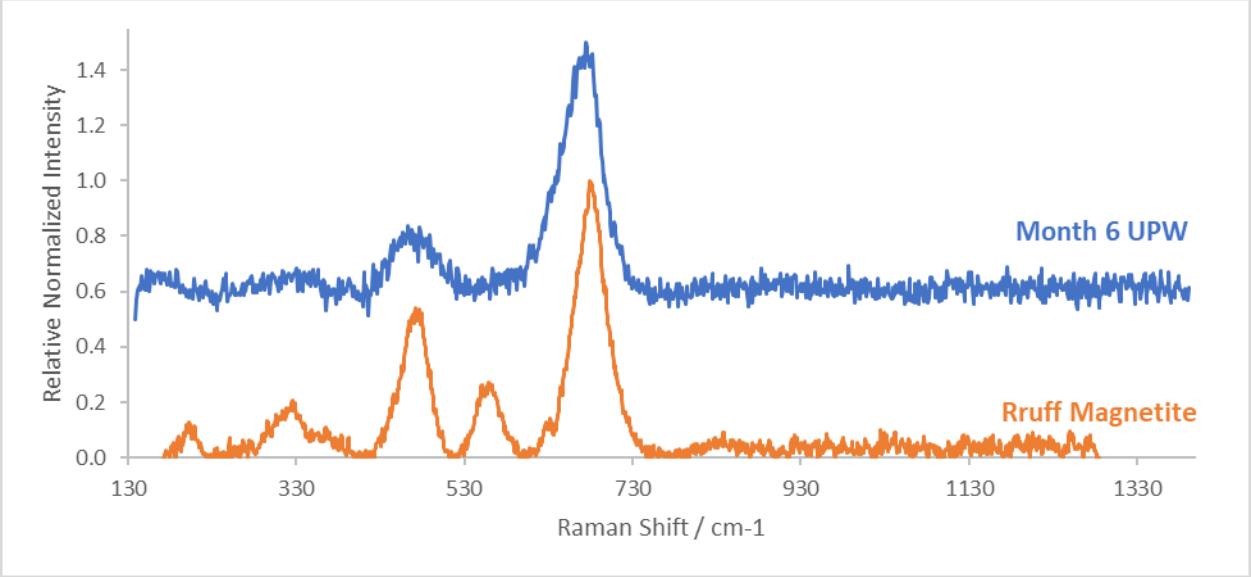

Figure 20. Raman spectra of a Craters of the Moon sample after reacting in ultra-pure water for 6 months (top) as compared to magnetite (bottom) from the online database www.rruff.info.

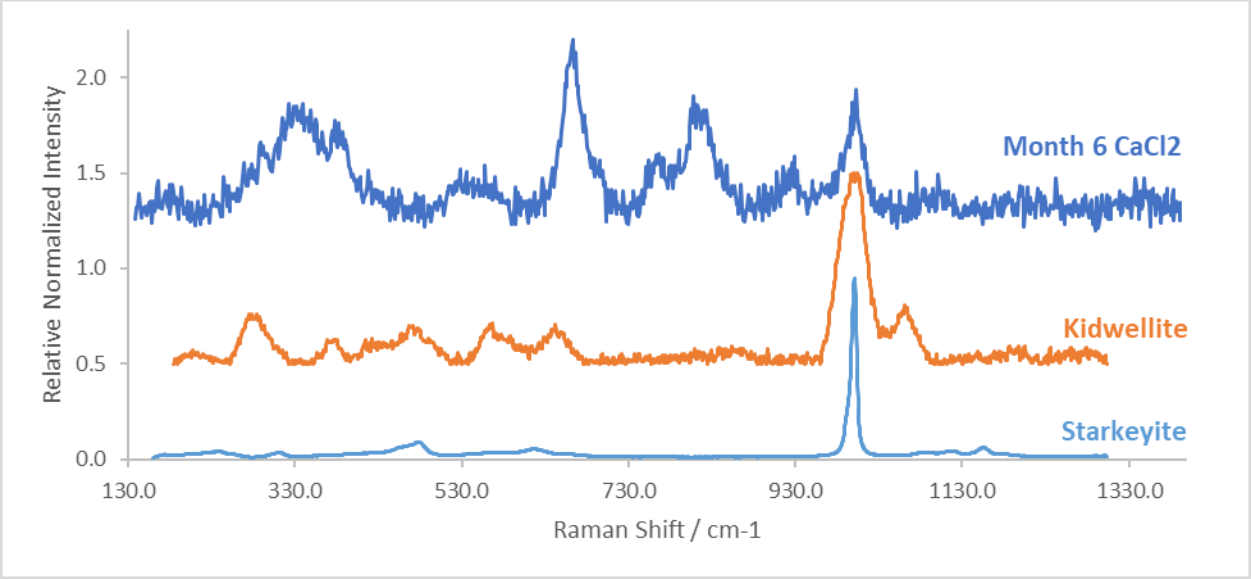

Figure 21. Raman spectra of a Craters of the Moon sample after reacting in $CaCl_2$ for six months as compared to the spectra of kidwellite and Starkeyite from the online database www.rruff.info.

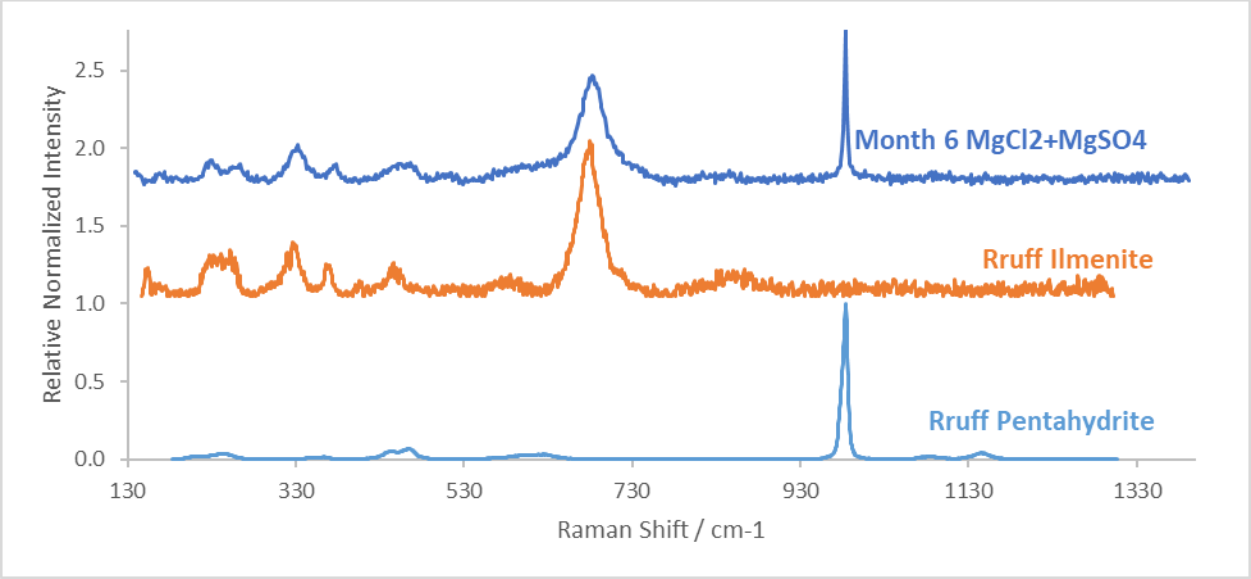

Figure 22. Raman Spectra of a Craters of the Moon sample after reacting in a mix solution of $MgCl_2$ and $MgSO_4$ as compared to ilmenite and pentahydrite from the online database www.rruff.info.

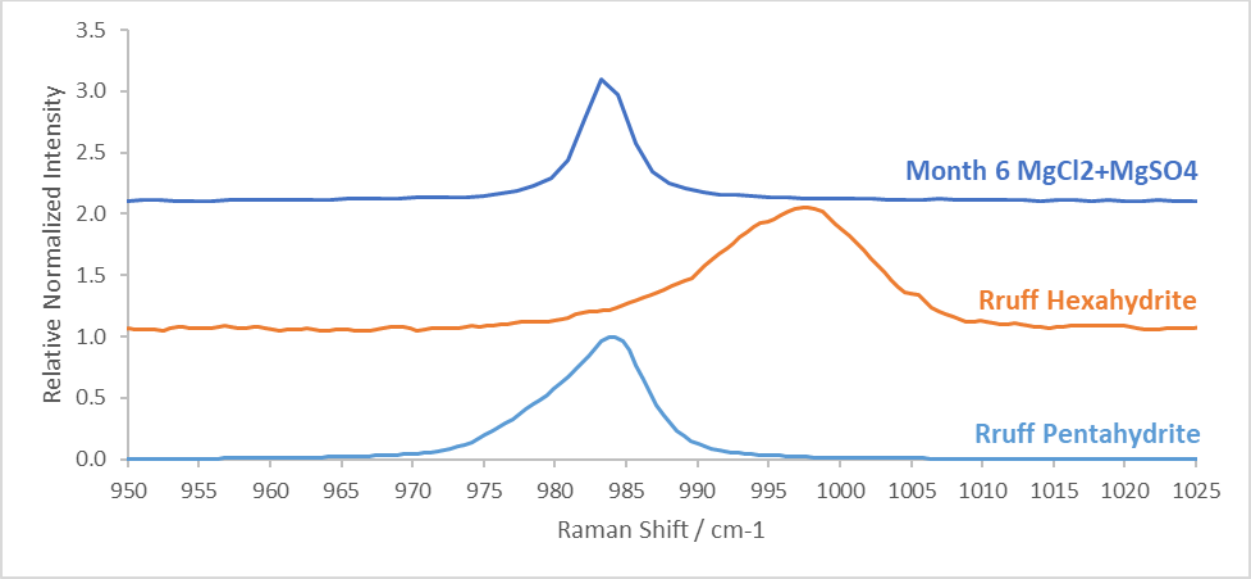

Figure 23. a close up of the Raman spectra of a Craters of the Moon sample after reacting in a mix solution of $MgCl_2$ and $MgSO_4$ as compared to the spectra of pentahydrite and hexahydrite from the online database www.rruff.info. The peak position of the reacted sample shows a better match for pentahydrite than hexahydrite.

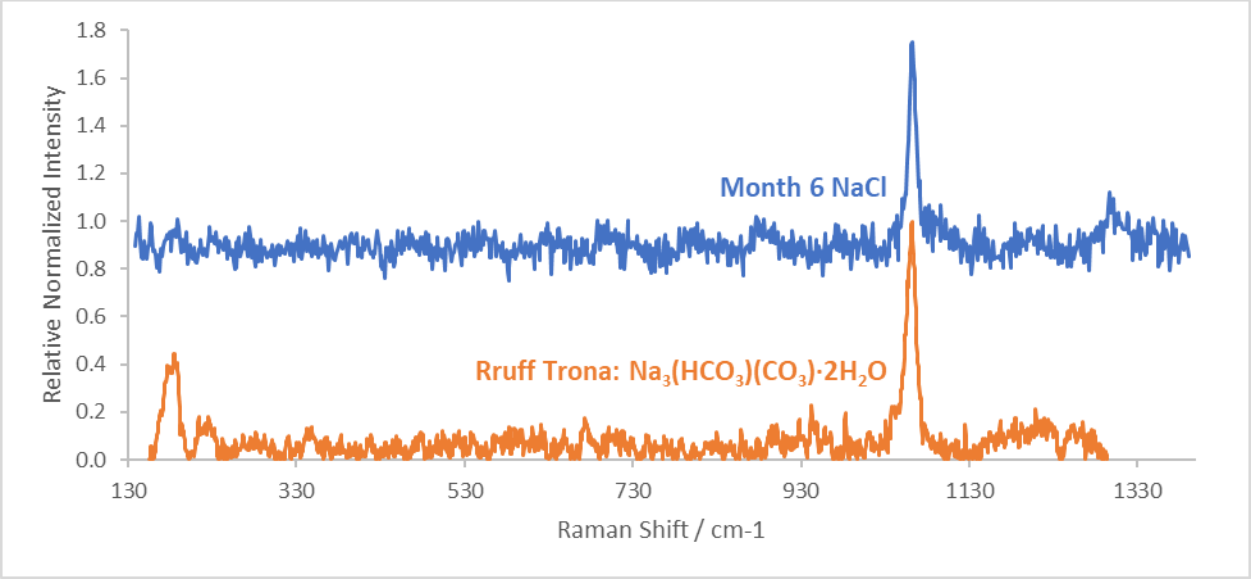

Figure 24. Raman spectra of a Craters of the Moon sample after reacting in a solution of NaCl after 6 months (top) as compared to the spectra of Trona ($Na_3(HCO_3)(CO_3)\cdot 2H_2O$) from the online database www.rruff.info.

Month 12

During the final collection period, no changes were observed with four of the primary minerals, pyroxene, olivine, plagioclase, and ilmenite. Despite collecting 192 spectra, no sample of quartz was observed. Olivine showed the least change while pyroxene had the most noise on average in the spectra. Iron oxides, sulfate, and carbonates were observed as secondary minerals.

Samples reacting in sodium-bearing brines exhibit hydrated states of iron oxides during this reaction period as well as iron oxides that have already been observed (fig. 25). Spectra of hematite and magnetite appear in chips after reacting in sulfate solutions, $CaCl_2$, and ultra-pure water solutions.

Samples reacting in magnesium sulfate-bearing brines continue to best fit pentahydrite (fig. 26), although no spectra of the secondary mineral pentahydrite alone were observed. One spectra from the $MgSO_4$ solution was collected that could be indicative of either calcite and motukoreaite ($Mg_6Al_3(OH)_{18}[Na(H_2O)_6](SO_4)_2{\cdot}6H_2O$) (fig. 27). Further spectra of samples reacted in magnesium cation solutions contained significantly more noise, making phase determination with *CrystalSleuth* more difficult.

Additional sulfate hydration states were observed in spectra collected from samples reacted in Na_2SO_4; however, the best fit for these samples is thenardite, or the hydrated sulfate minerals aluminite ($KAl_3(SO_4)_2(OH)_6$) or blödite ($Na_2Mg(SO_4)_2 \cdot 4H_2O$) (fig. 28). Spectra from the $NaClO_4$ brine experiments include spectra indicative of the hydrated sulfate mineral alunite

(fig. 28) and a few spectra that we were unable to identify beyond a close match with several phases that include a hydrated phosphate group (fig. 29).

Samples reacted in Na_2SO_4 exhibit the first observations of carbonates in these solutions during this period (fig. 30). Before this sampling, carbonates were only observed in NaCl and Mg- cation solutions.

Basalt chips reacted in NaCl show no hydrated sulfate minerals, but a spectra very similar to anatase is observed within one sample (fig. 31). The samples reacted in $CaCl_2$ show few iron oxide peaks, but a number of spectra consistent with aluminum oxide and titanium oxide were observed (fig. 32). One sample reacting in $CaCl_2$ shows a decent match to reinhardbraunsite ($Ca_5(SiO_4)_2(OH,F)_2$) (fig.33). This spectra, however, is fairly noisy and includes other peaks that may be indicative of other minerals such as hematite.

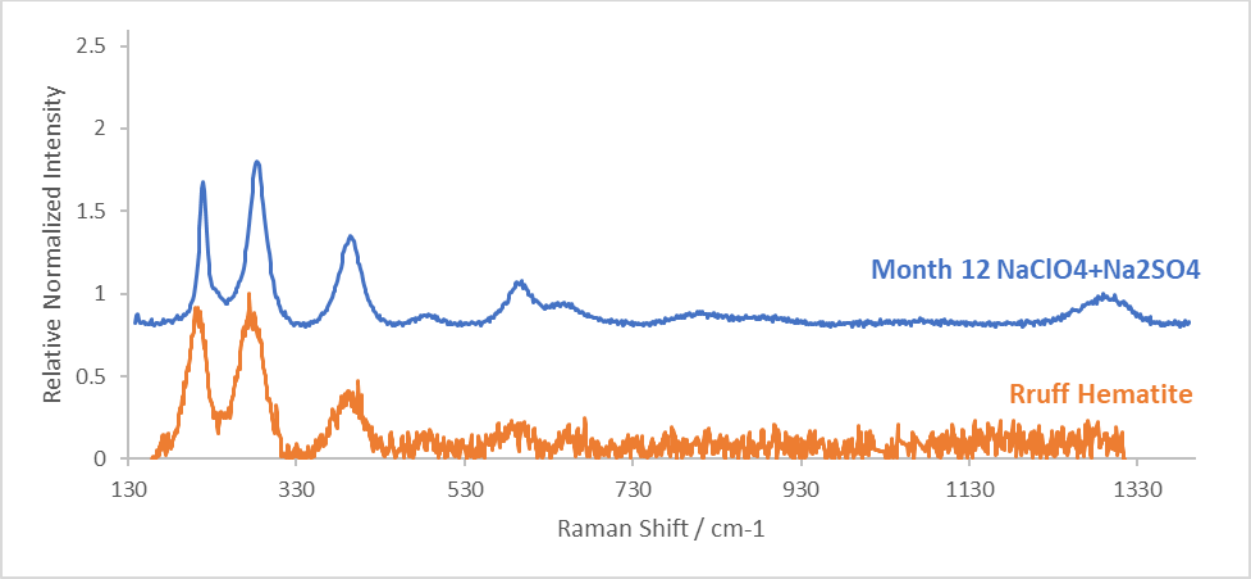

Figure 25. Raman spectra of a Craters of the Moon sample after reacting in $NaClO_4$ and Na_2SO_4 for 12 months as compared to spectra of hematite from the online database www.rruff.info

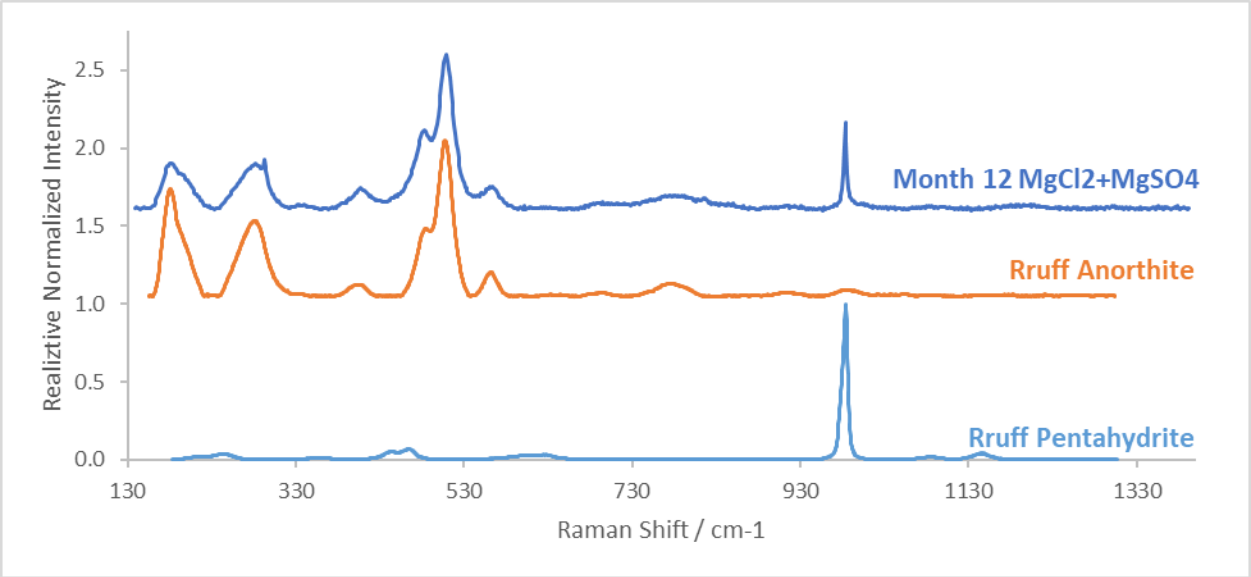

Figure 26. Raman spectra of a Craters of the Moon sample after reacting in a solution of $MgCl_2$ and $MgSO_4$ for 365 days (A) as compared to anorthite (B) and pentahydrite (C) from the online database www.rruff.info.

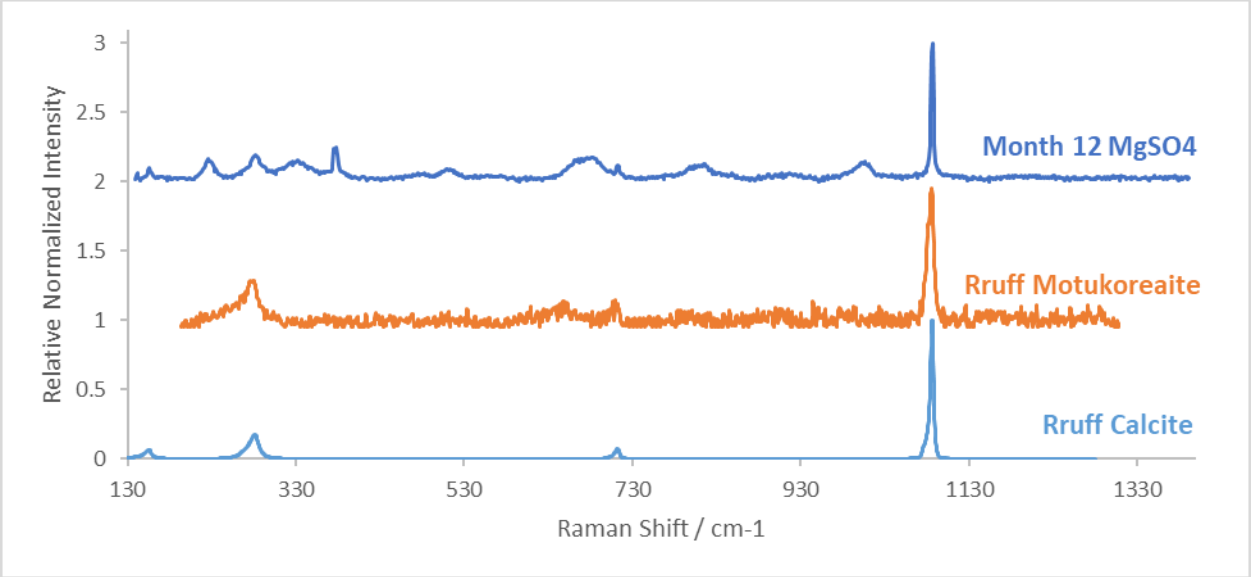

Figure 27. Raman spectra of a Craters of the Moon sample after reacting in $MgSO_4$ for 12 months as compared to spectra of motukoreaite ($Mg_6Al_3(OH)_{18}[Na(H_2O)_6](SO_4)_2{\cdot}6H_2O$) and calcite from the online database www.rruff.info.

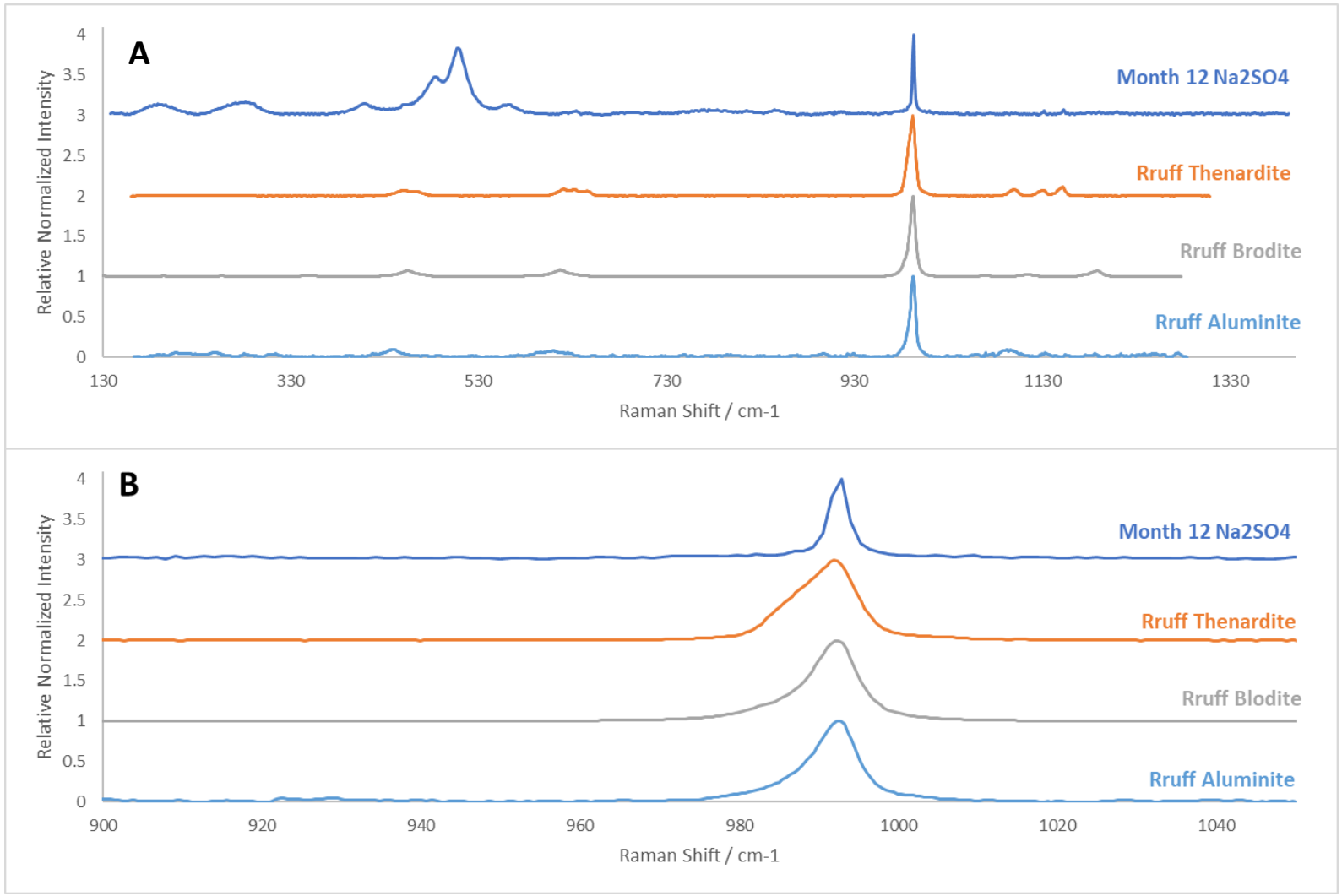

Figure 28. Raman Spectra of a Craters of the Moon sample after reacting in Na_2SO_4 for 12 months as compared to spectra of thenardite, blodite, and aluminite from the online database www.rruff.info. Panel A shows the full spectra collected and panel B shows the wavenumbers from 900 to 1050 to highlight the closeness in peak position of the four spectras.

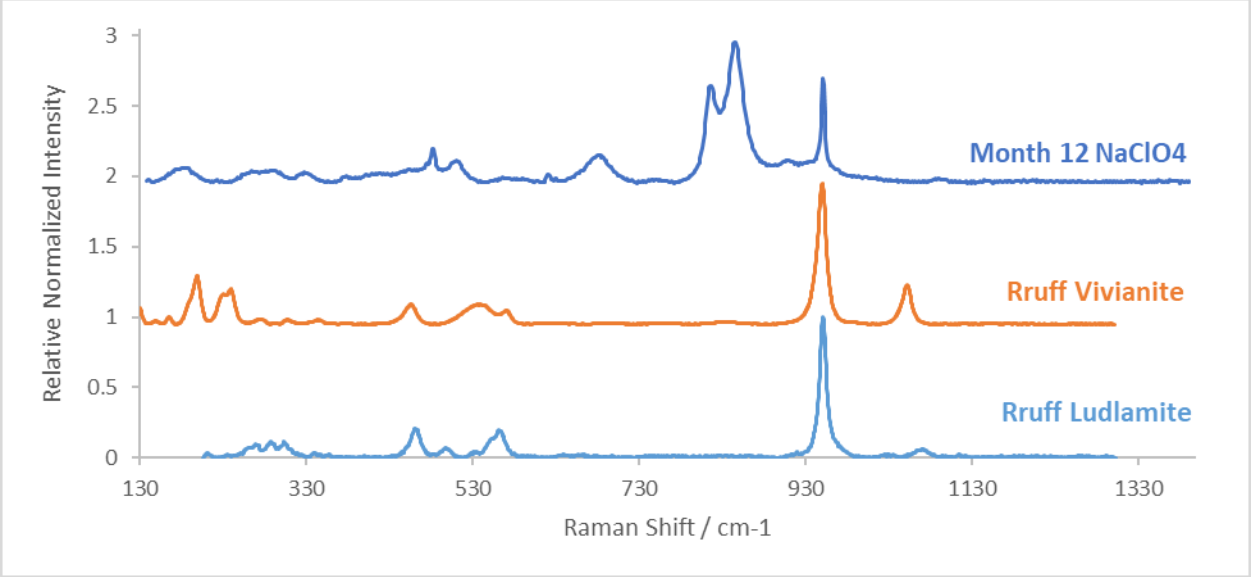

Figure 29. Raman spectra of a Craters of the Moon sample after reacting in $NaClO_4$ for 12 months as compared to spectra of vivianite $Fe^{2+}{}_3(PO_4)_2{\cdot}8H_2O$ () and ludlamite ($Fe^{2+}{}_3(PO_4)_2{\cdot}4H_2O$) from the online database www.rruff.info. Each spectra shares a peak at 951 wavenumbers which is correlated to a hydrated iron-PO_4 bond. The peak at 819 and 850 is correlated with forsterite.

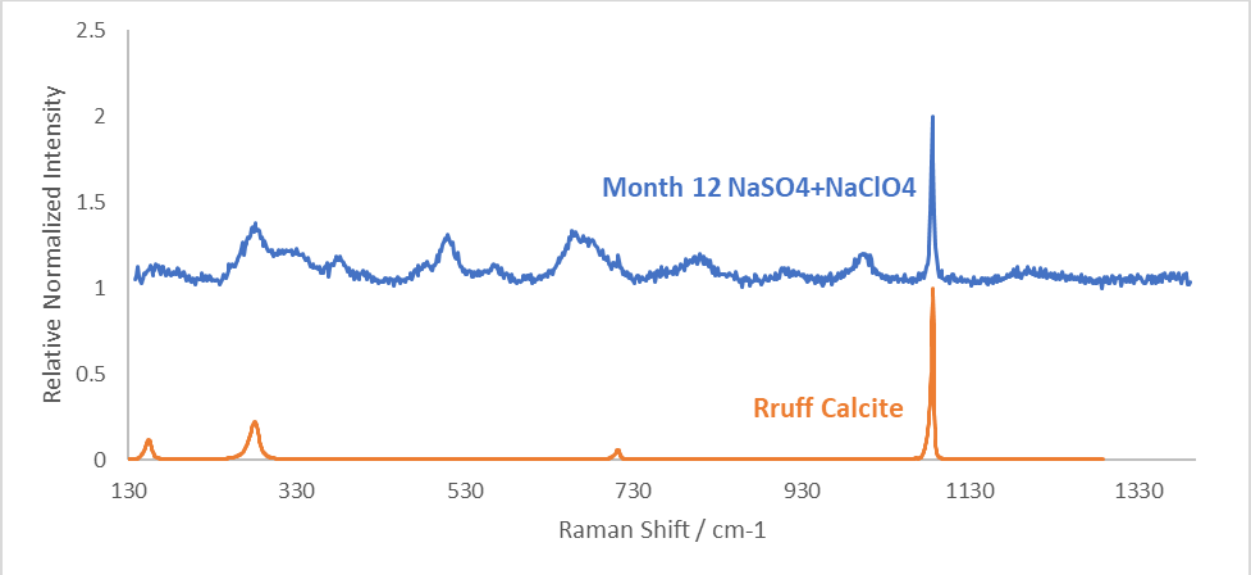

Figure 30. Raman spectra of a Craters of the Moon sample after reacting in a mixed solution of $NaClO_4$ and Na_2SO_4 for 12 months as compared to a spectra of calcite from the online database www.rruff.info.

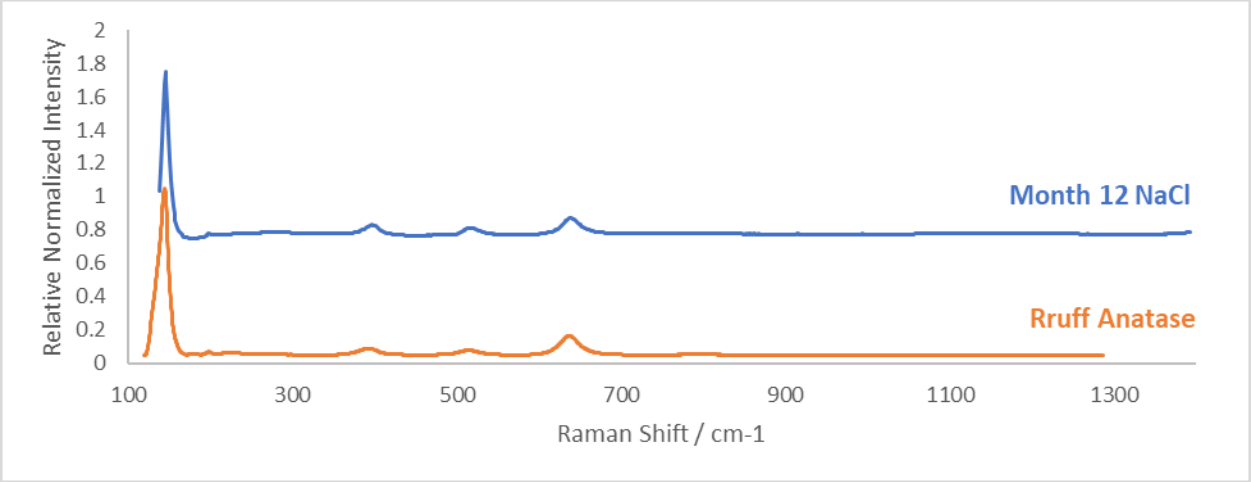

Figure 31. Raman spectra of a Craters of the Moon sample after reacting in a solution of NaCl for 12 months as compared to a spectra of anatase (TiO_2) from the online database www.rruff.info.

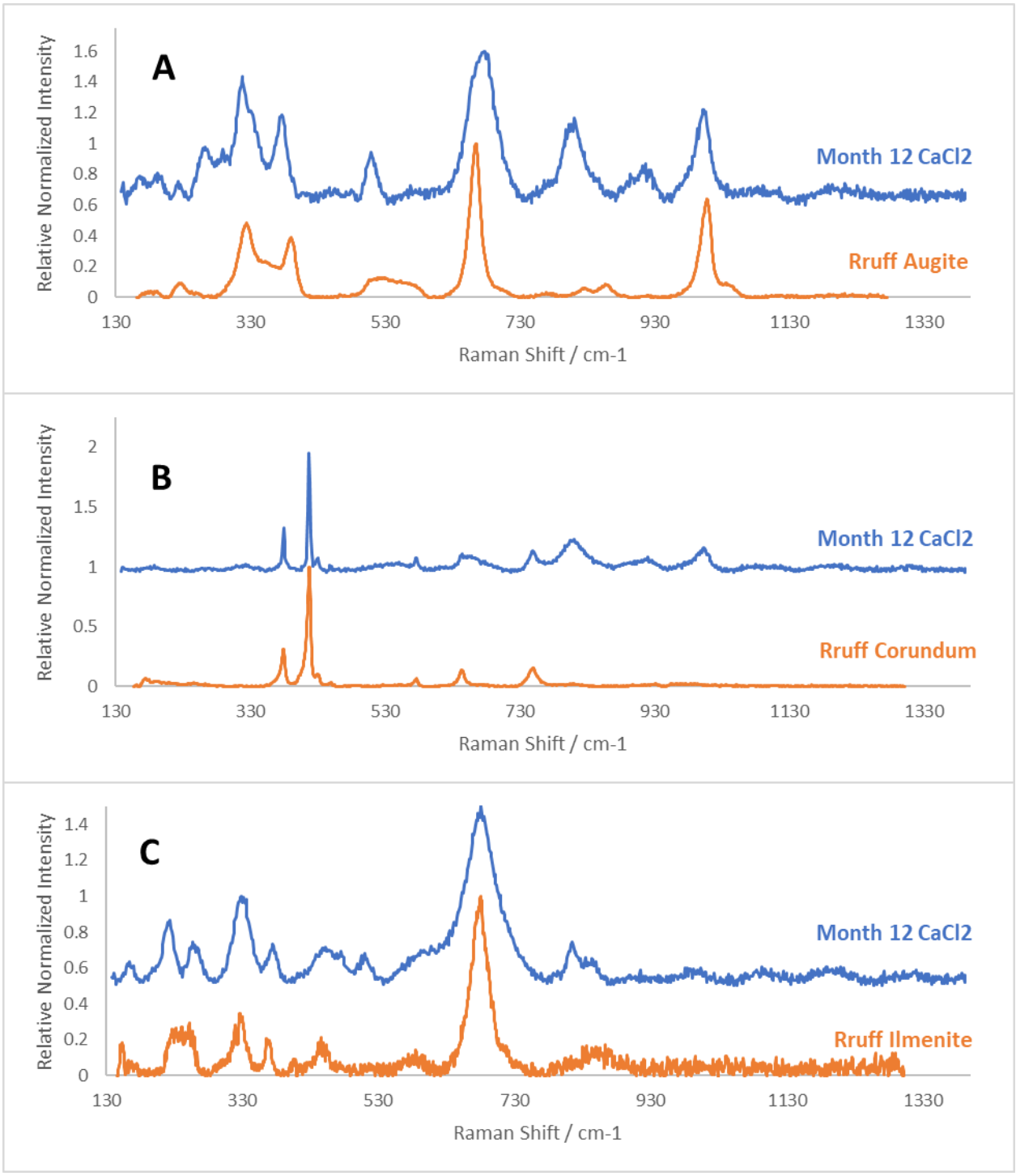

Figure 32. Raman spectra of three Craters of the Moon samples after reacting in a solution of $CaCl_2$ as compared to spectra of augite ($(Ca,Mg,Fe)_2Si_2O_6$), corundum (Al_2O_3), and ilmenite ($Fe^{2+}Ti^{4+}O_3$) from the online database www.rruff.info.

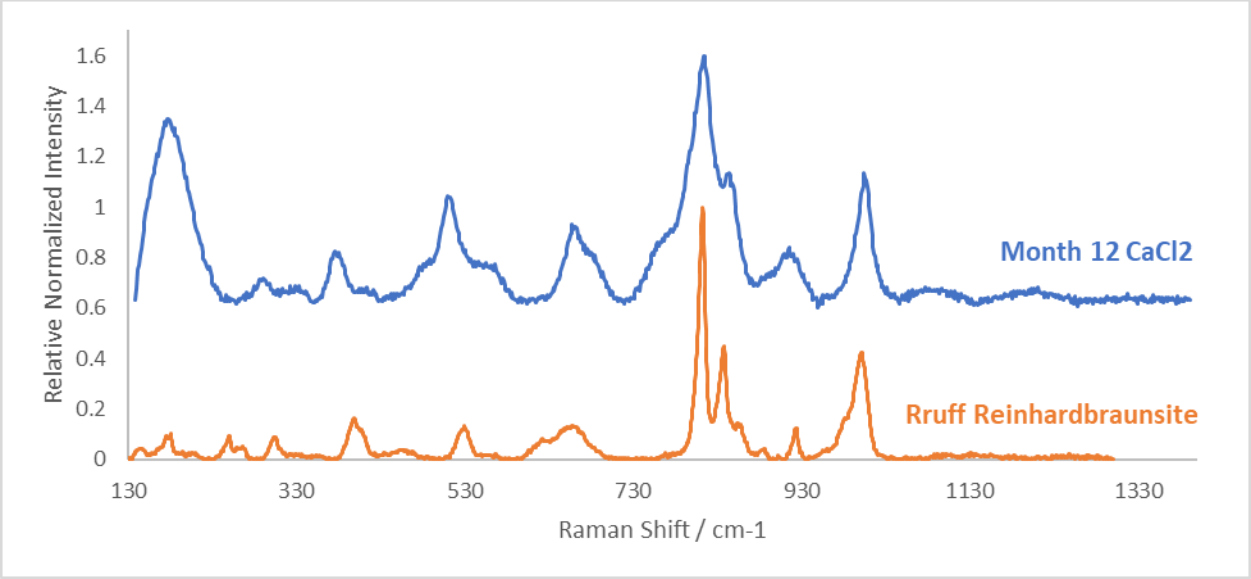

Figure 33. Raman spectra of a Craters of the Moon sample after reacting in a solution of $CaCl_2$ as compared to a spectra of reinhardbraunsite ($Ca_5(SiO_4)_2(OH)$) from the online database www.rruff.info. From this spectra, it is hypothesized this spectra shows a hydrated calcium silicate. The large peak at the lower wavenumbers of the sample is an artifact created from the calculated background level from the WiRE 4.2 software and is not a peak attributed to the mineral.

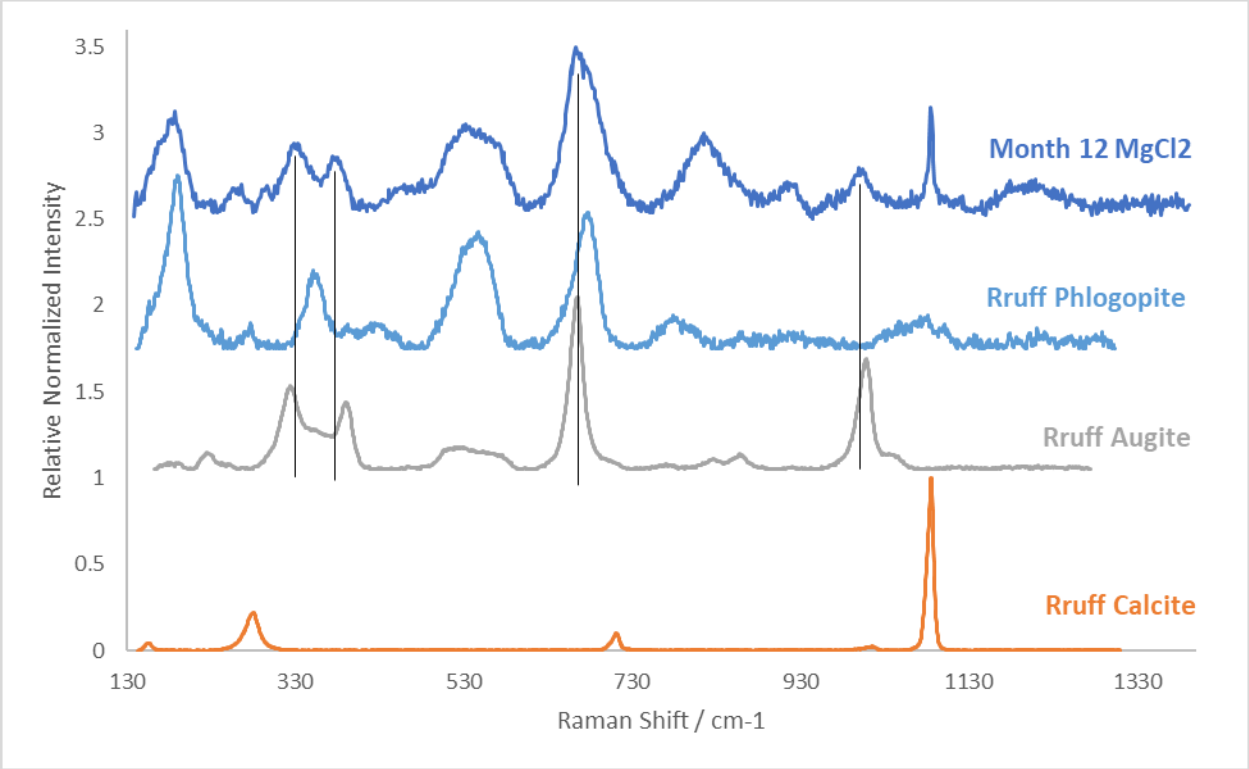

Figure 34. Raman spectra of a Craters of the Moon sample after reacting in $MgCl_2$ after 12 months as compared to spectra of phlogopite, augite, and calcite from the online database www.rruff.info. The vertical bars highlight how the peaks in the reacted sample don't line up with the peaks of augite nor phlogopite. With more noise from the spectra taken as well as inherited noise of the spectra from the database, accurate identification of the minerals present can only be referenced from common peaks and trends of hydrated states.

Discussion

Overview

From the first sampling period to the end of this experiment, iron oxide minerals were observed more frequently in ultra-pure water and sulfate brines, compared to other solutions. The COTM chips in all solutions exhibit qualitative observations of dissolution and secondary mineral formation (fig. 35).

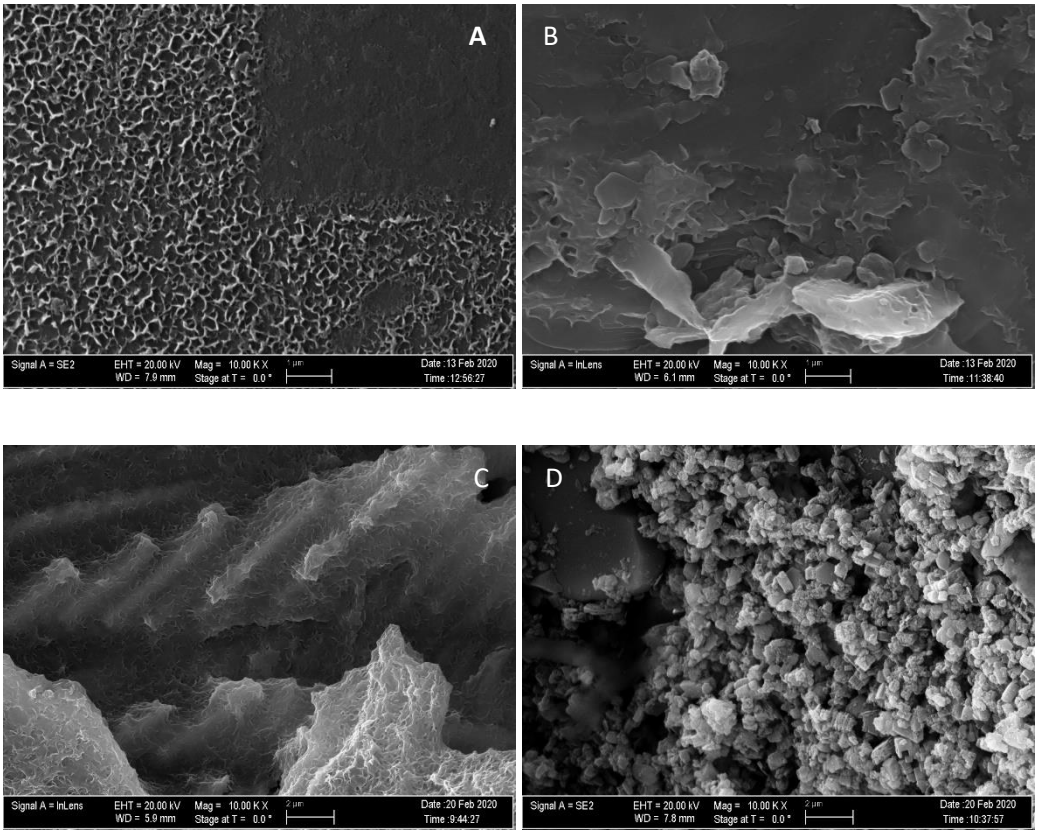

Figure 35. Scanning electron microscope (SEM) images of four Craters of the Moon samples after reacting in Na_2SO_4 (A), UPW (B), $MgSO_4$ (C), and $NaClO_4$ (D) for 12 months. Each image is taken at 10,000x.

From the beginning of the experiment, some of the first secondary minerals to form were iron oxides such as hematite and magnetite. Interestingly, as the experiment continued more spectra showed hydrated sulfate minerals compared to iron oxides. While this is possibly due to

a selection bias, it is worth noting that no hydrated sulfate minerals were observed in the control sample and it can be reasoned that hydrated sulfate minerals formed due to the environment inside the reaction chambers

For each chip, 15 spectra were initially taken each at different locations. About one in 15 attempts oversaturated the detector requiring an abort and an alteration of the spectrometer settings. About 10% of the spectra returned either background noise or spectra that were too low in counts to render a smooth enough curve to precisely measure the peak positions. Of the spectra that successfully collected data, about 90% of those were spectra of the primary minerals alone or in combination with each other. This resulted in three to five spectra for each sampling period that showed a secondary mineral or something else of interest. . As the experiment continued, the spectra contained more noise, making it difficult to clearly identify mineral spectral matches. Thus, more spectra were collected in these later experiments in order to produce the results described above. This necessity for taking multiple spectra within a small area is important for future experiments and missions as a movement of less than one millimeter could result in locating a mineral or organic molecule that is mission critical. Failure to take multiple spectra at a target risks returned data that is either noisy due to poor focus, too low of power to the laser, or fluorescence; or data that doesn't represent the diversity of the location due to a low sample size. This experiment collected 3,705 Raman spectra and despite the large number of spectra collected, it is very possible that some secondary minerals went undetected. If the Raman spectrometer is to be used to the best of its ability, a setup that will either take multiple spectra within a small zone, not unlike a raster plot, or a collection series where multiple spectra taken one after another at a single target with a slight alteration in power or duration will achieve the best results for the team utilizing this instrument. This process of multiple

collections of a single target with varying power ensures that if the sample will oversaturate the detector at a higher power, there will be a collection from a lower power available. This will ultimately ensure that time and resources will not be wasted because a single data collection came back unusable, given that from a signal being sent, data being collected, and a return signal of the data may take anywhere from up to half an hour.

One key limitation for Raman spectroscopy is the lack of robust libraries of collected spectra to compare unknown samples to known minerals and organic compounds. The RRUFF™ Project has been a pivotal resource in the analysis of the spectra collected in this work. While many spectra exist in the library are of excellent quality, of the 9764 mineral spectra as of April 2020 the library only 4088 samples have high resolution, excellent quality spectra. The remaining spectra are of low quality and either contain too much noise to be useful or do not exhibit any characteristics worth classifying. Scientists have worked to collect metadata of minerals and fluid inclusions so as to have a published work that have the basic structure of a compendium of mineral peaks (Frezzotti et al., 2012). What is missing, that will be essential to the usefulness of the Mars missions, will be a library of spectra that not only include mineral spectra taken at standard temperature and pressure, but a fuller spectral library that includes minerals and fluids stable at varying temperatures and pressures. Scientists are working to collect and publish such varying spectra of minerals based on varying conditions with implication for Mars (Chou et al., 1990; Dünnwald and Otto, 1989; Frezzotti et al., 2012; Gough et al., 2011; Israel et al., 1997; Martinez et al., 2004; Mazzetti and Thistlethwaite, 2002; Nuding et al., 2014; Prasad, 1999; Steiger et al., 2011; Wang et al., 2009, 2006). However, until a comprehensive library is available, the analysis of Raman spectroscopy will require thorough literature searches.

Another limitation for the Raman spectroscopy on Mars is fluorescence. This phenomenon causes peaks in the spectrum that are not indicative of the underlying matrix and could oversaturate the detector completely. This limitation was not observed in this experiment as the porcelain painter's dish used to hold the samples did not produce any fluorescence, nor did the samples produce additional peaks that could be attributed to fluorescence. About 10% of the spectra taken, however, oversaturated the detector even at 10% power. After observing an oversaturated signal, I aborted the collection and reduced power to 5%. This reduction of power typically achieved the goal of reducing the amount of signal return, but the drawback was an increase in noise in the spectra. The SuperCam spectrometer will only have a 532nm green laser so any substances that cause fluorescence will have to be either left without further Raman investigation, or require sample preparation which nullifies a key advantage to the Raman spectrometer.

Despite these limitations, the Raman spectrometer possesses key advantages that outweigh the limitations stated above. The Raman spectrometer onboard the Mars 2020 rover will have the capability to identify minerals and possibly discern the hydration state of these minerals.

Mineral group identification

The iron oxide minerals are some of the most discernable of the major mineral groups discussed in this work. Of the minerals, hematite has the most diversity in the spectral library (fig. 36), and from previous studies hematite also has a peak near 1320 *(Das and Hendry, 2011)*. The RRUFF™ Project does not contain this peak as the spectra from the project generally go from 129 to 1301 wavenumbers, however our experiment collected spectra out to 1350

wavenumbers. One limitation from this experiment is the inability to accurately discern magnetite from other iron bearing minerals like ilmenite and pyroxene. This is due to each mineral having a broad peak around 680 and a noticeable amount of noise causing uncertainty in precision. These minerals have some minor peaks based on the RRUFF™ database, but as the spectra of pyroxene from this work contains a fair amount of noise, it is inconclusive to say whether a sample is pyroxene or an iron oxide with peaks in this region.

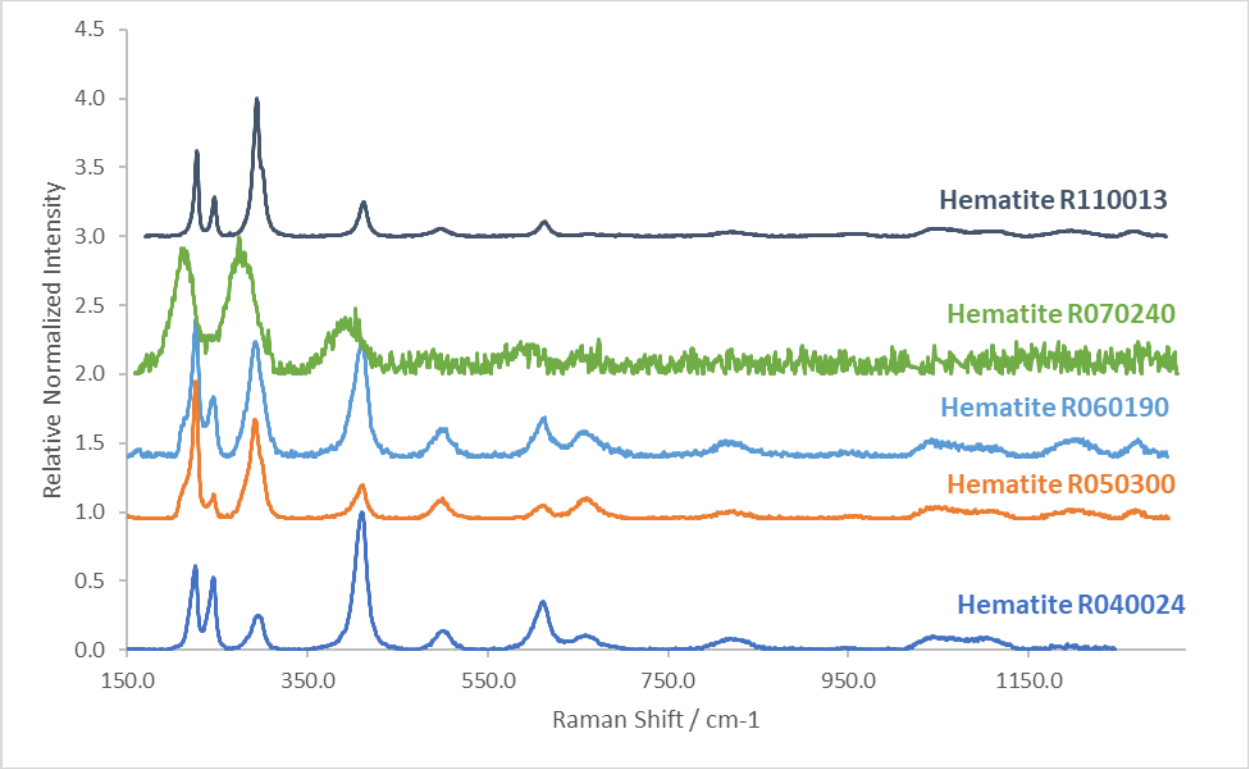

Figure 36. Raman spectra of several hematite with their RRUFF™ database identification number. While each sample was confirmed, the peak at 292 is of different intensities, the peak at 405 is at 409 in R110013, the two peaks near 615 and 665 are not the same for each spectra, and R070240 shares no peaks with the other hematite samples.

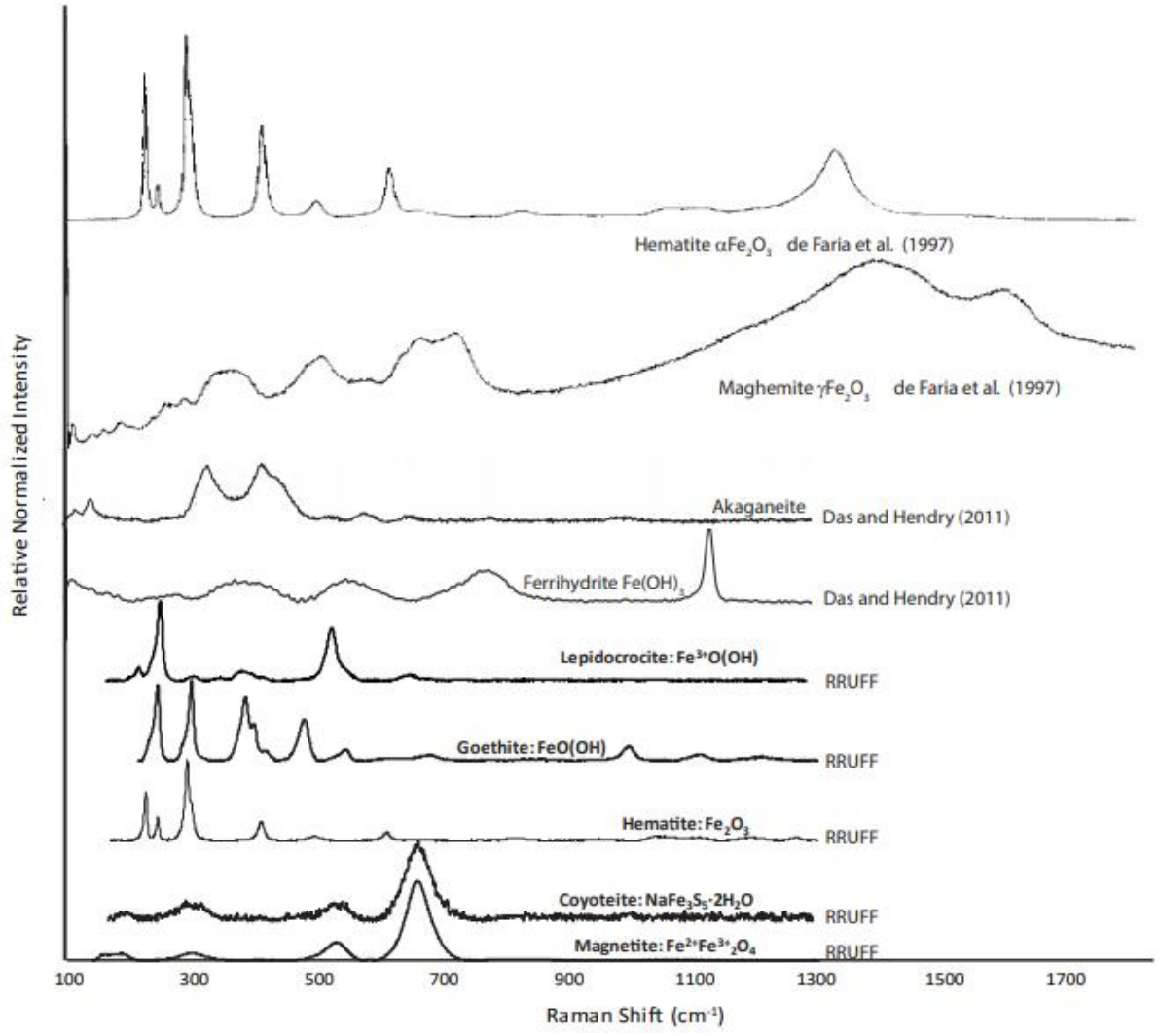

Figure 37. Raman spectra of various iron oxides with their ideal chemistry. Spectra are from the RRUFF™ database www.rruff.info.. The iron oxides represented highlight how some states present peaks unique to that species of mineral, but some iron oxides such as coyoteite and magnetite appear to be the exact same spectra despite the differences in ideal chemistry. Hematite from de Faria et al. (1997) includes a peak near 1300 which is absent from the magnetite spectra from RRUFF™.

Table 4. Raman excitation peak positions of the iron oxides listed in figure 5. Bolded values are primary peaks and the positions are based on the processed, unoriented files of the minerals in the online database www.rruff.info.

Mineral	Raman exhitation position (wavenumber/cm-1)								
goethite		247	**300**		**386**	416	481	547	
lepidocrocite	216	**250**	311	349	**380**				
hematite	**226**	246	**293**			412			1326
Coyoteite	200						527	**663**	
magnetite							532	**667**	

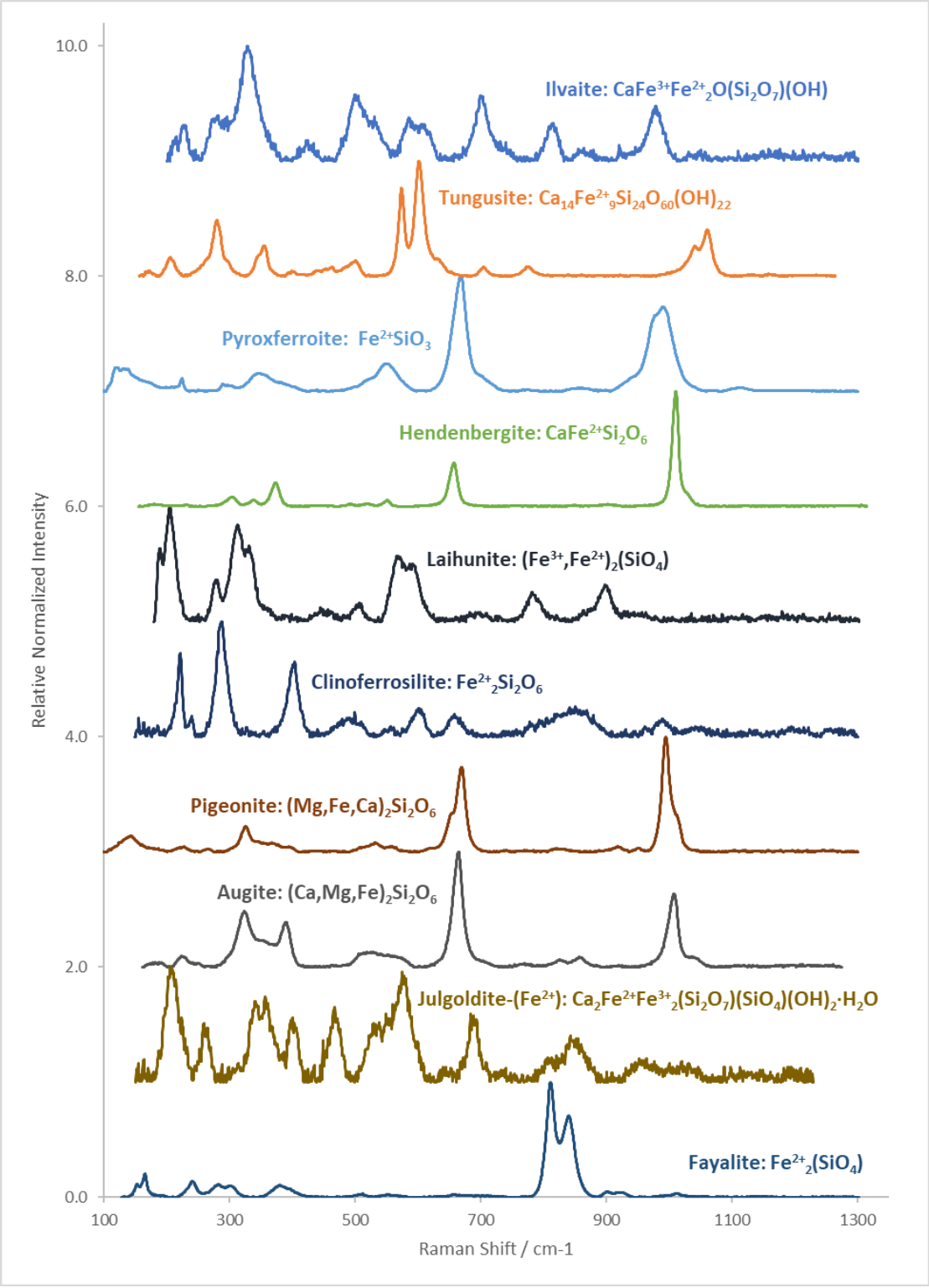

Figure 38. Raman spectra of iron silicates from the online database www.rruff.info. Each silicate has a spectra modestly distinctive, but many of the spectra include a broad peak near 680 and 1050. This common peak among iron silicates can cause a misclassification if the secondary peaks are not strong or if too much noise distorts the spectra.

Table 5. Raman peak position of iron silicates from figure 31. Spectra values are from the online database www.rruff.info and are a laser emitting 532nm green light. The bold values are the highest primary peaks.

Mineral	Raman excitation position (wavenumber/cm-1)								
Ilvaite		**328**		500		701		979	
Tungusite	280	355		574	**601**				1061
Pyroxferroite				550	**668**			991	
Hedenbergite		374			657				**1011**
Laihunite	188	**205**	281	313	566	587	898		
Clinoferrosilite	221	**290**	404						
Pigeonite		325			670			**995**	
Augite		324	391		**665**				1008
Julgoldite-(Fe2+)	**205**	259	341	357	400	465	576	693	
Fayalite							**811**	840	

The identification of sulfate minerals bears mentioning of how the hydration state of a mineral will shift or completely alter the Raman spectrum. Sulfate minerals produce subtle differences from each other (fig. 39). These minerals vary in their primary peak position by 20 wavenumbers and do not exhibit any other major secondary peaks that are discernable above noise or natural variations in the host rock. Because of this low margin for error, the spectra for sulfate minerals that have a high amount of noise could create issues for *CrystalSleuth* to correctly identify the mineral. However, this issue was overcome by reducing the range of the spectrum for the program to analyze. This successfully allows the program to fit the peak without being inundated with information irrelevant to the most significant difference within these minerals. This process, however, will be difficult to replicate for the Mars 2020 mission as the Raman on the SuperCam has a spectral resolution of four wavenumbers, so minerals differing by less may not appear. Thus, any need to identify sulfates with better precision will require other instruments onboard the Mars 2020 rover. Some sulfates like jarosite and amarantite contain additional peaks that assist in identification, but for the majority of these minerals the primary

peak ranging from 980 to 1100 are the only identification of the mineral using the Raman spectrometer.

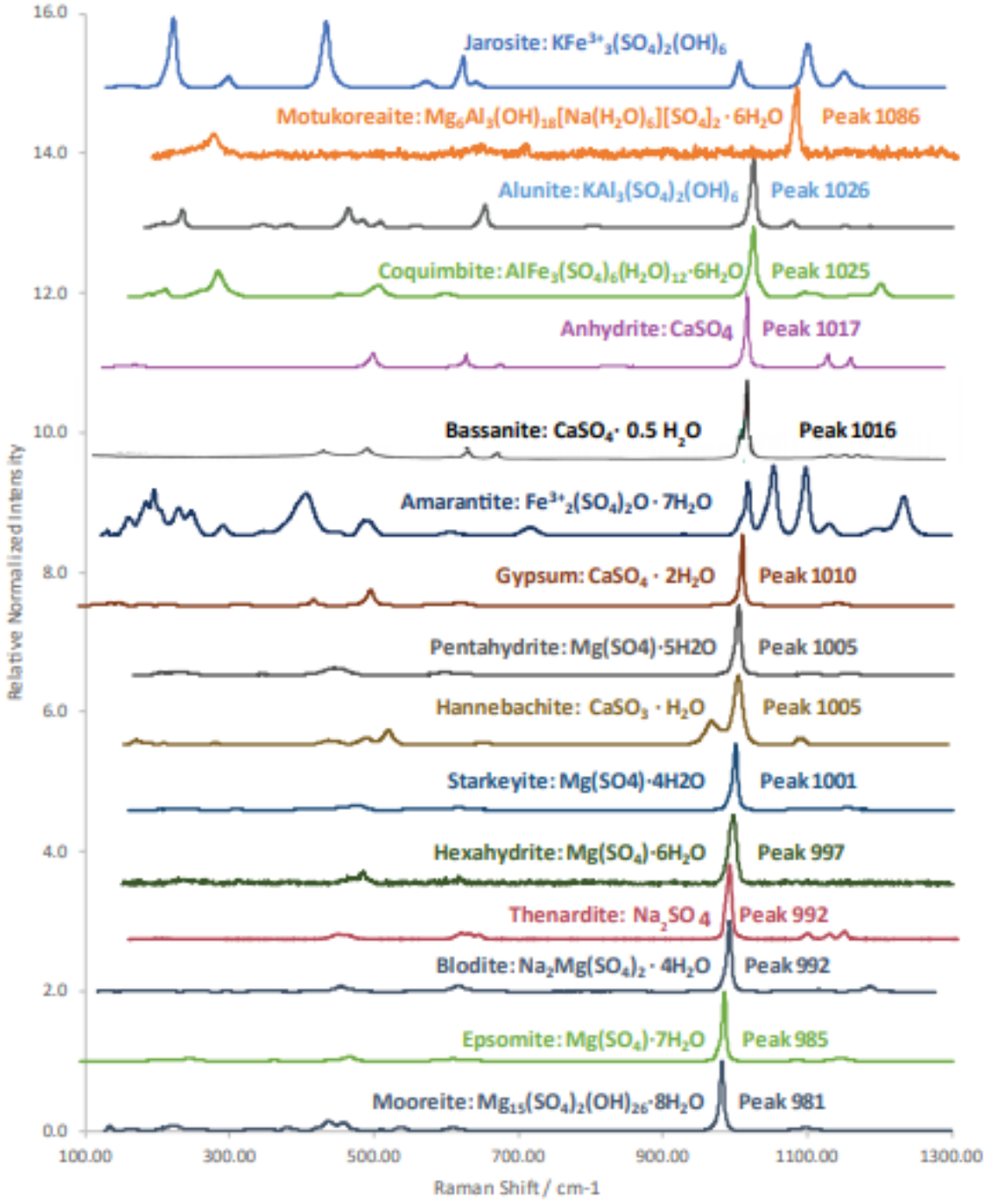

Figure 39. Raman spectra of multiple magnesium sulfate minerals associated with their name, chemical composition, and their primary peak position from the online database www.rruff.info. Bassanite spectra is at standard pressure and 400K, image from Prasad (1999).The peaks for amarantite are 1018, primary peak 1053, and 1098. Additional peaks for jarosite are at primary peak 222 and 434. Spectra are in order of increasing primary peak position of the major sulfate peak.

Many of the carbonate minerals, like the sulfates, exhibit a consistent spectrum shape of a single, intense peak that is shifted by a few wavenumbers. Carbonate in solution will produce a peak at 1064 wavenumbers (Martinez et al., 2004), and the carbonate minerals with different cations and varying hydration states show a shift in the carbonate ion peak from 1085 in rhodochrosite ($Mn(CO_3)$) to 1122 in huntite ($CaMg_3(CO_3)_4$). With few exceptions such as dolomite, siderite, and magnesite, the only discernable peak is the carbonate peak. Therefore, similar tactics were employed here to focus the Crystal Sleuth mineral search only the section of the spectra that identifies carbonate minerals. The carbonate minerals each have the possibility to produce spectra similar to calcite as each have few peaks except for a strong, narrow peak within 25 wavenumbers of each other (fig.40). Aragonite, calcite and rhodochrosite have the same primary peak at 1085, which can make identification without additional compositional information about the phase. The same limitation occurs here as does the sulfate group; each mineral has a primary peak within a narrow range. While this limitation will require the same secondary analysis if the goal is to gain more precise information between the carbonate minerals, one benefit is that the range of carbonate minerals overlaps by a single wavenumber. Motukoreaite, $(Mg_6Al_3(OH)_{18}[Na(H_2O)_6](SO_4)_2 \cdot 6H_2O)$, has a wavenumber of 1086 which is higher than the aragonite and rhodochrosite shared peak of 1085, and is the same peak position as calcite. This could be an issue if the spectrum collected has a significant amount of noise that covers the small peak near 300 for rhodochrosite. Except for this occurrence, the two mineral classes have clear ranges that will give the Mars 2020 and ESA ExoMars teams a clear, general understanding of what mineral group the Raman spectrometer is observing.

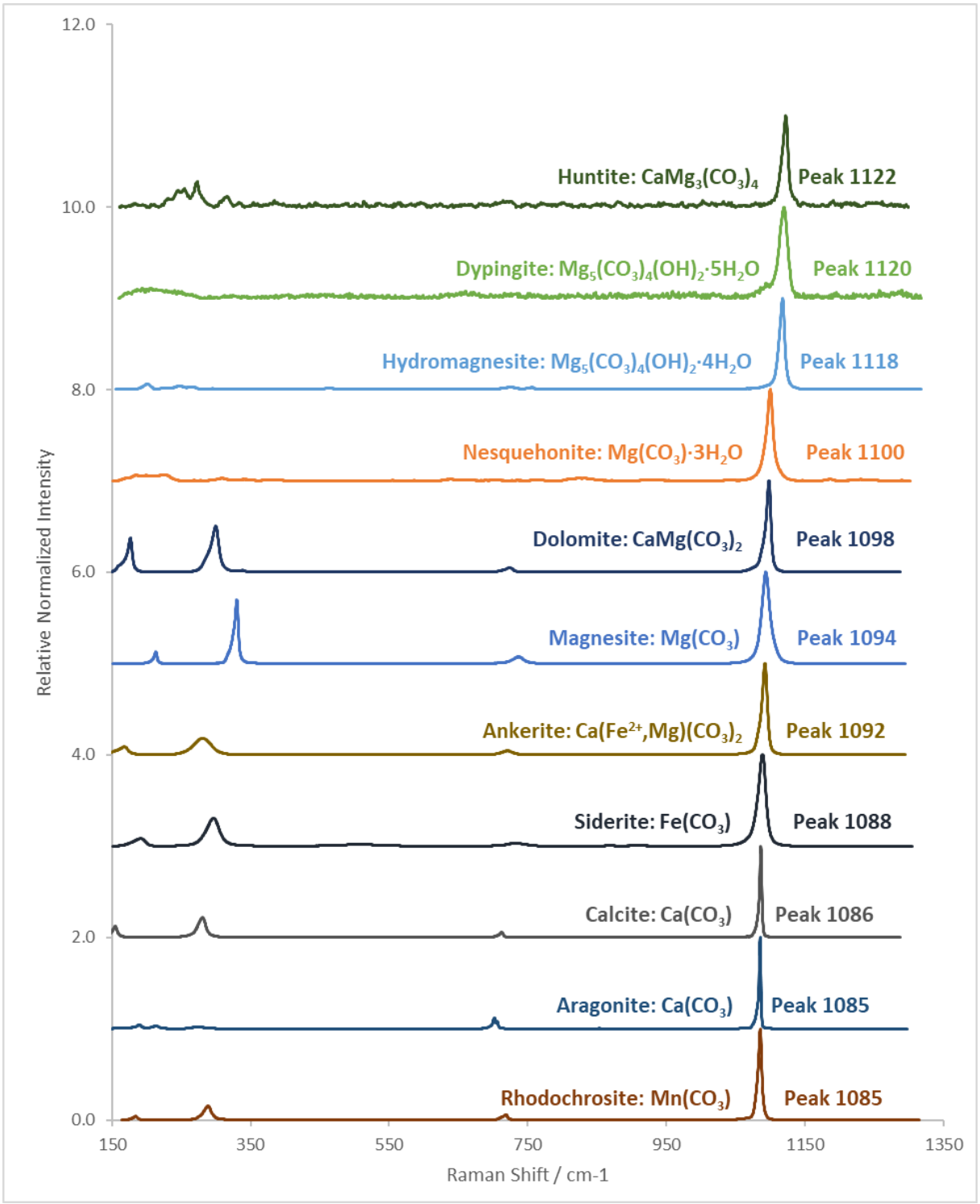

Figure 40. Raman spectra of various carbonate minerals highlighting their shift in wavenumbers correlating to their ideal chemistry. Spectra are from the RRUFF™ database www.rruff.info. Order of spectra is by increasing primary peak position.

Raman spectra consistent with macfayallite was observed in one sample reacting in $MgSO_4$ and $MgCl_2$ at the one month extraction period. The spectra is not a perfect fit; the primary and secondary peak are shifted in different directions. This shift in the spectra could be due to either differences in calibration or merely from a slight change in orientation. A change in the spectra is not too uncommon as the RRUFF™ database includes many spectra of minerals where the ideal chemistry is the same but the spectra varies (fig. 41). With this near fit for macfallite, it is within reason that the sample is macfallite. Raman spectra of Mn-oxide minerals also exhibit trends of carbonates and sulfates where a minor change in hydrated state or crystal structure will slightly shift the primary peak, but also exhibit completely different spectra shapes as like the Fe-oxide minerals (fig. 37).

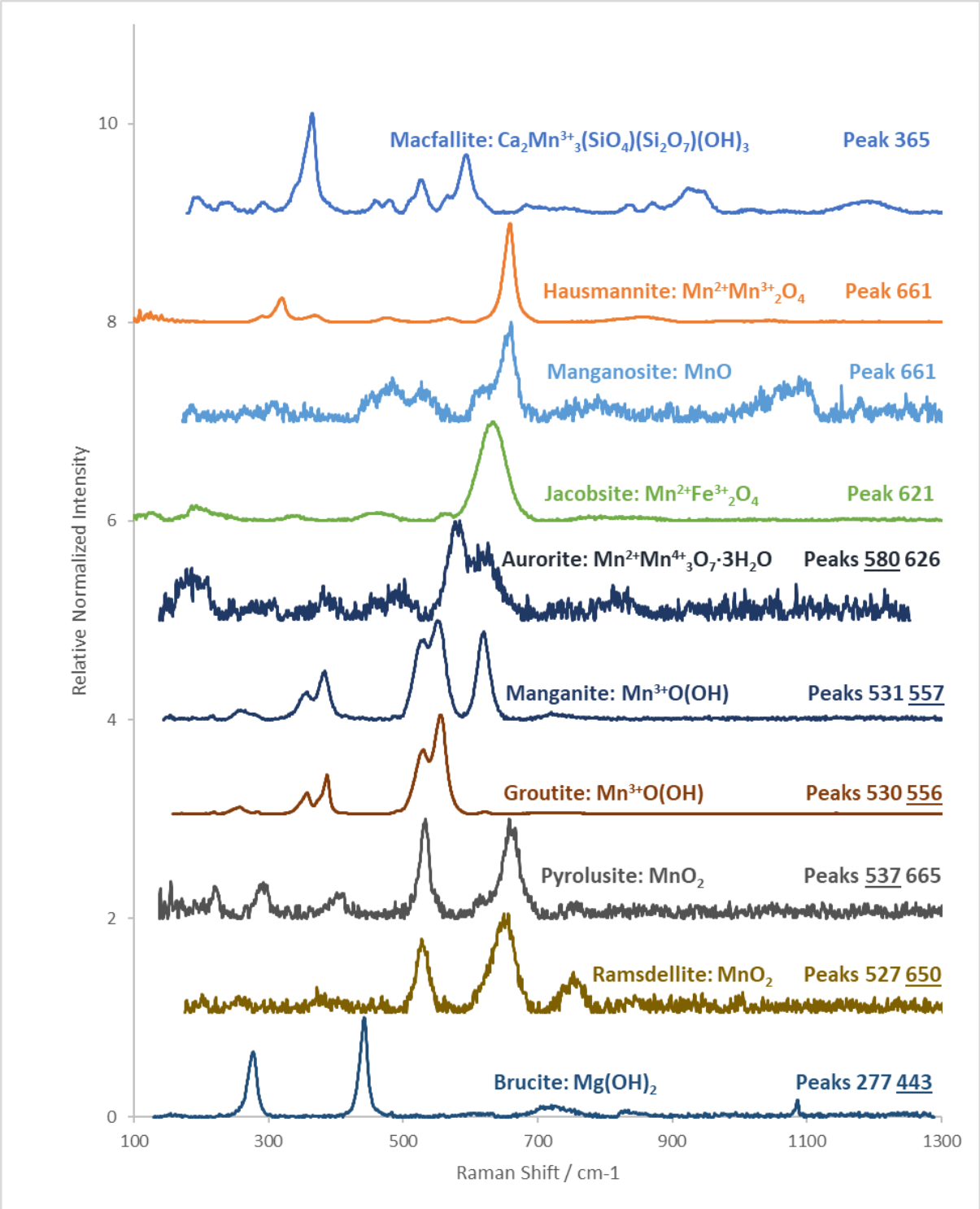

Figure 41. Raman spectra of Mn oxide minerals from the online database www.rruff.info. Primary peak positions are underlined when more than one major peak is present.

The spectra that fit with thenardite possibly represent a mineral that precipitated onto the basalt during reaction or this might be salt from the brine that did not react with the basalt and merely crystalized onto the surface. Due to the simplicity of the mineral and how it is, chemically, one of the salts of the brine, it is impossible to say where this is from the basalt or from the brine but it is plausible to suggest the target is from the brine.

Trends in hydrated sulfate minerals

The basalt chips analyzed from the month 3 samples produced more spectra where more iron oxides were observed in the samples and were the first instances where hydrated sulfate minerals were observed. Samples that reacted in a $MgSO_4$ or $MgCl_2$ solution produced more hydrated sulfate spectra that fit more robustly with pentahydrite. Thenardite is also observed at this sampling period but is not as hydrated as pentahydrite or hexahydrite. One theory is when the basalt chips are removed from the brines the sulfate hydration state is determined by the relative humidity during the sample analysis, rather than the conditions in the reactor (Wang et al., 2009). This model suggests that once the brines are out of an aqueous environment the sulfate minerals are controlled by the relative humidity of the laboratory and the hydrated states of the sulfates at the time of measurement is the meta-stable state closest to equilibrium at that moment. One spectra of interest is shown in figure 27 where *CrystalSleuth* suggests a good fit with motukoreaite. This hydrated mineral is unique from the sulfate minerals related to epsomite as it includes aluminum in addition to sulfate. This more complex hydrated mineral still fits the

trend of being a hexahydrated mineral so this is not an outlier of what has been observed so far for magnesium cation solutions.

A deviation from this trend of magnesium cation solutions producing pentahydrite minerals and sodium solutions producing hexahydrite minerals is from the Na_2SO_4 brine in the one year samples minerals indicative of blodite ($Na_2Mg(SO_4)_2 \cdot 4H_2O$) or aluminite ($Al_2(SO_4)(OH)_4 \cdot 7H_2O$) show a good fit with the spectra produced in this sample as does thenardite, an ephemeral mineral of sodium sulfate. While it is chemically possible to produce blodite or aluminite, it is more plausible that the spectra is produced from a crystal of the Na_2SO_4 salt from the brine that formed on the surface due to this latter explanation being more simplistic.

Other secondary minerals

As the experiment continues to its conclusion after 12 months of reaction, more complex hydrated states appear in measurements. Hydrated iron phosphates appear to arise in samples reacting in a sodium perchlorate brine in the form of vivianite ($Fe^{2+}_3(PO_4)_2 \cdot 8H_2O$) or ludlamite ($Fe^{2+}_3(PO_4)_2 \cdot 4H_2O$), yet the WDS analysis measured 0.04% of a phosphorus oxide in the material by weight percent. If this measurement is accurate to the fitted spectrum chemistry, it must mean that any available phosphorus was quickly reacted to form these hydrated minerals. The complexity of the hydrated states also appears in NaCl brines at the six month collection with the identification of trona ($Na_3(HCO_3)(CO_3) \cdot 2H_2O$).

One hydrated state that is of interest is the observation of opal in the 3 month ultra-pure water sample, which is probable considering the amount of silicon and oxygen in the environment and how opaline structures have been identified in Gale Crater (Ruff et al., 2011). With the abundance of water some amount of opal is possible, but with only one occurrence of

this mineral it is difficult to make any further interpretations of its formation mechanism or likelihood of formation in saltier environments since it was not observed in any of the saturated brine reactors. It is also difficult to make a table of hydrated silica spectra from the RRUFF™ Project as opal has no ideal chemistry of silica to water molecules and can vary from location to location and within one mine. Because of this variability in the molecular bonding of silica and water, a sample of opal may not correlate to known spectra of opal in a database (fig. 42) and may be either misidentified as another mineral or would require additional instruments to confidently suggest the formation of opal.

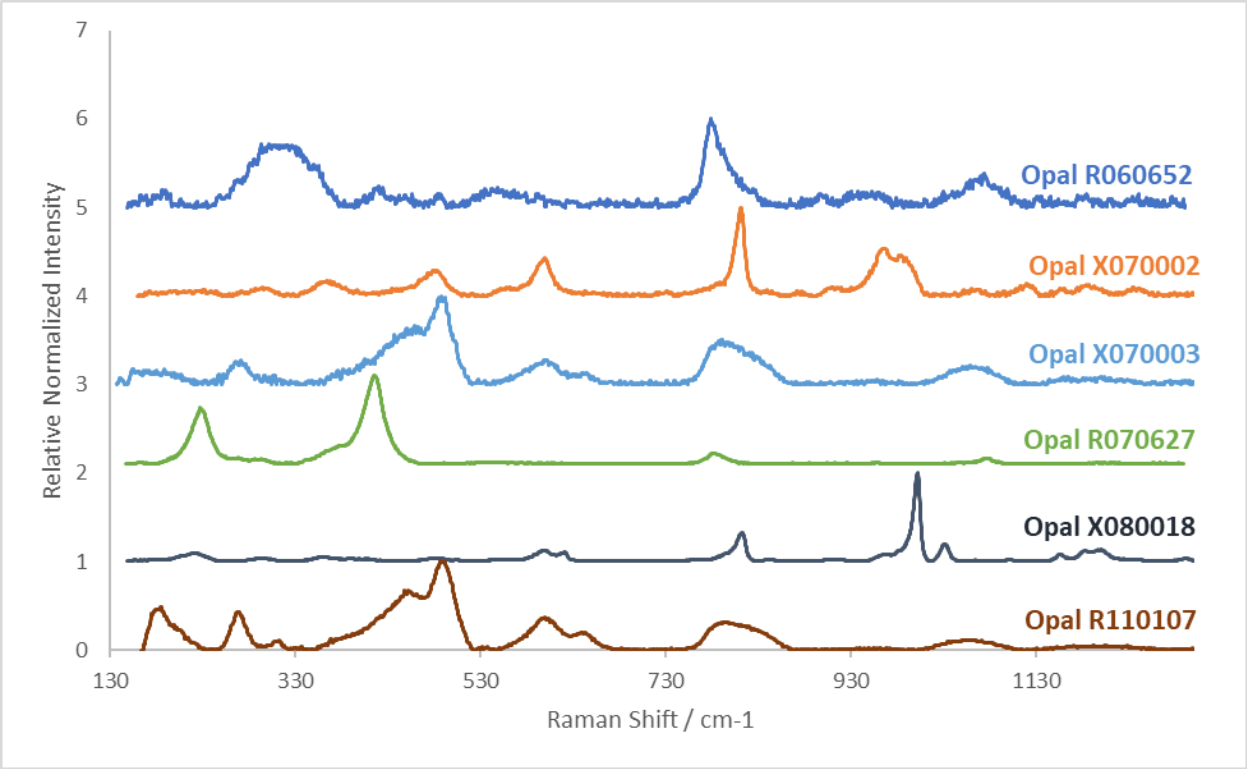

Figure 42. Raman spectra of various opal from the online database www.rruff.info. Some spectra share a primary peak from 780 to 820, but this range is too great for one to for one to confidently say a spectra is opal without a secondary analysis.

One question that has arisen is why some brines show a higher number of secondary or hydrated minerals as compared to others. And, more to the point, why do sodium sulfate and sodium perchlorate produce spectra consistent with pentahydrite while magnesium chloride and

magnesium sulfate produce spectra aligned with hexahydrite? Experiments have looked at the meta-stable relationship of magnesium sulfate minerals and how a change in relative humidity or temperature will change the equilibrium of the system to favor one hydrated state over another (Boukhalfa, 2010; Steiger et al., 2011; Vaniman et al., 2004), but no experiment in the literature search has looked at whether the presence of basalt will affect the hydration state of the minerals; either by the release of ions or as a intermolecular attraction to adjust the rate of hydration/dehydration based on the thermodynamic model suggested by Wang et al. (Wang et al., 2009).

If this trend is not merely due to selection bias or by a fault in calibration, the next task would be to perform additional tests to ensure this hydration trend is not by mere chance, and how the presence or absence of certain cations could affect the hydration state of the precipitated mineral

Focusing on the anion chemistry of the solutions is inconclusive in determining if there is a trend into the abundance, strength of signature, or types of secondary minerals created (table X). This is similar in outcomes to a study that looked at denticle length in a pyroxene and if the aqueous chemistry could be ascertained by the denticle characteristics (Phillips-Lander et al., 2017). Our results also find little determining factors in anion characteristics that play a significant role in the alterations of basalt. However, even though the secondary minerals do not implicitly signify the solute of the brine, the existence of these carbonates and sulfates is important based on the significance it suggests of the pH of the brine from which it formed.

Implications

Previous studies have tried to rationalize the plausibility of how orbital, lander, and rover observations see evidence for carbonates in the Martian dust and sediment if a prevailing theory for the history of Mars includes a highly acidic and oxidizing environment (Dehouck et al., 2016, 2012; Fairen et al., 2004; Horgan et al., 2019; Kim et al., 2017; Moyano-Cambero et al., 2017; Saheb et al., 2011). Studies show that under an acidic environment, carbonate minerals become unstable and will breakdown into dissolve CO_2 gas and H_2O (Pismenskaya et al., 2020). This dissolution of carbonates and bicarbonates would suggest an acidic environment during the Martian past. However, if we observe carbonates with the Raman spectrometer during our next two rover missions, this would provide support for a more neutral pH environment during the period of time we estimate for that sediment formation.

One novel approach to utilize the Raman spectrometer with respect to the salting out of sulfates due to dissolved CO_2 gasses in liquid brines is to use it as a tool for estimating the amount of dissolved CO_2 in the brine (Bonales et al., 2013). Such techniques would compare known spectra of end-member brines at different concentrations of CO_2 gas, pressures, and temperatures to compare how the spectra changes at the peak positions of CO_2. This alteration of brines has the potential to explain possible geochemical interactions from salting out of sulfates or carbonates seen within a brines.

Prior orbital scanning of Jezero Crater provides a compelling argument for carbonates in lacustrine fluvial features within the crater (Horgan et al., 2019). Along with detecting carbonates in general, CRISM imaging also suggests hydration of carbonates within

the fluvial system, which can be used to further aim the rover team with utilizing the Raman spectrometer for scanning of carbonates.

The observation of an opaline mineral in this experiment suggests that the Raman spectrometer could have the ability to observe hydrated silicates. This would have implications to the conditions of that area of Mars as studies have looked at the dissolution of silicas (Burns, 1993; Daval et al., 2017; Ruff et al., 2011). These experiments show the limits of silica dissolution as well detail the area around "Home plate" in Gusev Crater. This observation also suggests areas of Mars that were less oxidizing than nearby areas, alluding to hydrothermal activity. If this were the case, then the next Mars missions may be able to use Raman spectrum observations that correlate to opal to further investigate an area for hydrothermal activities.

From the Mars 2020 proposal information packet, the Raman spectrometer using the 532nm green laser will be on the SuperCam and have a discernable range of four wavenumbers. This quite broad range is limiting in identifying the specific chemistry and hydration state of some minerals, given how some minerals like magnesite and dolomite are at the limit of resolution for the Raman spectrometer, this will still be useful in discerning the groups of sulfate, carbonate, and Mn-oxide group apart from each other, especially if the mineral in question has only one peak that falls in the middle of the grouping. This factor can provide insight for rover commanders in deciding which targets are best for completing the missions with the best utilization of time and resources remaining.

This work shows how secondary minerals created from the alteration of Mars analogous basalt in near saturated brines can be observed with the Raman spectrometer and how one can discern secondary mineral groups based on where a peak is located within a range of known peaks. Even with the limitations of a broad, low resolution spectrometer, a spectra exhibiting a

strong peak can be utilized to gauge the mineral group to support claims of pH of the solution the secondary mineral precipitated from. This insight can lead scientists to further investigate an area with more precise, resource heavy instruments to better understand what the Raman spectrometer has detected.

Since evidence of hydrated carbonates is seen with CRISM, the Raman spectrometer will play a large role in identifying such mineral groups at a distance of about 7 meters. This ability to use the instrument without needing the rover to be close to a target allows the Raman to take observations of targets either in a location too precarious for the rover team to maneuver, or take spectra of many locations within the 7 meter radius to aid in deciding where to take the rover next.

Table 6. Summary of minerals observed on a Craters of the Moon chip for each time period with minerals grouped by major chemical similarities. The final section "other" lists minerals that were observed but do not chemically fit into any of the major groups above. Spectra where a secondary mineral was observed is shaded in the respective color of the major group of that mineral. Minerals that are a possibility but are not confident matches (e.g. magnesite in the Month 12 Na_2SO_4 solution) are excluded from this table.

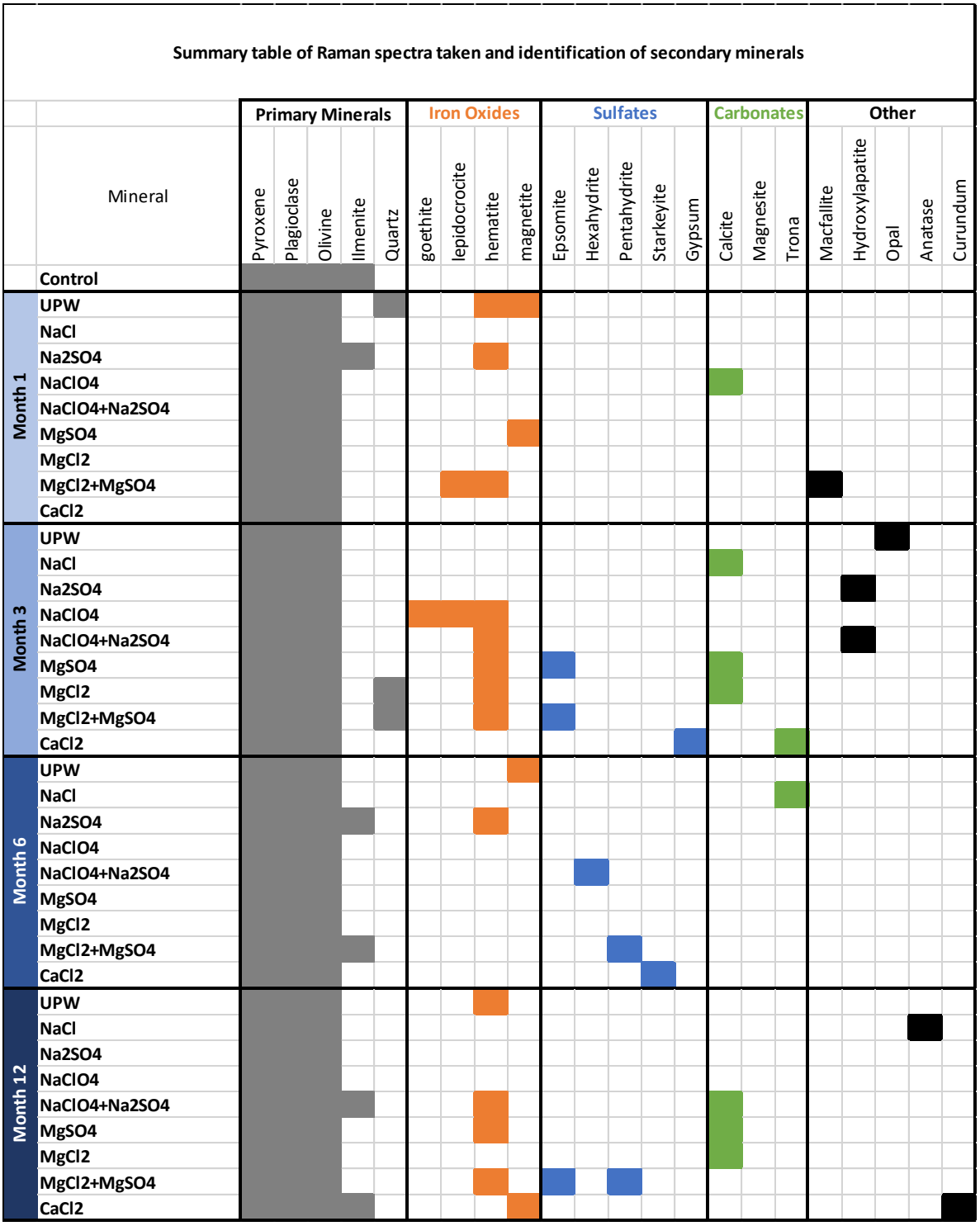

Conclusion

The Raman spectrometer is able to detect secondary minerals formed after a Mars analogous basalt reacted in near saturated brines within weeks of incorporation and for up to a year in duration. The basalt exhibited signs of dissolution and precipitation by the detection of iron oxides and hydrated minerals on the surface of the chips. A trend of which hydrated state is present on the surface is correlated to the cation of the brine. This tool is of great value as a non-destructive analysis of geochemisty of minerals present and will benefit our understanding of other worlds as well as hard to reach areas of Earth as we seek to understand the environments around us. The Raman spectrometer will also achieve mission goals while instilling our stewardship goals of being as conservative to the environment being studied and to leave as few alterations to the location as possible so what we study is from the location being studied and not a remnant of our presence.

This thesis fills shows that a Raman spectrometer will be able to observe secondary mineralization of a Mars analogous basalt after reacting in a near-saturated brine. This observation and the discernibility of major mineral groups will be impactful for the Mars missions in understanding the mineralogy of the Martian soil and the conditions of the Martian past that affect the solubility of minerals. If future missions to Mars will include a Raman spectrometer of more precise measurements, this thesis will work to support our theories in the impact of near saturated brines and the hydrated state of the secondary minerals.

This has the added importance of supporting theories of mineral transport of the Martian environment at present and in the past that are necessary for our current understanding of the necessary requirements for life.

References

Abotalib, A.Z., Heggy, E., 2019. A deep groundwater origin for recurring slope lineae on Mars. Nat. Geosci. 12, 235–241. https://doi.org/10.1038/s41561-019-0327-5

Adcock, C.T., Udry, A., Hausrath, E.M., Tschauner, O., 2018. Craters of the Moon National Monument basalts as unshocked compositional and weathering analogs for martian rocks and meteorites. Am. Mineral. 103, 502–516. https://doi.org/10.2138/am-2018-6193

Baker, V.R., Strom, R.G., al, et, 1991. Ancient Oceans, Ice Sheets and the Hydrological Cycle on Mars. Nat. Lond. 352, 589.

Banin, A., Han, F.X., Kan, I., Cicelsky, A., 1997. Acidic volatiles and the Mars soil. J. Geophys. Res. Planets 102, 13341–13356. https://doi.org/10.1029/97JE01160

Beck, A.W., Murchie, S.L., Viviano, C.E., 2020. A search for early- to mid-Noachian chloride-rich deposits on Mars. Icarus 338, 113552. https://doi.org/10.1016/j.icarus.2019.113552

Benison, K.C., Goldstein, R.H., Wopenka, B., Burruss, R.C., Pasteris, J.D., 1998. Extremely Acid Permian Lakes and Ground Waters in North America. Nature 392, 911.

Berger, G., Meunier, A., Beaufort, D., 2014. Clay mineral formation on Mars: Chemical constraints and possible contribution of basalt out-gassing. Planet. Space Sci., Planetary Geology Field Symposium, Kitakyushu, Japan, 2011: Planetary Geology and Terrestrial Analogs 95, 25–32. https://doi.org/10.1016/j.pss.2013.05.024

Berger, G., Toplis, M.J., Treguier, E., d'Uston, C., Pinet, P., 2009. Evidence in favor of small amounts of ephemeral and transient water during alteration at Meridiani Planum, Mars. Am. Mineral. 94, 1279–1282. https://doi.org/10.2138/am.2009.3230

Bhattacharya, J.P., Payenberg, T.H.D., Lang, S.C., Bourke, M., 2005. Dynamic river channels suggest a long-lived Noachian crater lake on Mars. Geophys. Res. Lett. 32. https://doi.org/10.1029/2005GL022747

Bibring, J.-P., Langevin, Y., Mustard, J.F., Poulet, F., Arvidson, Raymond, Gendrin, A., Gondet, B., Mangold, N., Pinet, P., Forget, F., Berthé, M., Bibring, J.-P., Gendrin, A., Gomez, C., Gondet, B., Jouglet, D., Poulet, F., Soufflot, A., Vincendon, M., Combes, M., Drossart, P., Encrenaz, T., Fouchet, T., Merchiorri, R., Belluci, G., Altieri, F., Formisano, V., Capaccioni, F., Cerroni, P., Coradini, A., Fonti, S., Korablev, O., Kottsov, V., Ignatiev, N., Moroz, V., Titov, D., Zasova, L., Loiseau, D., Mangold, N., Pinet, Patrick, Douté, S., Schmitt, B., Sotin, C., Hauber, E., Hoffmann, H., Jaumann, R., Keller, U., Arvidson, Ray, Mustard, J.F., Duxbury, T., Forget, François, Neukum, G., 2006. Global Mineralogical and Aqueous Mars History Derived from OMEGA/Mars Express Data. Science 312, 400–404. https://doi.org/10.1126/science.1122659

Bish, D.L., William Carey, J., Vaniman, D.T., Chipera, S.J., 2003. Stability of hydrous minerals on the martian surface. Icarus 164, 96–103. https://doi.org/10.1016/S0019-1035(03)00140-4

Bonales, L.J., Muñoz-Iglesias, V., Prieto-Ballesteros, O., 2013. Raman spectroscopy as a tool to study the solubility of CO2 in magnesium sulphate brines: application to the fluids of Europa's cryomagmatic reservoirs. Eur. J. Mineral. 25, 735–743. https://doi.org/10.1127/0935-1221/2013/0025-2312

Boukhalfa, C., 2010. Sulfate removal from aqueous solutions by hydrous iron oxide in the presence of heavy metals and competitive anions: Macroscopic and spectroscopic analyses. Desalination 250, 428–432. https://doi.org/10.1016/j.desal.2009.09.070

Boynton, W.V., Taylor, G.J., Evans, L.G., Reedy, R.C., Starr, R., Janes, D.M., Kerry, K.E., Drake, D.M., Kim, K.J., Williams, R.M.S., Crombie, M.K., Dohm, J.M., Baker, V., Metzger, A.E., Karunatillake, S., Keller, J.M., Newsom, H.E., Arnold, J.R., Brückner, J.,

Englert, P. a. J., Gasnault, O., Sprague, A.L., Mitrofanov, I., Squyres, S.W., Trombka, J.I., d'Uston, L., Wänke, H., Hamara, D.K., 2007. Concentration of H, Si, Cl, K, Fe, and Th in the low- and mid-latitude regions of Mars. J. Geophys. Res. Planets 112. https://doi.org/10.1029/2007JE002887

Brass, G.W., 1980. Stability of brines on Mars. Icarus 42, 20–28. https://doi.org/10.1016/0019-1035(80)90237-7

Bridges, J., Burchell, M., Changela, H., FOSTER, N., CREIGHTON, J., CARPENTER, J., GURMAN, S., Franchi, I., BUSEMANN, H., 2010. Iron oxides in comet 81P/Wild 2. Meteorit. Planet. Sci. 45, 55–72. https://doi.org/10.1111/j.1945-5100.2009.01005.x

Burns, R.G., 1993. Rates and mechanisms of chemical weathering of ferromagnesian silicate minerals on Mars. Geochim. Cosmochim. Acta 57, 4555–4574. https://doi.org/10.1016/0016-7037(93)90182-V

Carr, M.H., 1979. Formation of Martian flood features by release of water from confined aquifers. J. Geophys. Res. 84, 2995. https://doi.org/10.1029/JB084iB06p02995

Carrier, B.L., Kounaves, S.P., 2015. The origins of perchlorate in the Martian soil. Geophys. Res. Lett. 42, 3739–3745. https://doi.org/10.1002/2015GL064290

Carter, J., Poulet, F., Bibring, J.-P., Mangold, N., Murchie, S., 2013. Hydrous minerals on Mars as seen by the CRISM and OMEGA imaging spectrometers: Updated global view. J. Geophys. Res. Planets 118, 831–858. https://doi.org/10.1029/2012JE004145

Chemtob, S.M., Nickerson, R.D., Morris, R.V., Agresti, D.G., Catalano, J.G., 2017. Oxidative Alteration of Ferrous Smectites and Implications for the Redox Evolution of Early Mars. J. Geophys. Res. Planets 122, 2469–2488. https://doi.org/10.1002/2017JE005331

Chevrier, V.F., Rivera-Valentin, E.G., 2012. Formation of recurring slope lineae by liquid brines on present-day Mars: LIQUID BRINES ON MARS. Geophys. Res. Lett. 39, n/a-n/a. https://doi.org/10.1029/2012GL054119

Chou, I.-M., Pasteris, J.D., Seitz, J.C., 1990. High-density volatiles in the system C-O-H-N for the calibration of a laser Raman microprobe. Geochim. Cosmochim. Acta 54, 535–543. https://doi.org/10.1016/0016-7037(90)90350-T

Chou, I.-M., Wang, A., 2017. Application of laser Raman micro-analyses to Earth and planetary materials. J. Asian Earth Sci., Asian Orogeny and Continental Tectonics from Geochemical Perspectives, A Special Issue in Memory of Professor Bor-ming Jahn for His Scientific Contributions and Service (Part I) 145, 309–333. https://doi.org/10.1016/j.jseaes.2017.06.032

Clifford, S.M., Parker, T.J., 2001. The Evolution of the Martian Hydrosphere: Implications for the Fate of a Primordial Ocean and the Current State of the Northern Plains. Icarus 154, 40–79. https://doi.org/10.1006/icar.2001.6671

Cull, S.C., Arvidson, R.E., Catalano, J.G., Ming, D.W., Morris, R.V., Mellon, M.T., Lemmon, M., 2010. Concentrated perchlorate at the Mars Phoenix landing site: Evidence for thin film liquid water on Mars: PHOENIX-CONCENTRATED PERCHLORATE. Geophys. Res. Lett. 37, n/a-n/a. https://doi.org/10.1029/2010GL045269

Cutts, J.A., Blasius, K.R., Briggs, G.A., Carr, M.H., Greeley, R., Masursky, H., 1976. North Polar Region of Mars: Imaging Results from Viking 2. Science 194, 1329–1337.

Das, S., Hendry, M.J., 2011. Application of Raman spectroscopy to identify iron minerals commonly found in mine wastes. Chem. Geol. 290, 101–108. https://doi.org/10.1016/j.chemgeo.2011.09.001

Daval, D., Bernard, S., Rémusat, L., Wild, B., Guyot, F., Micha, J.S., Rieutord, F., Magnin, V., Fernandez-Martinez, A., 2017. Dynamics of altered surface layer formation on dissolving silicates. Geochim. Cosmochim. Acta 209, 51–69. https://doi.org/10.1016/j.gca.2017.04.010

Dehouck, E., Chevrier, V., Gaudin, A., Mangold, N., Mathé, P.-E., Rochette, P., 2012. Evaluating the role of sulfide-weathering in the formation of sulfates or carbonates on Mars. Geochim. Cosmochim. Acta 90, 47–63. https://doi.org/10.1016/j.gca.2012.04.057

Dehouck, E., Gaudin, A., Chevrier, V., Mangold, N., 2016. Mineralogical record of the redox conditions on early Mars. ICARUS 271, 67–75. http://dx.doi.org.ezproxy.lib.ou.edu/10.1016/j.icarus.2016.01.030

Dickinson, W.W., Rosen, M.R., 2003. Antarctic permafrost: An analogue for water and diagenetic minerals on Mars. Geology 31, 199–202. https://doi.org/10.1130/0091-7613(2003)031<0199:APAAFW>2.0.CO;2

Dodd, M.S., Papineau, D., Grenne, T., Slack, J.F., Rittner, M., Pirajno, F., O'Neil, J., Little, C.T.S., 2017. Evidence for early life in Earth's oldest hydrothermal vent precipitates. Nature 543, 60–64. https://doi.org/10.1038/nature21377

Dünnwald, J., Otto, A., 1989. An investigation of phase transitions in rust layers using raman spectroscopy. Corros. Sci. 29, 1167–1176. https://doi.org/10.1016/0010-938X(89)90052-8

Edwards, C.S., Christensen, P.R., Hamilton, V.E., 2008. Evidence for extensive olivine-rich basalt bedrock outcrops in Ganges and Eos chasmas, Mars. J. Geophys. Res. Planets 113. https://doi.org/10.1029/2008JE003091

Ehlmann, B.L., Edwards, C.S., 2014. Mineralogy of the Martian Surface. Annu. Rev. Earth Planet. Sci. 42, 291–315. https://doi.org/10.1146/annurev-earth-060313-055024

Fairen, A.G., Fernandez-Remolar, D., Dohm, J.M., Baker, V.R., Amils, R., 2004. Inhibition of carbonate synthesis in acidic oceans on early Mars. Nat. Lond. 431, 423–6. http://dx.doi.org.ezproxy.lib.ou.edu/10.1038/nature02911

Fairén, A.G., Schulze-Makuch, D., Rodríguez, A.P., Fink, W., Davila, A.F., Uceda, E.R., Furfaro, R., Amils, R., McKay, C.P., 2009. Evidence for Amazonian acidic liquid water on Mars—A reinterpretation of MER mission results. Planet. Space Sci. 57, 276–287. https://doi.org/10.1016/j.pss.2008.11.008

Feldman, W.C., Prettyman, T.H., Maurice, S., Plaut, J.J., Bish, D.L., Vaniman, D.T., Mellon, M.T., Metzger, A.E., Squyres, S.W., Karunatillake, S., Boynton, W.V., Elphic, R.C., Funsten, H.O., Lawrence, D.J., Tokar, R.L., 2004. Global distribution of near-surface hydrogen on Mars. J. Geophys. Res. Planets 109. https://doi.org/10.1029/2003JE002160

Frezzotti, M.L., Tecce, F., Casagli, A., 2012. Raman spectroscopy for fluid inclusion analysis. J. Geochem. Explor. 112, 1–20. https://doi.org/10.1016/j.gexplo.2011.09.009

Golden, D.C., Ming, D.W., Morris, R.V., Mertzman, S.A., 2005. Laboratory-simulated acid-sulfate weathering of basaltic materials: Implications for formation of sulfates at Meridiani Planum and Gusev crater, Mars. J. Geophys. Res. Planets 110. https://doi.org/10.1029/2005JE002451

Gooding, J.L., 1978. Chemical weathering on Mars thermodynamic stabilities of primary minerals (and their alteration products) from mafic igneous rocks. Icarus 33, 483–513. https://doi.org/10.1016/0019-1035(78)90186-0

Goudge, T.A., Fassett, C.I., Head, J.W., Mustard, J.F., Aureli, K.L., 2016. Insights into surface runoff on early Mars from paleolake basin morphology and stratigraphy. Geology 44, 419–422. https://doi.org/10.1130/G37734.1

Gough, R.V., Chevrier, V.F., Baustian, K.J., Wise, M.E., Tolbert, M.A., 2011. Laboratory studies of perchlorate phase transitions: Support for metastable aqueous perchlorate solutions on Mars. Earth Planet. Sci. Lett. 312, 371–377. https://doi.org/10.1016/j.epsl.2011.10.026

Greenwood, J.P., Blake, R.E., 2006. Evidence for an acidic ocean on Mars from phosphorus geochemistry of Martian soils and rocks. Geology 34, 953–956. https://doi.org/10.1130/G22415A.1

Grotzinger, J.P., Arvidson, R.E., Bell, J.F., Calvin, W., Clark, B.C., Fike, D.A., Golombek, M., Greeley, R., Haldemann, A., Herkenhoff, K.E., Jolliff, B.L., Knoll, A.H., Malin, M., McLennan, S.M., Parker, T., Soderblom, L., Sohl-Dickstein, J.N., Squyres, S.W., Tosca, N.J., Watters, W.A., 2005. Stratigraphy and sedimentology of a dry to wet eolian depositional system, Burns formation, Meridiani Planum, Mars. Earth Planet. Sci. Lett., Sedimentary Geology at Meridiani Planum, Mars 240, 11–72. https://doi.org/10.1016/j.epsl.2005.09.039

Grotzinger, J.P., Gupta, S., Malin, M.C., Rubin, D.M., Schieber, J., Siebach, K., Sumner, D.Y., Stack, K.M., Vasavada, A.R., Arvidson, R.E., Calef, F., Edgar, L., Fischer, W.F., Grant, J.A., Griffes, J., Kah, L.C., Lamb, M.P., Lewis, K.W., Mangold, N., Minitti, M.E., Palucis, M., Rice, M., Williams, R.M.E., Yingst, R.A., Blake, D., Blaney, D., Conrad, P., Crisp, J., Dietrich, W.E., Dromart, G., Edgett, K.S., Ewing, R.C., Gellert, R., Hurowitz, J.A., Kocurek, G., Mahaffy, P., McBride, M.J., McLennan, S.M., Mischna, M., Ming, D.,

Milliken, R., Newsom, H., Oehler, D., Parker, T.J., Vaniman, D., Wiens, R.C., Wilson, S.A., 2015. Deposition, exhumation, and paleoclimate of an ancient lake deposit, Gale crater, Mars. Science 350. https://doi.org/10.1126/science.aac7575

Haskin, L.A., Wang, A., Jolliff, B.L., McSween, H.Y., Clark, B.C., Des Marais, D.J., McLennan, S.M., Tosca, N.J., Hurowitz, J.A., Farmer, J.D., Yen, A., Squyres, S.W., Arvidson, R.E., Klingelhöfer, G., Schröder, C., de Souza, P.A., Ming, D.W., Gellert, R., Zipfel, J., Brückner, J., Bell, J.F., Herkenhoff, K., Christensen, P.R., Ruff, S., Blaney, D., Gorevan, S., Cabrol, N.A., Crumpler, L., Grant, J., Soderblom, L., 2005. Water alteration of rocks and soils on Mars at the Spirit rover site in Gusev crater. Nature 436, 66–69.

Hausrath, E.M., Brantley, S.L., 2010. Basalt and olivine dissolution under cold, salty, and acidic conditions: What can we learn about recent aqueous weathering on Mars? J. Geophys. Res. Planets 115. https://doi.org/10.1029/2010JE003610

Hazen, R., 2012. The story of Earth.

Hecht, M.H., Kounaves, S.P., Quinn, R.C., West, S.J., Young, S.M.M., Ming, D.W., Catling, D.C., Clark, B.C., Boynton, W.V., Hoffman, J., DeFlores, L.P., Gospodinova, K., Kapit, J., Smith, P.H., 2009. Detection of Perchlorate and the Soluble Chemistry of Martian Soil at the Phoenix Lander Site. Science 325, 64–67. https://doi.org/10.1126/science.1172466

Horgan, B.H.N., Anderson, R.B., Dromart, G., Amador, E.S., Rice, M.S., 2019. The mineral diversity of Jezero crater: Evidence for possible lacustrine carbonates on Mars. Icarus 113526. https://doi.org/10.1016/j.icarus.2019.113526

Horgan, B.H.N., Smith, R.J., Cloutis, E.A., Mann, P., Christensen, P.R., 2017. Acidic weathering of basalt and basaltic glass: 1. Near-infrared spectra, thermal infrared spectra, and

implications for Mars. J. Geophys. Res. Planets 122, 172–202. https://doi.org/10.1002/2016JE005111

Hurowitz, J.A., Fischer, W.W., Tosca, N.J., Milliken, R.E., 2010. Origin of acidic surface waters and the evolution of atmospheric chemistry on early Mars. Nat. Geosci. Lond. 3, 323–326. http://dx.doi.org/10.1038/ngeo831

Israel, E.J., Arvidson, R.E., Wang, A., Pasteris, J.D., Jolliff, B.L., 1997. Laser Raman spectroscopy of varnished basalt and implications for in situ measurements of Martian rocks. J. Geophys. Res. Planets 102, 28705–28716. https://doi.org/10.1029/97JE02399

Jones, M.T., Pearce, C.R., Oelkers, E.H., 2012. An experimental study of the interaction of basaltic riverine particulate material and seawater. Geochim. Cosmochim. Acta 77, 108–120. https://doi.org/10.1016/j.gca.2011.10.044

Kieffer, H.H., 2007. Cold jets in the Martian polar caps. J. Geophys. Res. Planets 112. https://doi.org/10.1029/2006JE002816

Kim, S., Marrs, C., Nemer, M., Je-Hun Jang, J., 2017. Solubility Model for Ferrous Iron Hydroxide, Hibbingite, Siderite, and Chukanovite in High Saline Solutions of Sodium Chloride, Sodium Sulfate, and Sodium Carbonate. ACS Earth Space Chem. 1, 647–663. https://doi.org/10.1021/acsearthspacechem.7b00065

Kite, E.S., 2019. Geologic Constraints on Early Mars Climate. Space Sci. Rev. 215, 10. https://doi.org/10.1007/s11214-018-0575-5

Kounaves, S.P., Hecht, M.H., Kapit, J., Quinn, R.C., Catling, D.C., Clark, B.C., Ming, D.W., Gospodinova, K., Hredzak, P., McElhoney, K., Shusterman, J., 2010. Soluble sulfate in the martian soil at the Phoenix landing site: SULFATE AT THE PHOENIX LANDING SITE. Geophys. Res. Lett. 37, n/a-n/a. https://doi.org/10.1029/2010GL042613

Lafuente, B., Downs, R.T., Yang, H., Stone, N., 2015. The power of databases: the RRUFF project, in: Highlights in Mineralogical Crystallography. De Gruyter, Inc., Berlin/München/Boston, GERMANY, pp. 1–30.

Legett, C., Pritchett, B.N., Elwood Madden, A.S., Phillips-Lander, C.M., Elwood Madden, M.E., 2018. Jarosite dissolution rates in perchlorate brine. Icarus 301, 189–195. https://doi.org/10.1016/j.icarus.2017.06.031

Marshall, C.P., Edwards, H.G.M., Jehlicka, J., 2010. Understanding the Application of Raman Spectroscopy to the Detection of Traces of Life. Astrobiology 10, 229–243. https://doi.org/10.1089/ast.2009.0344

Marshall, C.P., Marshall, A.O., 2014. Raman spectroscopy as a screening tool for ancient life detection on Mars. Philos. Trans. R. Soc. Math. Phys. Eng. Sci. 372, 20140195–20140195. https://doi.org/10.1098/rsta.2014.0195

Martínez, G.M., Renno, N.O., 2013. Water and Brines on Mars: Current Evidence and Implications for MSL. Space Sci. Rev. 175, 29–51. https://doi.org/10.1007/s11214-012-9956-3

Martínez, G.M., Renno, N.O., Elliott, H.M., 2012. The evolution of the albedo of dark spots observed on Mars polar region. Icarus 221, 816–830. https://doi.org/10.1016/j.icarus.2012.09.008

Martinez, I., Sanchez-Valle, C., Daniel, I., Reynard, B., 2004. High-pressure and high-temperature Raman spectroscopy of carbonate ions in aqueous solution. Chem. Geol. 207, 47–58. https://doi.org/10.1016/j.chemgeo.2004.02.003

Massé, M., Beck, P., Schmitt, B., Pommerol, A., McEwen, A., Chevrier, V., Brissaud, O., Séjourné, A., 2014. Spectroscopy and detectability of liquid brines on mars. Planet. Space Sci. 92, 136–149. https://doi.org/10.1016/j.pss.2014.01.018

Mazzetti, L., Thistlethwaite, P.J., 2002. Raman spectra and thermal transformations of ferrihydrite and schwertmannite. J. Raman Spectrosc. 33, 104–111. https://doi.org/10.1002/jrs.830

McEwen, A.S., Dundas, C.M., Mattson, S.S., Toigo, A.D., Ojha, L., Wray, J.J., Chojnacki, M., Byrne, S., Murchie, S.L., Thomas, N., 2014. Recurring slope lineae in equatorial regions of Mars. Nat. Geosci. 7, 53–58. https://doi.org/10.1038/ngeo2014

McGraw, L.E., McCollom, N.D.S., Phillips-Lander, C.M., Elwood Madden, M.E., 2018. Measuring Perchlorate and Sulfate in Planetary Brines Using Raman Spectroscopy. ACS Earth Space Chem. 2, 1068–1074. https://doi.org/10.1021/acsearthspacechem.8b00082

Milliken, R.E., Grotzinger, J.P., Thomson, B.J., 2010. Paleoclimate of Mars as captured by the stratigraphic record in Gale Crater. Geophys. Res. Lett. 37. http://dx.doi.org.ezproxy.lib.ou.edu/10.1029/2009GL041870

Ming, D.W., Mittlefehldt, D.W., Morris, R.V., Golden, D.C., Gellert, R., Yen, A., Clark, B.C., Squyres, S.W., Farrand, W.H., Ruff, S.W., Arvidson, R.E., Klingelhöfer, G., McSween, H.Y., Rodionov, D.S., Schröder, C., Souza, P.A. de, Wang, A., 2006. Geochemical and mineralogical indicators for aqueous processes in the Columbia Hills of Gusev crater, Mars. J. Geophys. Res. Planets 111. https://doi.org/10.1029/2005JE002560

Möhlmann, D., Thomsen, K., 2011. Properties of cryobrines on Mars. Icarus 212, 123–130. https://doi.org/10.1016/j.icarus.2010.11.025

Moyano-Cambero, C.E., Trigo-Rodríguez, J.M., Benito, M.I., Alonso-Azcárate, J., Lee, M.R., Mestres, N., Martínez-Jiménez, M., Martín-Torres, F.J., Fraxedas, J., 2017. Petrographic and geochemical evidence for multiphase formation of carbonates in the Martian orthopyroxenite Allan Hills 84001. Meteorit. Planet. Sci. 52, 1030–1047. https://doi.org/10.1111/maps.12851

Nikolakakos, G., Whiteway, J.A., 2018. Laboratory study of adsorption and deliquescence on the surface of Mars. Icarus, Mars Polar Science VI 308, 221–229. https://doi.org/10.1016/j.icarus.2017.05.006

Nuding, D.L., Rivera-Valentin, E.G., Davis, R.D., Gough, R.V., Chevrier, V.F., Tolbert, M.A., 2014. Deliquescence and efflorescence of calcium perchlorate: An investigation of stable aqueous solutions relevant to Mars. Icarus 243, 420–428. https://doi.org/10.1016/j.icarus.2014.08.036

Ojha, L., Wilhelm, M.B., Murchie, S.L., McEwen, A.S., Wray, J.J., Hanley, J., Massé, M., Chojnacki, M., 2015. Spectral evidence for hydrated salts in recurring slope lineae on Mars. Nat. Geosci. 8, 829–832. https://doi.org/10.1038/ngeo2546

Peretyazhko, T.S., Ming, D.W., Rampe, E.B., Morris, R.V., Agresti, D.G., 2018. Effect of Solution pH and Chloride Concentration on Akaganeite Precipitation: Implications for Akaganeite Formation on Mars. J. Geophys. Res. Planets 123, 2211–2222. https://doi.org/10.1029/2018JE005630

Peslier, A.H., Hervig, R., Yang, S., Humayun, M., Barnes, J.J., Irving, A.J., Brandon, A.D., 2019. Determination of the water content and D/H ratio of the martian mantle by unraveling degassing and crystallization effects in nakhlites. Geochim. Cosmochim. Acta. https://doi.org/10.1016/j.gca.2019.04.023

Peter. Vandenabeele, 2013. Practical Raman spectroscopy: an introduction / Peter Vandenabeele, Ghent University, Belgium., Analytical techniques in the sciences. Wiley, Chichester, West Sussex, United Kingdom.

Phillips-Lander, C.M., Elwood Madden, A.S., Hausrath, E.M., Elwood Madden, M.E., 2019. Aqueous alteration of pyroxene in sulfate, chloride, and perchlorate brines: Implications for post-Noachian aqueous alteration on Mars. Geochim. Cosmochim. Acta 257, 336–353. https://doi.org/10.1016/j.gca.2019.05.006

Phillips-Lander, C.M., Legett, C., Madden, A.S.E., Madden, M.E.E., 2017. Can we use pyroxene weathering textures to interpret aqueous alteration conditions? Yes and No. Am. Mineral. 102, 1915–1921. https://doi.org/10.2138/am-2017-6155

Pismenskaya, N., Laktionov, E., Nikonenko, V., Attar, A., Auclair, B., Pourcelly, G., 2020. Dependence of composition of anion-exchange membranes and their electrical conductivity on concen-V.

Prasad, P.S.R., 1999. Raman intensities near gypsum–bassanite transition in natural gypsum. J. Raman Spectrosc. 30, 693–696. https://doi.org/10.1002/(SICI)1097-4555(199908)30:8<693::AID-JRS434>3.0.CO;2-8

Primm, K.M., Gough, R.V., Chevrier, V.F., Tolbert, M.A., 2017. Freezing of perchlorate and chloride brines under Mars-relevant conditions. Geochim. Cosmochim. Acta 212, 211–220. https://doi.org/10.1016/j.gca.2017.06.012

Raman, C.V., Krishnan, K.S., 1928. A New Type of Secondary Radiation. Nature 121, 501. https://doi.org/10.1038/121501c0

Rampe, E.B., Ming, D.W., Blake, D.F., Bristow, T.F., Chipera, S.J., Grotzinger, J.P., Morris, R.V., Morrison, S.M., Vaniman, D.T., Yen, A.S., Achilles, C.N., Craig, P.I., Des Marais,

D.J., Downs, R.T., Farmer, J.D., Fendrich, K.V., Gellert, R., Hazen, R.M., Kah, L.C., Morookian, J.M., Peretyazhko, T.S., Sarrazin, P., Treiman, A.H., Berger, J.A., Eigenbrode, J., Fairén, A.G., Forni, O., Gupta, S., Hurowitz, J.A., Lanza, N.L., Schmidt, M.E., Siebach, K., Sutter, B., Thompson, L.M., 2017. Mineralogy of an ancient lacustrine mudstone succession from the Murray formation, Gale crater, Mars. Earth Planet. Sci. Lett. 471, 172–185. https://doi.org/10.1016/j.epsl.2017.04.021

Rapin, W., Chauviré, B., Gabriel, T.S.J., McAdam, A.C., Ehlmann, B.L., Hardgrove, C., Meslin, P.-Y., Rondeau, B., Dehouck, E., Franz, H.B., Mangold, N., Chipera, S.J., Wiens, R.C., Frydenvang, J., Schröder, S., 2018. In Situ Analysis of Opal in Gale Crater, Mars. J. Geophys. Res. Planets 123, 1955–1972. https://doi.org/10.1029/2017JE005483

Rennó, N.O., Bos, B.J., Catling, D., Clark, B.C., Drube, L., Fisher, D., Goetz, W., Hviid, S.F., Keller, H.U., Kok, J.F., Kounaves, S.P., Leer, K., Lemmon, M., Madsen, M.B., Markiewicz, W.J., Marshall, J., McKay, C., Mehta, M., Smith, M., Zorzano, M.P., Smith, P.H., Stoker, C., Young, S.M.M., 2009. Possible physical and thermodynamical evidence for liquid water at the Phoenix landing site. J. Geophys. Res. Planets 114. https://doi.org/10.1029/2009JE003362

Robertson, K., Bish, D., 2011. Stability of phases in the Mg(ClO4)2·nH2O system and implications for perchlorate occurrences on Mars. J. Geophys. Res. Planets 116. https://doi.org/10.1029/2010JE003754

Ruff, S.W., Farmer, J.D., Calvin, W.M., Herkenhoff, K.E., Johnson, J.R., Morris, R.V., Rice, M.S., Arvidson, R.E., Bell, J.F., Christensen, P.R., Squyres, S.W., 2011. Characteristics, distribution, origin, and significance of opaline silica observed by the Spirit rover in Gusev crater, Mars. J. Geophys. Res. Planets 116. https://doi.org/10.1029/2010JE003767

Rull, F., Maurice, S., Hutchinson, I., Moral, A., Perez, C., Diaz, C., Colombo, M., Belenguer, T., Lopez-Reyes, G., Sansano, A., Forni, O., Parot, Y., Striebig, N., Woodward, S., Howe, C., Tarcea, N., Rodriguez, P., Seoane, L., Santiago, A., Rodriguez-Prieto, J.A., Medina, J., Gallego, P., Canchal, R., Santamaría, P., Ramos, G., Vago, J.L., on behalf of the RLS Team, 2017. The Raman Laser Spectrometer for the ExoMars Rover Mission to Mars. Astrobiology 17, 627–654. https://doi.org/10.1089/ast.2016.1567

Saheb, M., Neff, D., Bellot-Gurlet, L., Dillmann, P., 2011. Raman study of a deuterated iron hydroxycarbonate to assess long-term corrosion mechanisms in anoxic soils. J. Raman Spectrosc. 42, 1100–1108. https://doi.org/10.1002/jrs.2828

Schon, S.C., Head, J.W., Fassett, C.I., 2012. An overfilled lacustrine system and progradational delta in Jezero crater, Mars: Implications for Noachian climate. Planet. Space Sci. 67, 28–45. https://doi.org/10.1016/j.pss.2012.02.003

Schröder, C., Klingelhöfer, G., Tremel, W., 2004. Weathering of Fe-bearing minerals under Martian conditions, investigated by Mössbauer spectroscopy. Planet. Space Sci., Planet Mars. Sponsors: Centre National d'Etudes Spatiales (CNES); Centre National de la Recherche Scientifique (CNRS); Observatoire de Paris 52, 997–1010. https://doi.org/10.1016/j.pss.2004.07.018

Schuttlefield, J.D., Sambur, J.B., Gelwicks, M., Eggleston, C.M., Parkinson, B.A., 2011. Photooxidation of Chloride by Oxide Minerals: Implications for Perchlorate on Mars. J. Am. Chem. Soc. 133, 17521–17523. https://doi.org/10.1021/ja2064878

Smith, M.L., Claire, M.W., Catling, D.C., Zahnle, K.J., 2014. The formation of sulfate, nitrate and perchlorate salts in the martian atmosphere. Icarus 231, 51–64. https://doi.org/10.1016/j.icarus.2013.11.031

Smith, R.J., Horgan, B.H.N., Mann, P., Cloutis, E.A., Christensen, P.R., 2017. Acid weathering of basalt and basaltic glass: 2. Effects of microscopic alteration textures on spectral properties. J. Geophys. Res. Planets 122, 203–227. https://doi.org/10.1002/2016JE005112

Solomon, S.C., Aharonson, O., Aurnou, J.M., Banerdt, Wb., Carr, M.H., Dombard, A.J., Frey, H.V., Golombek, M.P., Hauck, S.A., Head, J.W., Jakosky, B.M., Johnson, C.L., McGovern, P.J., Neumann, G.A., Phillips, R.J., Smith, D.E., Zuber, M.T., 2005. New Perspectives on Ancient Mars. Sci. Wash. 307, 1214–1220. http://dx.doi.org/10.1126/science.1101812

Steiger, M., Linnow, K., Ehrhardt, D., Rohde, M., 2011. Decomposition reactions of magnesium sulfate hydrates and phase equilibria in the MgSO4–H2O and Na+–Mg2+–Cl−–SO42−–H2O systems with implications for Mars. Geochim. Cosmochim. Acta 75, 3600–3626. https://doi.org/10.1016/j.gca.2011.03.038

Toner, J.D., Catling, D.C., Light, B., 2014. The formation of supercooled brines, viscous liquids, and low-temperature perchlorate glasses in aqueous solutions relevant to Mars. Icarus 233, 36–47. https://doi.org/10.1016/j.icarus.2014.01.018

Tosca, N.J., McLennan, S.M., 2009. Experimental constraints on the evaporation of partially oxidized acid-sulfate waters at the martian surface. Geochim. Cosmochim. Acta 73, 1205–1222. https://doi.org/10.1016/j.gca.2008.11.015

Vago, J.L., Westall, F., Coates, A.J., Jaumann, R., Korablev, O., Ciarletti, V., Mitrofanov, I., Josset, J.-L., De Sanctis, M.C., Bibring, J.-P., Rull, F., Goesmann, F., Steininger, H., Goetz, W., Brinckerhoff, W., Szopa, C., Raulin, F., Westall, F., Edwards, H.G.M., Whyte, L.G., Fairén, A.G., Bibring, J.-P., Bridges, J., Hauber, E., Ori, G.G., Werner, S.,

Loizeau, D., Kuzmin, R.O., Williams, R.M.E., Flahaut, J., Forget, F., Vago, J.L., Rodionov, D., Korablev, O., Svedhem, H., Sefton-Nash, E., Kminek, G., Lorenzoni, L., Joudrier, L., Mikhailov, V., Zashchirinskiy, A., Alexashkin, S., Calantropio, F., Merlo, A., Poulakis, P., Witasse, O., Bayle, O., Bayón, S., Meierhenrich, U., Carter, J., García-Ruiz, J.M., Baglioni, P., Haldemann, A., Ball, A.J., Debus, A., Lindner, R., Haessig, F., Monteiro, D., Trautner, R., Voland, C., Rebeyre, P., Goulty, D., Didot, F., Durrant, S., Zekri, E., Koschny, D., Toni, A., Visentin, G., Zwick, M., van Winnendael, M., Azkarate, M., Carreau, C., 2017. Habitability on Early Mars and the Search for Biosignatures with the ExoMars Rover. Astrobiology 17, 471–510. https://doi.org/10.1089/ast.2016.1533

Vaniman, D.T., Bish, D.L., Chipera, S.J., Fialips, C.I., William Carey, J., Feldman, W.C., 2004. Magnesium sulphate salts and the history of water on Mars. Nature 431, 663–665. https://doi.org/10.1038/nature02973

Vaniman, D.T., Bish, D.L., Ming, D.W., Bristow, T.F., Morris, R.V., Blake, D.F., Chipera, S.J., Morrison, S.M., Treiman, A.H., Rampe, E.B., Rice, M., Achilles, C.N., Grotzinger, †. J. P., McLennan, S.M., Williams, J., Bell III, J.F., Newsom, H.E., Downs, R.T., Maurice, S., Sarrazin, P., 2014. Mineralogy of a Mudstone at Yellowknife Bay, Gale Crater, Mars. Science 343, 1–8. https://doi.org/10.1126/science.1243480

Viles, H., Ehlmann, B., Wilson, C.F., Cebula, T., Page, M., Bourke, M., 2010. Simulating weathering of basalt on Mars and Earth by thermal cycling. Geophys. Res. Lett. Wash. 37. http://dx.doi.org/10.1029/2010GL043522

Wang, A., Freeman, J.J., Jolliff, B.L., 2009. Phase transition pathways of the hydrates of magnesium sulfate in the temperature range 50°C to 5°C: Implication for sulfates on Mars. J. Geophys. Res. Planets 114. https://doi.org/10.1029/2008JE003266

Wang, A., Freeman, J.J., Jolliff, B.L., Chou, I.-M., 2006. Sulfates on Mars: A systematic Raman spectroscopic study of hydration states of magnesium sulfates. Geochim. Cosmochim. Acta 70, 6118–6135. https://doi.org/10.1016/j.gca.2006.05.022

Westall, F., 2005. Evolution. Life on the early Earth: a sedimentary view. Science 308, 366–367.

Wray, J.J., Squyres, S.W., Roach, L.H., Bishop, J.L., Mustard, J.F., Noe Dobrea, E.Z., 2010. Identification of the Ca-sulfate bassanite in Mawrth Vallis, Mars. Icarus 209, 416–421. https://doi.org/10.1016/j.icarus.2010.06.001

Yant, M., Rogers, A.D., Nekvasil, H., Zhao, Y.-Y.S., Bristow, T., 2016. Spectral characterization of acid weathering products on Martian basaltic glass. J. Geophys. Res. Planets 121, 516–541. https://doi.org/10.1002/2015JE004969

Appendix

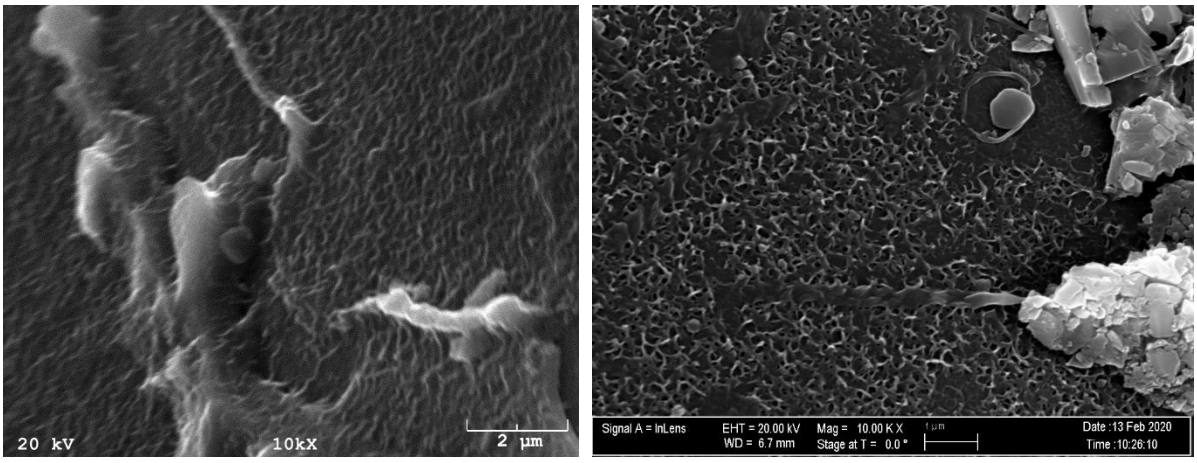

Figure 43. Scanning electron images of two samples of Craters of the Moon basalt at 10,000x after reacting in ultra-pure water for six months (left) and after reaction in ultra-pure water for 12 months (right). The image on the left is taken with the Jeol 840A and the right is imaged with the Zeiss Neon SEM. While the right has more clarity with a better resolution and more precise adjustments for astigmatism and aberration, both images show the details of the "corn chip" appearance of clay formation.

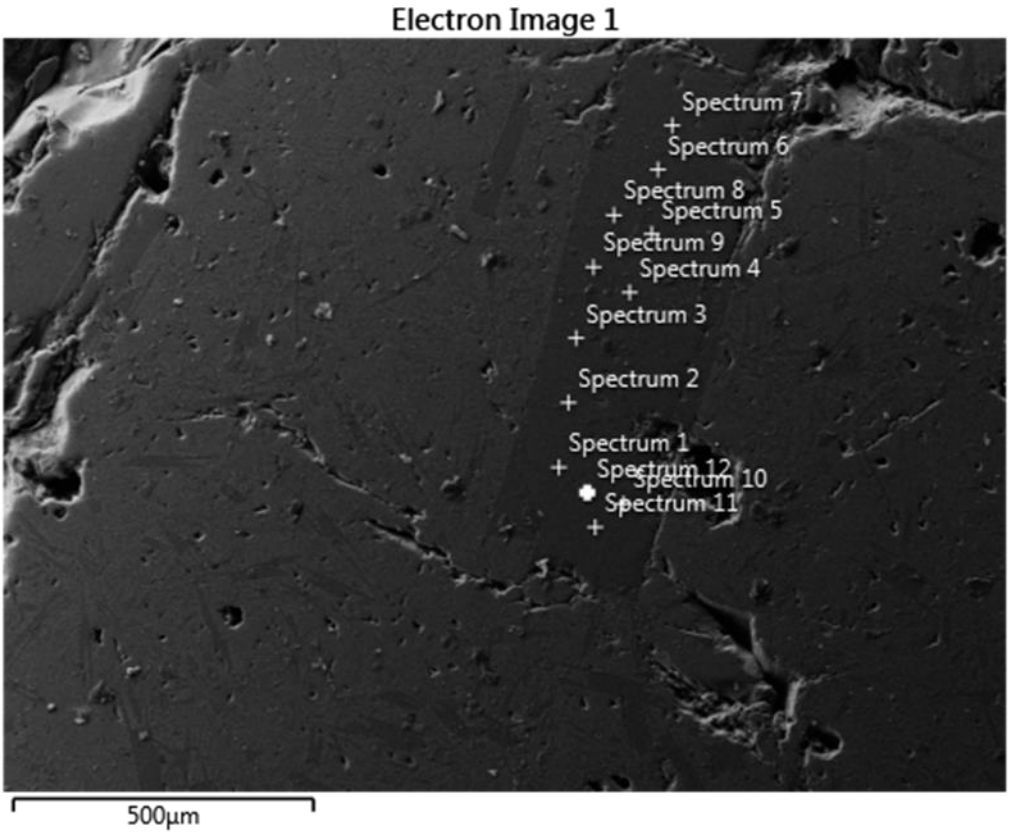

Figure 44. SEM image of a plagioclase crystal showing the location of the 12 spots used for EDS analysis. An olivine crystal can be seen at the top right corner of the image.

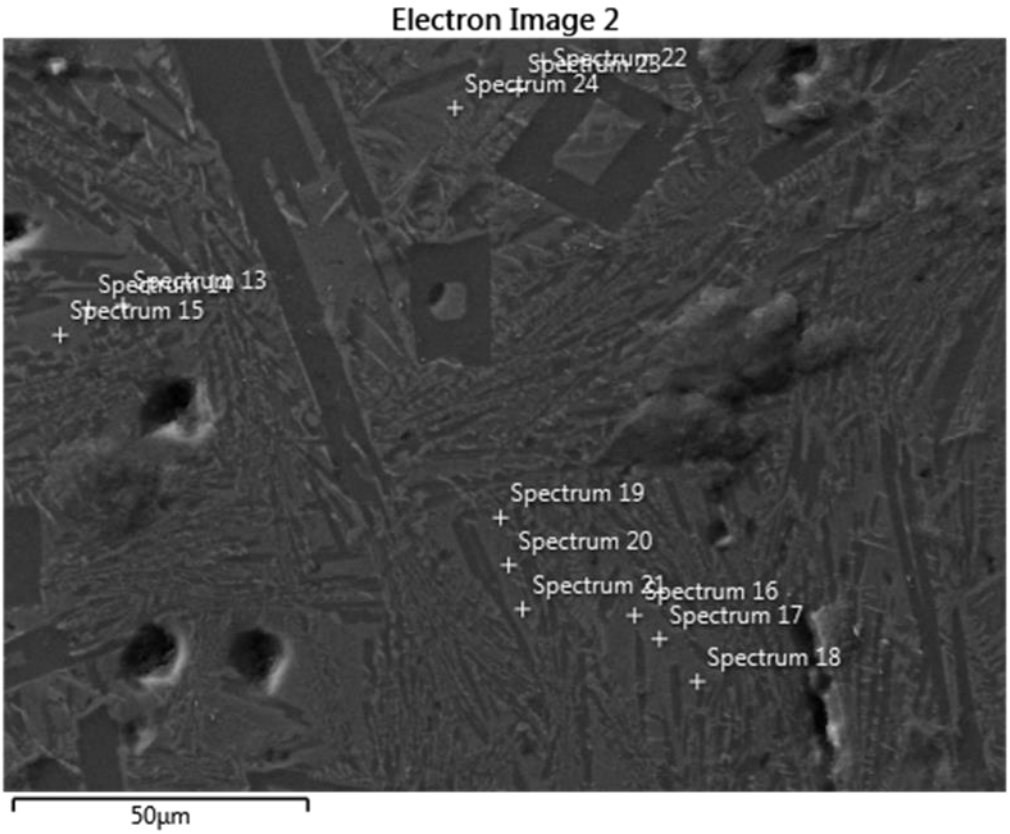

Figure 45. SEM image showing the location for EDS analysis for pyroxene. The image also shows the exsolution of the pyroxene matrix and the plagioclase crystal formations.

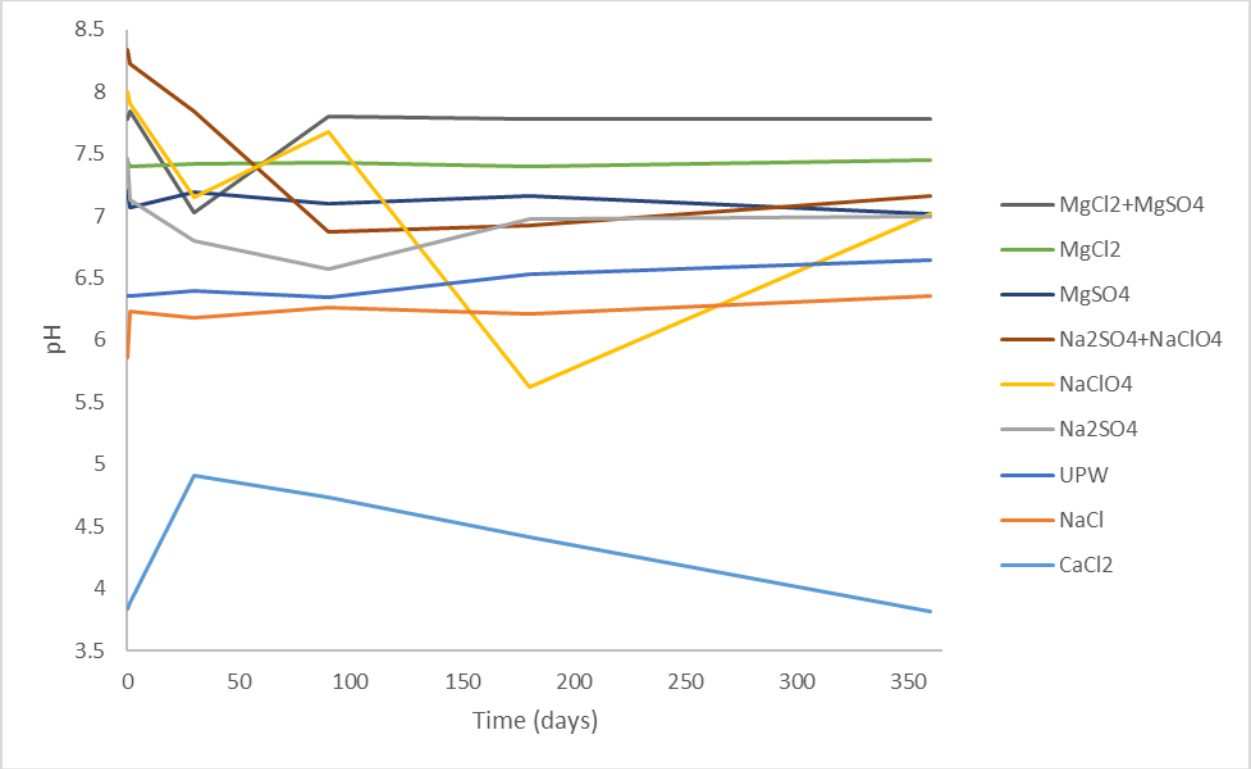

Figure 46. change of pH of the nine solutions over time. order of the solutions in the legend represent the ordinal placement of the solutions at the end of the 1-year experiment.